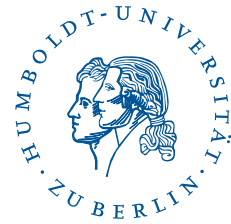


HUMBOLDT-UNIVERSITÄT ZU BERLIN



**LEBENSWISSENSCHAFTLICHE FAKULTÄT
INSTITUT FÜR BIOLOGIE**

**MASTERARBEIT
ZUM ERWERB DES AKADEMISCHEN GRADES
MASTER OF SCIENCE**

**”Die Reise der Spermien: Ein dreidimensionales
agentenbasiertes Modell”**

**”Decryption of the Journey of Sperm: A Three
Dimensional Agent Based Model”**

vorgelegt von

Jorin Diemer

geb. am 20.09.1990 in Berlin

angefertigt in der Arbeitsgruppe Theoretische Biophysik
am Institut für Biologie

Berlin, im Juni 2017

”Actually, to start with, a significant amount of sperm is lost when the penis is withdrawn from the vagina, especially if the penis is still erect when withdrawn, a regrettably common practice nowadays.”

Reynaud et al. [1]

Contents

1	Zusammenfassung	v
2	Abstract	vi
3	Introduction	1
3.1	The sperms journey through the reproductive tract	3
3.1.1	Vagina	5
3.1.2	Cervix	6
3.1.3	Uterus	8
3.1.4	Uterotubal junction - the bottleneck	10
3.1.5	Oviducts - site of storage and fertilization	11
4	Methods	14
4.1	Agent-based modeling	14
4.2	Implicit functions	15
4.3	Computational realization	15
5	Results	19
5.1	Mathematical description of the female reproductive tract	19
5.1.1	Vagina as cylinder	21
5.1.2	Cervix, cranial vagina and uterine body	22
5.1.3	Uterine horns to oviducts	28
5.2	Populating the reproductive tract	28
5.3	Agents and their movement	30
5.3.1	Active swimming	30
5.3.2	Alignment to the epithelium	34
5.3.3	Reaction to fluid flow	38
5.3.4	Muscle contractions	42
5.3.5	Modeling of pH and immune system	42
5.3.6	Environment of the microgrooves	43
5.3.7	Interaction with neighbors	44

5.4	Removing agents	45
5.5	Simulation results	45
5.5.1	Parameter setting <i>All_False</i>	47
5.5.2	Results with fluid flow, orgasm, wall interaction, pH change and immune response	49
5.5.3	Results without fluid flow	54
5.5.4	Results without wall interaction	55
5.5.5	Results with strong fluid flow	55
5.5.6	Runs <i>WFO_False</i> and <i>FO_False</i>	59
5.5.7	Interaction of sperm - proof of concept	59
6	Discussion	60
6.1	Sperm swimming in a linear fashion are more likely to reach oviducts .	62
6.2	Fluid flow fuels sperm passage through cervix	62
6.3	Wall interaction assists journey through the uterus	63
6.4	Influence of orgasm and pH	64
6.5	Sperms get stuck in microgrooves	65
6.6	Drawing random angles	65
7	Conclusion	66
8	Outlook	67
9	Acknowledgements	68
	Glossary	79
A	Appendix	87
E	Eigenständigkeitserklärung	104

1 Zusammenfassung

Auf ihrer Reise durch den weiblichen Genitaltrakt sind Spermien einer Vielzahl von Hindernissen ausgesetzt. Der weibliche Genitaltrakt und die Spermien kommunizieren über ein komplexes Netzwerk regulativer Interaktionen. Viele Mechanismen stehen unter Verdacht, die fittesten Spermien zu selektieren und diese Spermien auf ihrer Reise zur Eizelle zu unterstützen. Durch diese Mechanismen wird die Fertilisation garantiert und das Auftreten von Polyspermie verhindert.

Mathematisches Modellieren ist eine mächtige Methode zum Analysieren von komplexen, biologischen Systemen und kann benutzt werden um Nadelöhre in diesen Systemen zu identifizieren. In dieser Arbeit wird das erste agentenbasierte Modell präsentiert, welches den gesamten weiblichen Säugetierreproduktionstrakt sowie dessen Interaktionen mit Spermien beschreibt. Der Reproduktionstrakt wurde mithilfe von impliziten Funktionen definiert. Die Spermien wurden als individuelle Einheiten, ausgestattet mit Verhaltensregeln, beschrieben.

Mit Hilfe des Modells konnten zwei Prozesse identifiziert werden, welche höchst wahrscheinlich eine Schlüsselrolle in der Reproduktion der Säugetiere spielen. Die Wechselwirkung der Spermien mit Flüssigkeitsströmen und die Ausrichtung an den Epithelwänden scheinen von eminenter Bedeutung zu sein. Das vorgestellte Modell ist leicht erweiterbar und in der Lage Hypothesen über die Migration der Spermien zu testen. Mit kleinen Modifikationen, welche in dieser Arbeit thematisiert werden, ist das Modell potenziell in der Lage Licht in den Prozess der Spermienselektion zu bringen.

2 Abstract

On their journey through the female reproductive tract sperms encounter a variety of obstacles. The female reproductive tract and the sperms themselves have developed a complex interplay of regulatory interactions. Selecting only the fittest sperms, these mechanism potentially guide sperms towards the female oocyte, enable fertilization and coincidentally prohibit polyspermy.

Mathematical modeling provides a powerful method to decipher complex biological systems and can be used in order to identify bottle necks in sperm selection. In this thesis the first agent-based 3D model describing the entire mammalian female reproductive tract and its interactions with sperms is presented. The reproductive tract was described with a set of implicit functions. Sperms were modeled as decision making entities equipped with a set of behavioral rules.

Two processes were identified, which most likely play key roles during mammalian reproduction. These processes are the interaction between sperms and fluid flows as well as the alignment of sperms to the compartment wall. The resulting model is effortlessly extendable and able to test hypotheses about sperm migration. Consequently, with some future modifications, discussed in this work, the model is potentially able to elucidate processes in sperm selection.

3 Introduction

Most mammals are viviparous, i.e. they give birth to living offspring and fertilization takes place inside the female reproductive tract [2]. For successful fertilization one sperm has to fuse with the female oocyte. Therefore, sperms have to travel from the site of semen deposition through the entire female genital tract, which is orders of magnitude larger than the sperm itself (Table 1).

In mammals tens of millions to billions of sperms are deposited in the female genital tract [3]. The female genital tract faces a complex task. On one hand it has to assist sperms on their way to the female oocyte, on the other hand it has to assure that only the fittest sperms reach the site of fertilization. As in the end only one sperm should fertilize the egg.

How is this severe selection process achieved? Besides aiding the propagation of sperms, progression of pathogens into the genital tract has to be inhibited. Consequently, the female reproductive tract needs defense mechanisms against viruses, bacteria and parasites. However, these defense mechanisms should not hamper the migration of sperm. Therefore, the female reproductive tract interacts in multiple ways with the spermatozoa to support sperm migration, while preventing pathogens from entering the reproductive tract.

Fertilization by more than one sperm is called polyspermy and considered a pathological process since the 1960s [4]. Dispermy (fertilization by two sperms) results in triploidy. Triploidy, arising from an extra haploid set of chromosomes, is present in 6 % of spontaneous abortions [5]. During *in vitro* fertilization (IVF) a higher incidence of polyspermy is observed [6]. IVF becomes more and more spread in humans [7] and is of major importance in rescuing endangered animal species [8]. Consequently, a reduction in the rate of polyspermy would be of substantial (economical and emotional) importance [6]. Besides beneficial outcomes for IVF another circumstance could be unraveled. Between 1989 and 2005 sperm concentration in human semen decreased by 32.2% (from 73.6 to 49.9 million per *ml*) [9]. A minimal sperm concentration of 20 million sperms per *ml* is required for fertilization [10]. So would a further decline in semen concentration lead to infertility of a whole species?

Many hypotheses on how sperms are guided and selected on their way to the oocyte have been established [11, 12, 13, 14, 15, 16, 17]. Testing and validating hypotheses, would lead to a more pronounced understanding of sperm selection and potentially answer the question, which mechanisms sort out which sperms. Investigating this question would help to optimize IVF and estimate the significance of the decline of human sperm concentration. Sperm selection and transition can hardly be studied *in vivo*, because it takes place inside the female reproductive tract.

In order to describe and understand complex biological systems, mathematical models can be extremely beneficial. Hypotheses and experimental knowledge can be integrated into a coherent picture. Modeling potentially describes time courses of system compounds, which cannot be measured in experiments. Additionally, computational modeling can help to quantify processes. In a mathematical model, the influence of small perturbations on the system's behavior can be investigated [18]. Biological systems are often highly interconnected, so that their dynamical behavior cannot be captured by observation of single components.

In general models can be described with many different approaches [19]. These approaches include equation-based and graph-based models, as well as agent-based models. In equation-based models, a set of differential equations describes the dynamics of a system. Deterministic description of a system can be realized by a set of ordinary differential equations (ODEs). Using stochastic or partial differential equations, stochastic and spatial system properties can be incorporated [20]. Boolean networks are an example for graph-based models. A Boolean model describes a system as a network of Boolean variables. The temporal update of the system is defined by a set of logical rules. In agent-based modeling (ABM) an agent is a freely moving, decision making entity, which is enabled to interact with its environment and other agents by a set of rules. ABMs easily include spatial properties of a system.

Each modeling approach has its advantages and disadvantages. In order to investigate the journey of sperms, a model approach should be able to describe spatial properties. Furthermore, the properties of sperms should be adaptable, in dependence of their local environment, i.e. they should interact with their surroundings. Boolean networks fail to describe spatial properties and for an equation-based approach a deeper insight into

Table 1: Dimension of mammalian reproduction.

T_l : Length of reproduction tract, s_l : Length of spermatozoa, s_{speed} : Speed of spermatozoa

Species	Deposition site	T_l [cm]	s_l [μm]	s_{speed} [$\frac{\mu m}{s}$]
<i>Homo sapiens</i>	cranial vagina	29[21]	57 [22]	77.4 ± 14.1 [23] 49 – 63 [24]
<i>Bos taurus</i> (bull)	cranial vagina	110[21]	65 [25] 54 [22]	140 ^a 114.4 ± 2.37 [26]
<i>Sus scrofa</i> (wild boar)	uterus	195[21]	55 [22]	92.9 ± 3.4 [27]

^aDr. Müller (IZW) , personal communication

the model kinetics is required [20]. In contrast, constructing an ABM is possible in the absence of complete knowledge of a system. Apart from that, modeling one sperm as one agent is an intuitive approach and ABM is suitable to test, elaborate and approve hypotheses[19]. Therefore, the method of ABM was used to create a dynamical model for the propagation of sperms.

The mathematical model could help to confirm or even quantify, but also to reject the current hypotheses about sperm propagation, leading to a more pronounced understanding of sperm selection. This in turn could help to optimize *in vitro* sperm selection in order to increase fertilization rates and to decrease incidence of polyspermy.

3.1 The sperms journey through the reproductive tract

The following section summarizes current knowledge and hypotheses of the mammalian female reproductive tract and its interaction with semen and sperms. The knowledge is drawn from different species, i.e. from human, mouse, pig and cattle. This knowledge is combined in order to describe typical properties common in many species. The journey of sperms through the reproductive tract is described below, starting in the vagina. The other considered compartments are cervix, uterine body, uterine horns (e.g. in cattle and pigs), uterotubal junctions and oviducts. For each compartment general properties and hypotheses on how these influence sperms are pointed out. This

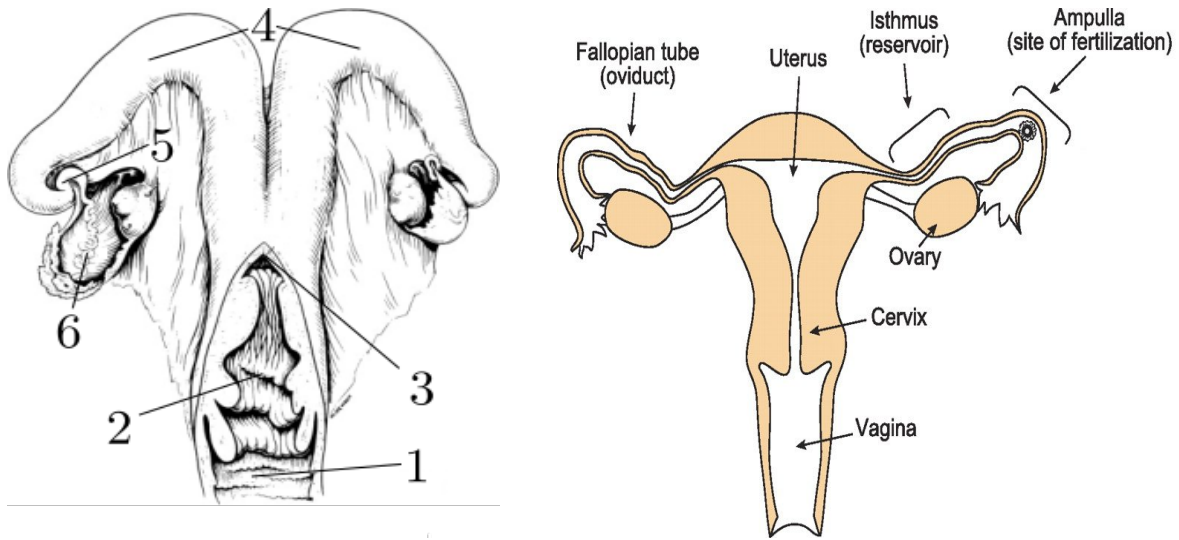


Figure 1: Comparison of bovine and human female reproductive tract.

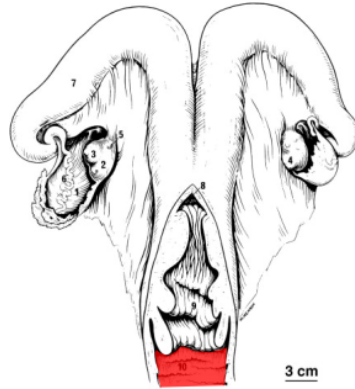
In the bovine reproductive tract the oviducts originate from the uterine horns, while in human the oviducts emerge directly from the uterine cavity. Bovine reproductive tract on the left: (1) vagina, (2) cervix, (3) uterine body, (4) uterine horns, (5) uterotubal junction, (6) oviduct. Adapted from [3].

Human reproductive tract on the right: Here isthmus and ampulla are indicated. They are part of the oviducts. In the isthmus sperms are stored and ripened (capacitated), while fertilization takes place in the ampulla [28]. The human female reproduction does not possess uterine horns.

is important to understand potential selection steps and bottle-necks.

That one sperm reaches the oocyte might look like a simple matter of chance, but there exists strong evidence that regulating mechanisms play a role in the passage of sperms through the reproductive tract [3]. Fertilization typically takes place within hours of ovulation, but often independent of insemination time. For this, sperms are stored in the isthmus (part of the oviduct) until ovulation takes place. Spermatozoa survival sometimes has to be prolonged up to five days in human until ovulation. In bats, insemination typically takes place in autumn, while ovulation occurs several months later in spring [29]. Sperms are stored for the whole time (198 days in *Noctule bat*) [30]. During this time sperms which are terminally differentiated cells lacking transcription and translation have to be kept alive. Which surroundings are provided by the female reproductive tract to keep sperms alive for such a long time?

3.1.1 Vagina

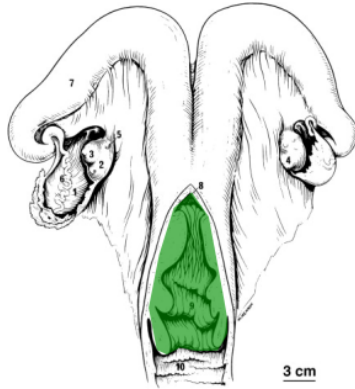


In mammals sperms are either deposited in the cranial vagina (e.g. in human and cattle) or inside the uterine body (e.g. in horse and pig) [3]. The cranial vagina is the head-directed end of the vagina,. The rest of the vagina is filled by the penis during copulation. So which environment do sperms of vaginal inseminators face after deposition?

The vagina is open to the exterior, especially during and shortly after mating, thus it is easily accessible for pathogens. One vaginal antimicrobial defense mechanism is the lowering of the pH by lactic acid [31]. In women the pH reaches values of approximately 4.5 [32], which makes it microbicidal to yeast, bacteria causing urinary tract infections and HIV (human immunodeficiency virus) [33]. However, the hostile environment created to antagonize invading pathogens also impacts deposited sperms. Decreasing pH with lactic acid immobilizes bull sperms [34], with a sigmoidal response curve [35]. The spermicidal effect would consequently drastically hamper the chance of fertilization. The pH of human seminal plasma is 7.54 ± 0.03 [36] and is able to neutralize vaginal pH [3]. So it could, at least in the beginning, protect sperms from the acidic environment.

Additionally to the acidic environment the vagina reacts immunologically, by an invasion of neutrophils. In rabbits many leukocytes contained ingested sperms 3 - 24 h post coitus [37]. These harsh conditions suggest that many sperms are conceivably lost in the vagina. In order to circumvent this hazardous environment sperms probably move quickly into the cervix [12]. But is that advantageous? Which sperm-affecting properties holds the cervix?

3.1.2 Cervix



After deposition in the vagina, sperms migrate to the cervix, where they face large volumes of cervical mucus. Increasing viscosity negatively affects sperm swimming velocities [38]. Estradiol (an estrogen) controls the hydration level, often exceeding 96 % [39], which correlates with the penetrability to sperms [3]. Estrogen concentration peaks prior estrus, the phase in which the female is receptive. This is because cervical mucus is less viscous¹ prior estrus and the probability of fertilization increases. Much of the mucus flows into the vagina and after ovulation it becomes more viscous [40]. This outflow of fluid is caused by ciliary beating and smooth muscle contractions in the epithelium [11]. Could this fluid flow wash out sperms?

In 1989 Mullins and Saacke found that the cervix is penetrated from microgrooves (sometimes not much wider than the sperm head), which run all the way from vagina up to uterus [41]. Inspecting sperms in natural mated cows, they discovered that sperms were orientated towards the uterus and therefore proposed that these microgrooves serve as advantaged pathways. These pathways would protect sperms from strong fluid flows in the middle of the cervix. Higher fluid viscosities lead to smaller swimming velocity in human and bull sperms [38] and the cervical mucus in microgrooves is less dense than the mucus in the cervical lumen [41]. So sperms in microgrooves would encounter fluid with smaller density compared to mucus in the cervical lumen. This is an indicator for microgrooves as a privileged pathway. Meanwhile, this proposal has been supported by several more recent studies: Sperms tend to swim along surfaces and corners [42]. Furthermore sperms orientate into fluid flows of certain velocity and

¹more hydrated

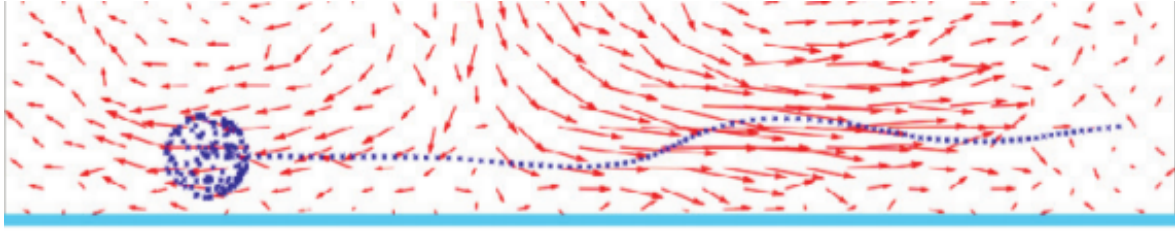


Figure 2: The sperm - a hydrodynamic pusher

Light blue line on the bottom indicates a compartment wall. Sperm shape is indicated by dark blue dots. Red arrows indicate the fluid field obtained by hydrodynamic simulations[46]. The fluid is pushed to the front and the back and replenished from the top, pressing the sperm against the wall.

viscosity [38, 43, 44, 45]. Sparse data is available about the velocity of fluid flows in the reproductive tract [3]. In mouse oviducts it was measured to be $18 \pm 1.6 \mu\text{m/s}$ [43]. Bull sperms undergo positive rheotaxis (the alignment into a flow) when fluids reach a velocity of $15 \mu\text{m/s}$ [45].

Aligning to surfaces and orientation into fluid flows could direct sperms towards the uterine cavity, but how do sperms sense a compartment wall?

The alignment to a surface or wall can be explained by the hydrodynamic nature of sperms and the conical shaped space of the beating flagella. First, sperms can be classified as a hydrodynamic pusher, which pushes fluids to the front and the back, while replenishing it from the sides [47]. Coming near a wall, fluid is refilled by only one side and the sperm is pressed against the wall (Figure 2) [46]. Second, the rotating flagella beats against the wall, pushing the sperm's posterior away from the surface. The sperm head keeps its distance to the surface. Consequently, the beating of the flagellum against the wall redirects the sperm towards it [38].

Because sperms align with surfaces and into fluid flow the microgrooves are a perfect environment for straight sperm movement.

So fluid flows can assist sperms and were shown to hinder pathogens on their progression [45]. *Tritrichomonas foetus* is a sexually transmitted parasite, causing bovine tritrichomonosis, a disease leading to infertility and abortion [48]. While sperms align into fluid flows and are able to move against them, *Tritrichomonas foetus* does not enter microgrooves and is swept away by fluid flows (Figure 3) [45].

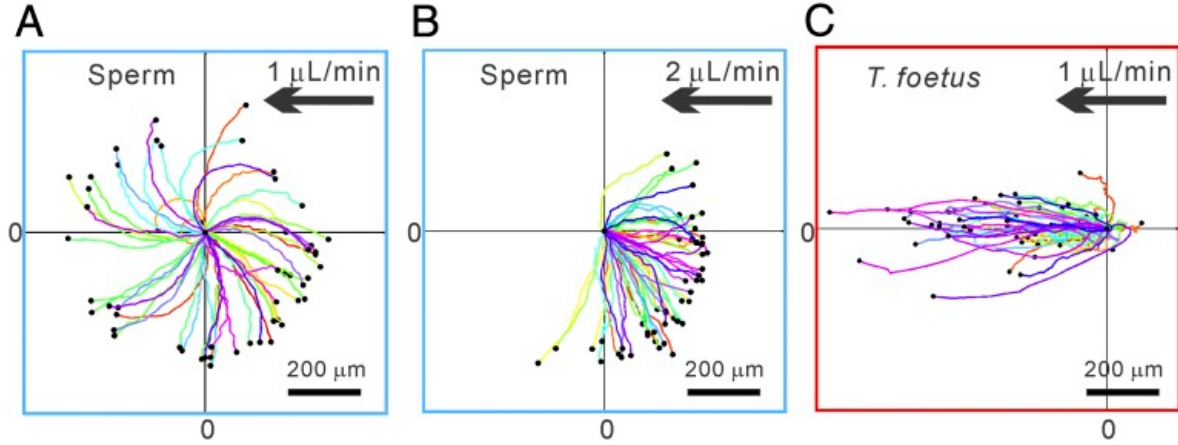


Figure 3: Bull sperms swim against fluid flow, while parasite *Trichomonas foetus* is swept away. Sperms began to orient into fluid flow at a flow rate of $1.13 \mu\text{L}/\text{min}$, corresponding to a fluid speed of $15.1 \mu\text{m}/\text{s}$ [45].

Besides the complex hydrodynamic and structural appearance of the cervix, it launches an immune response, similar to the one in the vagina (Section 3.1.1) [3]. However, this immune response is strongest after several hours [3], so sperms have sufficient time to pass the cervix.

3.1.3 Uterus



The uteri in mammals differ significantly in shape and size (Figure 1). In humans the uterine body is only $7 - 9 \text{ cm}$ long [16]. So a sperms could pass it in $14 - 18 \text{ min}$, assuming the swimming speed in aqueous medium of $5 \text{ mm}/\text{min}$ [49]. The exact rate of sperms transport through the uterus is difficult to determine. Therefore, women

would have to undergo hysterectomy², after insemination, in order to access sperms distribution. In three out of seven patients, which underwent hysterectomy, sperms were recovered from the oviduct within one hour [3].

In humans the size of the uterus is not a significant obstacle on the way to fertilization. However, in mammals with uterine horns the distance to travel is much larger. Bovine sperms must pass through the uterine body ($2.5 - 4\text{ cm}$) and the uterine horns ($35 - 45\text{ cm}$), before reaching the uterotubal junction (Figure 1, [3]). With a speed of $133\mu\text{m/s}$ [45] it would take approximately one hour to reach the uterotubal junctions on a direct path. Consequently, if sperms would swim in a directed manner, they would reach the oviducts before leukocytes begin to outnumber sperms.

As in vagina and cervix the sperms have to withstand the female immune response. In mouse uteri the number of leukocytes peaks several hours after mating [3]. Sperms have to pass through the uterine cavity before leukocytes begin to outnumber spermatozoa. As discussed above that would be possible by directed movement. Furthermore, sperms could benefit from muscle contraction inside the uterine wall [12]. These muscle contractions were shown to transport albumin microspheres ($5 - 40\mu\text{m}$ of diameter) from the cranial vagina into the uterine cavity and even up to the oviduct, in dependence of cycle stage [50]. Interestingly, occurrence of albumin beads was greater in the isthmus ipsilateral³ to the follicle. However, patterns of muscle contractions significantly changed in rats after mating [51]. Contraction waves had higher frequencies and amplitudes and propagated not only cranially, but also towards the vagina. The muscular movement could help to spread sperms in the whole uterine cavity, in order to increase the chance of sperms reaching the oviduct. In the cervix fluid flows and its complex structure seem to play an important role in sperm propagation (Section 3.1.2), while in the uterus muscle contractions are most likely to aid sperm migration. But before reaching the oviduct, the sperms have to pass the uterotubal junction.

²Hysterectomy - surgical removal of the uterus.

³Ipsilateral: on the same side.

3.1.4 Uterotubal junction - the bottleneck



The uterotubal junction (UTJ), being only 1 – 2 *mm* [52] in diameter in cattle, is a bottleneck on the way to fertilization. In addition to its small diameter, penetrating the uterotubal junction is often complicated by the presence of mucosal folds [52, 53]. In cattle the UTJ has a sigmoidal shape and is connected to muscular ligaments capable of compressing its lumen. This lumen is filled with mucus in pigs, cattle and humans [3]. For species which inseminate in the uterus, this mucus could act as a barrier to abnormal sperms, like the mucus in the cervix (Section 3.1.2).

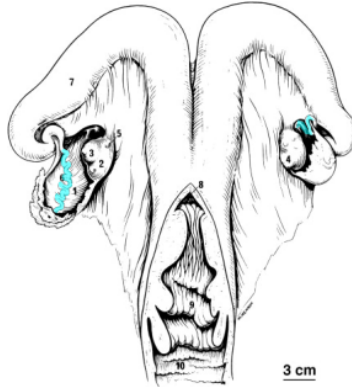
For hamster sperms, swimming in a linear fashion was advantageous compared to swimming in a non-linear (like hyperactivated sperms) fashion in order to pass the UTJ [54]. This indicates that uncapacitated sperms may have an advantage in passing the UTJ. Capacitation is a ripening process, which enables sperms to fertilize. However, this process takes place in the oviduct (Section 3.1.5). Consequently, sperms could pass into the oviduct, but once capacitated the way back into the uterine cavity is blocked by the UTJ. This means that reaching the oviduct is an irreversible process, for sperms that become capacitated.

The UTJ is, at least in mice, a barrier to sperms with mutations in membrane proteins [55, 56]. This indicates that at latest in the UTJ, the interaction between sperms and reproductive tract reaches a molecular level.

After surgical excision of both oviducts in women, sperms were recovered from the oviduct only minutes after insemination [57]. Sperms were probably transported by muscle contractions, which primarily serve to spread sperms in the cervix and the uterine body (Section 3.1.3). These muscle contractions can lead to an overshoot, so

that sperms arrive in the oviduct early. Be that as it may, the disadvantage of strong muscle contractions is that they can lead to large sheer forces, which damage sperms. Accordingly, the sperms which reach the oviducts rapidly are most likely not able to fertilize [11].

3.1.5 Oviducts - site of storage and fertilization



The oviducts significantly differ from all the other compartments, lacking an immune response after insemination [58]. Consequently, sperms do not have to encounter leukocytes in the oviducts. In the oviducts, sperms are saved from digestion. As already mentioned in Section 3.1, sperm's fertility and motility can be prolonged until ovulation. This was demonstrated in *in vitro* experiments, in which sperms were incubated with oviductal epithelium (human [59], cow [60, 61]). But how does the oviductal environment prolong sperm's life time?

In cows, nearly 40% of sperms bound to oviductal epithelial cells remained motile for 48 h, while none were motile when bound to tracheal cells or in medium alone [60]. Sperms bind to carbohydrates in the oviductal epithelium [62]. Binding of sperms to oviductal epithelium (Figure 4) creates a sperm storage site, which exists in various species [3]. In these storage sites sperms are enclosed by epithelial cells [29]. Sperm binding alters the gene expression in epithelial cells and new proteins are synthesized [63]. Some of these proteins were shown to prolong the life time of sperms [64]. Consequently, the prolonged life time of sperms originates in a complex interplay between the sperms and the oviductal epithelium. So, when bound to the epithelium, how do sperms reach the oocyte?

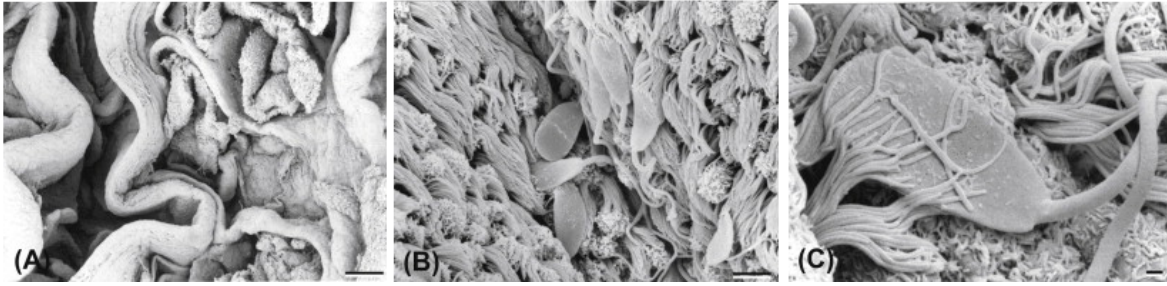


Figure 4: Bovine sperms in the oviductal sperm storage site. (A) A low magnification view of the isthmus (bar = $75\mu m$). (B) A higher magnification of a mucosal groove (bar = $5\mu m$). (C) A high magnification view of a sperm cell associated with the cilia of the epithelium (bar = $1\mu m$). Source: Figure adapted from reference [66]. Figure description taken from reference [3].

In the sperm storage sites capacitation takes place [16]. Capacitation is the ripening of sperms, which enables them to fertilize. Two changes due to capacitation may be responsible for the release of sperms from the storage site: modification of the plasma membrane as well as hyperactivation. Hyperactivated sperms show an increased flagellar beat amplitude [65]. A change in plasma membrane composition may decrease binding affinity, while hyperactivation could provide the necessary forces to detach from epithelium [65]. As mentioned before, sperms miss a transcriptional and translational machinery (Section 3.1). Consequently, the change in plasma membrane composition must be the result of the integration of proteins, synthesized in the oviductal epithelium, which again points to a complex interplay between sperms and the reproductive tract. However, sperms are able to leave the storage cite after capacitation. Sperms stay capacitated for only 1 – 4 hours. Further, capacitation takes place only once in a sperm’s life time. Therefore, capacitated sperms have to find the egg quite quickly [16].

From the storage site capacitated sperms are most likely guided to the egg by thermo- and chemotaxis, the movement directed along a temperature or chemical gradient [16]. Chemotaxis of sperms was observed in several species [16]. Interestingly, only capacitated sperms are chemotactically active. This chemotactically directed movement could guide the sperms quickly to the source of chemoattractant, the egg and its surrounding cumulus cells (Figure 5) [67].

After ovulation a temperature difference of $1.6 \pm 0.1^\circ C$ was measured from the cooler

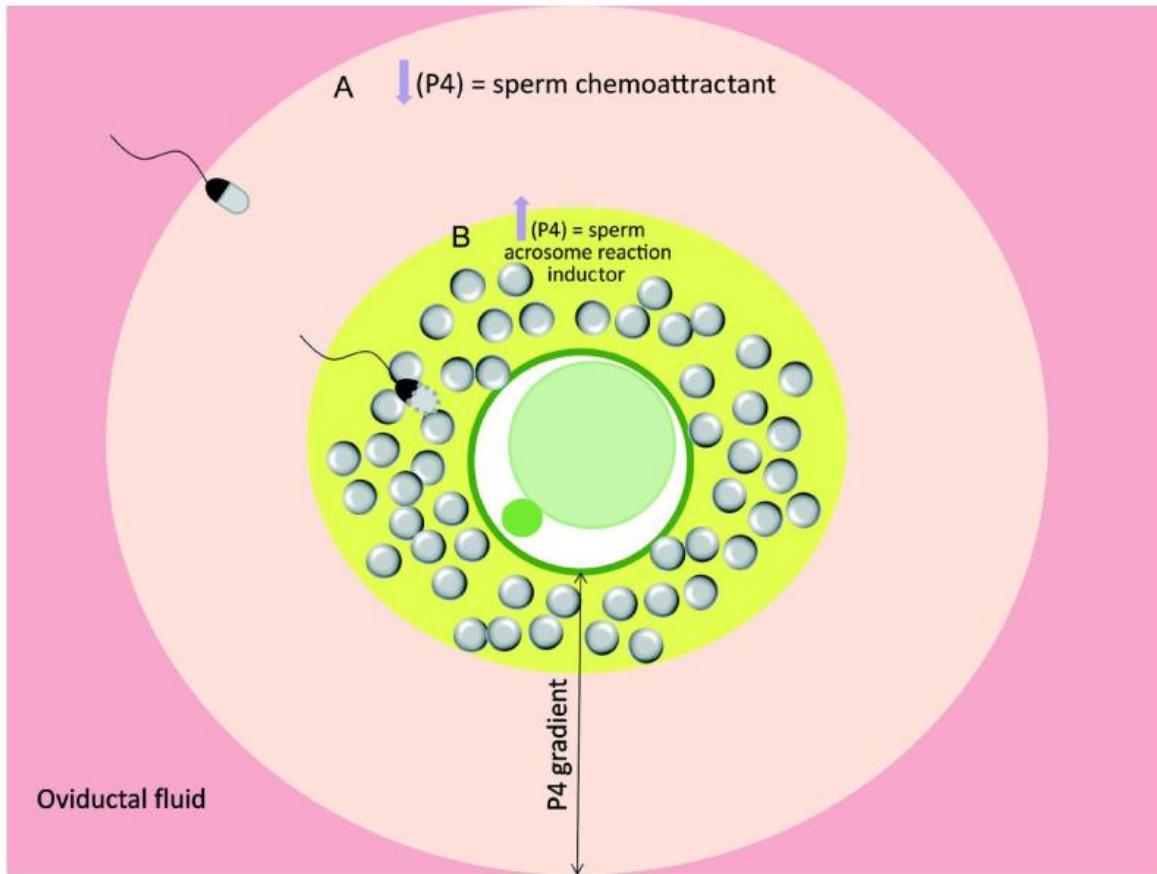


Figure 5: Site of Fertilization. Progesterone (P4) levels close to the fertilization location and its effect on sperms. A) Low progesterone levels acting like a chemo-attractant driving the sperms towards the oocyte. B) High progesterone levels secreted by cumulus cells induce acrosome reaction. [70]. Green circle: *zona pellucida*.

storage to the warmer fertilization site [68]. Human sperms were shown to be highly sensitive to temperature gradients, sensing a gradient of $0.014\text{ }^{\circ}\text{C}/\text{mm}$ [69]. Assuming a total temperature difference of nearly 2°C they could be guided for more than 14 cm by thermotaxis. However, if sperms are actually guided via thermotaxis *in vivo* remains to be validated.

On the other hand, it is unlikely that sperms are guided all the way from the storage site to the site of fertilization by chemotaxis alone, because the concentration field of the chemical attractant would be disrupted by fluid flows and muscle contractions [3].

In the end sperms reach the oocyte and its surrounding cells. There they undergo the acrosome reaction. A reaction which enables them to penetrate the *zona pellucida* and subsequently fertilize the egg (Figure 5).

4 Methods

Having the theoretical background it is now time to demonstrate, how this knowledge is used to build a model. Therefore, model concepts and techniques are presented in this section. In Section 3 the decision to use ABM for creating the model was propounded. The properties of ABM is described in more detail below. Further, the concept of implicit functions is shortly presented and the computational realization is sketched.

4.1 Agent-based modeling

In ABM a system is described as a collection of decision-making entities, called agents [71]. Agents behavior is defined by a set of rules, which could define interactions between the agents or with the agents environment. An ABM can easily incorporate space [19], which can be magnitudes larger than the agent. Albeit implementing interaction rules on single agent level, an observable outcome of an ABM are the population dynamics. This could help to analyze systems from a different viewpoint. Observing a flock of birds, it is reasonable to assume that synchronized movement is conducted by a single leader, giving flock-wide commands. Anyway, flocking behavior can be achieved by a set of simple locally defined interaction rules [72]. The sum of all these interactions leads to phenomena, which could not be foreseen. This capturing of emergent phenomena is one major advantage of ABMs [71]. Agent-based modeling is a bottom-up approach, enabling researchers to construct models in absence of complete or detailed knowledge. For the propagation of sperms in the reproductive tract ABM is an appropriate modeling approach, because data collection about the dynamics of sperm migration is difficult to access *in vivo*. Nevertheless, local interactions of sperms with their environment can be observed *in vitro*. Measuring sperm attributes and evaluating their interaction pattern *in vitro* could be used to create a model *in silico*, which then could potentially decipher the dynamics of the system. The interactions of sperms with the reproductive tract reach from large scale muscle contractions to interactions on molecular level, e.g. chemotaxis. These different scales can easily be united in agent-based modeling. As described in section 3 many hypothesis exist about the sperm guidance mechanisms. In an ABM hypothesis can be added, adapted or re-

moved without interference with the remaining system. Sections 5.1 - 5.3.6 describe the environment of the agents and their interaction with it.

4.2 Implicit functions

In the 1990s implicit surfaces have become progressively important to modeling of three-dimensional objects [73]. An implicit surface is defined by a three-dimensional implicit function. In general, an n -dimensional implicit function is defined by:

$$F(P_n) = 0 \quad (1)$$

Where P_n gives a set of points satisfying equation 1. Points P_n are defined to be on the surface of function F and define an enclosed volume [74]. Given a point X_n in an n -dimensional euclidean space, its position in respect to the described volume is defined by:

$$F(X_n) < 0, \text{ if } X_n \text{ is inside the volume} \quad (2)$$

$$F(X_n) = 0, \text{ if } X_n \text{ is on the surface of the volume} \quad (3)$$

$$F(X_n) > 0, \text{ if } X_n \text{ is outside the volume} \quad (4)$$

In three dimensions the surface of a sphere with radius (r) is given by:

$$x^2 + y^2 + z^2 - r^2 = 0 \quad (5)$$

Figure 6 shows the resulting surface setting $r = 4$.

The possibility to define if a point lies inside or outside the described volume, given by equations 2 to 4, makes the use of implicit functions for the description of the reproductive tract very useful.

4.3 Computational realization

The model was implemented in *Python* [75]. *Python* is an object oriented programming language. Having simple syntax *Python* is well readable. The readability of *Python* code enables it to be easily reused in future studies. Furthermore, it is quickly accessible for other scientists. Another advantage of *Python*, besides the readability, is that it

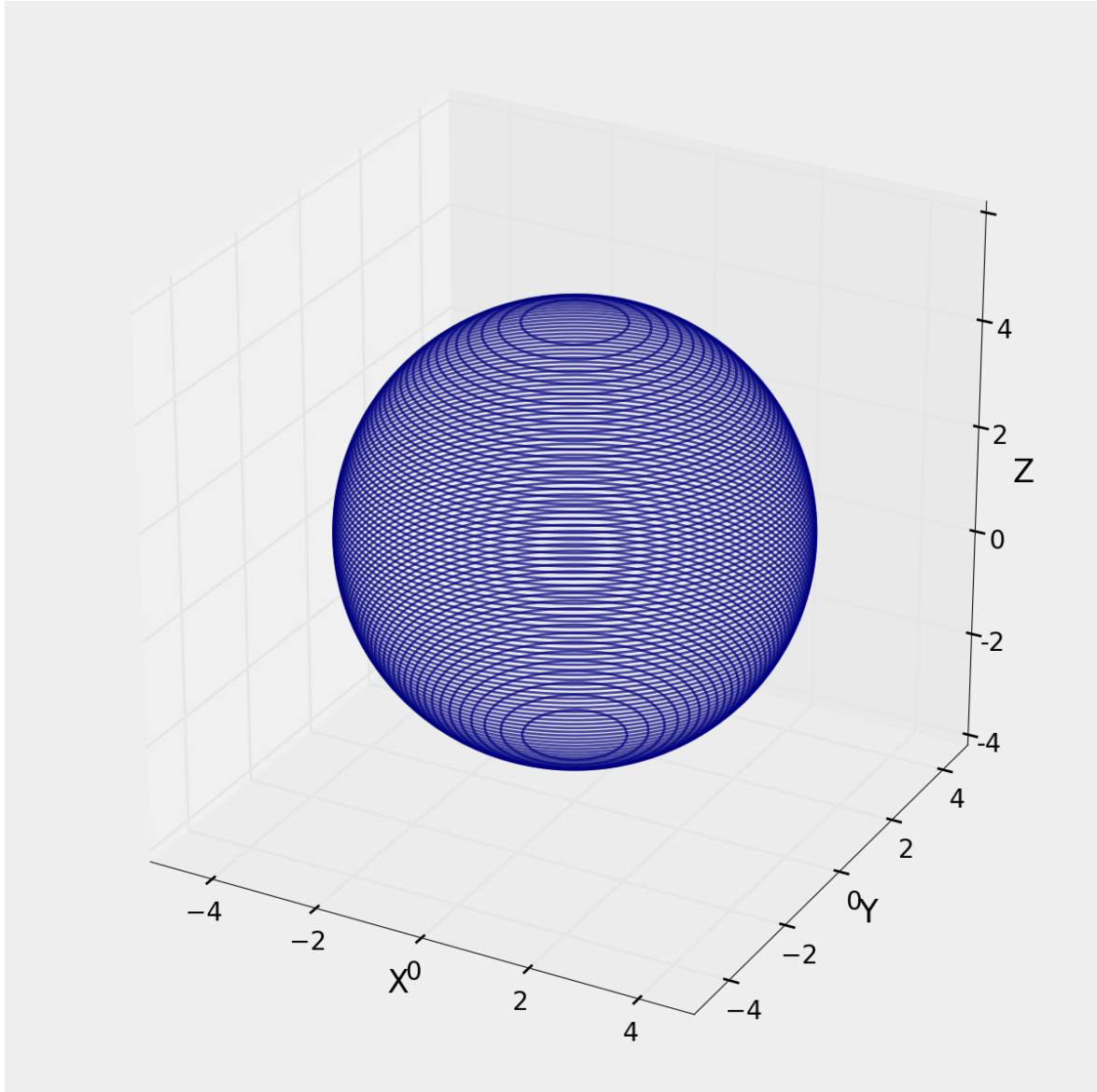


Figure 6: An example for an surface resulting from the spherical implicit function (Equation 5). Lines indicate null surface. Radius of the sphere was set to 4.

comes with a large package library. The usage of packages enables the programmer to increase productivity.

Visualization was realized utilizing two *Python* packages. The *matplotlib* package [76] was used for visualization of the reproductive tract and agent display during simulation. It was further used to display the results. In order to produce movies of moving sperms, data was saved in .vtk-files. *Visualization Toolkit* [77] is a visualization systems used by many researchers for three dimensional visualization. In order to visualize the exported vtk files the *Paraview* [78] software was used.

Running the model with large numbers of agents, becomes quickly computationally expensive. Therefore, simulation was parallelized using a bash script, which started simulation processes on different cores simultaneously. Figure 7 shows the simulation work flow.

Five servers were used for simulations. Some characteristic entities of the servers used for simulations are:

- 1 server with 32 CPU cores 2.9 GHz each and 256 GB RAM
- 1 server with 24 CPU cores 3.3 GHz each and 96 GB RAM
- 1 server with 24 CPU cores 3.5 GHz each and 96 GB RAM
- 2 server with 64 CPU cores 2.3 GHz each and 512 GB RAM

With help of the parallel computing it was possible to simulate large numbers of agents. However, using the bash script for parallelization is only possible without agent - agent interactions.

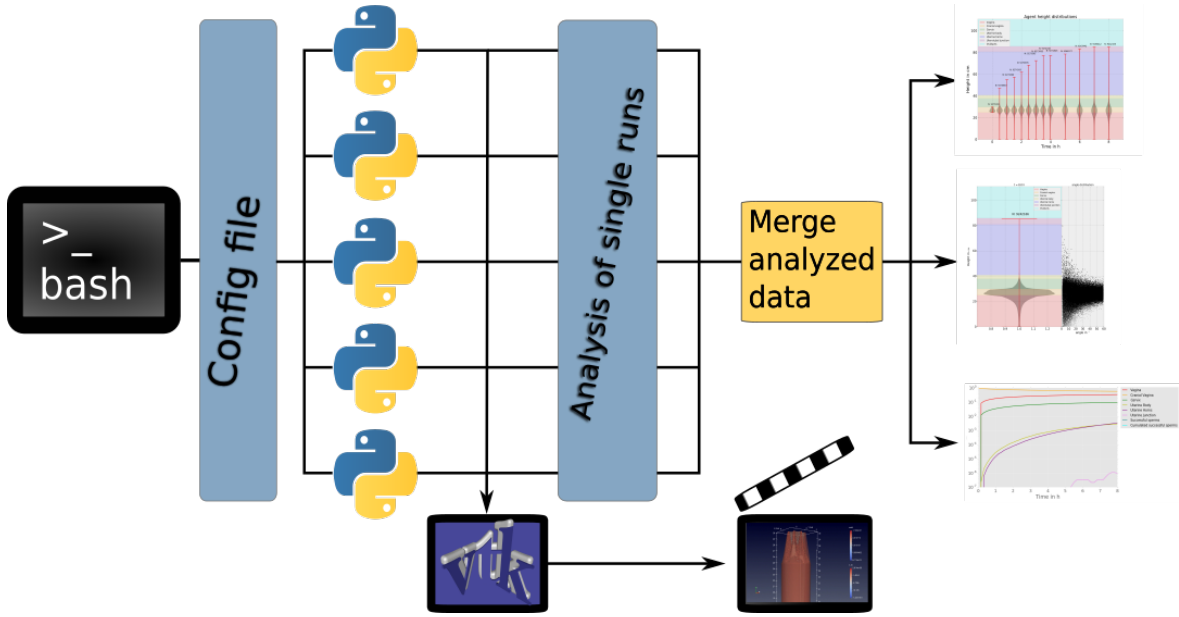


Figure 7: Simulation workflow. The bash script starts *Python* model, supplying the configuration file. The configuration file holds the simulation parameters. During simulation vtk-data can be exported. Later this data can be used to create movies with help of *paraview*. After a simulation results are stored. Due to large output files each run is analyzed individually and files resulting from first analysis are merged. These merged results are then used for further analysis. *Python* logo from [79]. *VTK* logo from [80]

5 Results

The results are divided in three major subsections: i) the modeling of the reproductive tract with implicit functions, ii) the realization of agent's movement and interaction, iii) the simulation results are shown.

5.1 Mathematical description of the female reproductive tract

In order to restrict the agents to a certain volume, a boundary ought to be defined which hinders the agent's progression. In case of sperms, this volume would be the female reproductive tract and consequently the boundary would be the epithelium. In order to approximate the shape of the bovine reproductive tract, a set of three dimensional implicit functions was chosen to describe specified regions. All used equations can be classified as variations of cylindrical or conical functions. Given an agent's position they return a value. If this value is below zero, the agent is defined to be inside the reproductive tract, otherwise (i.e. the value is zero or above) the agent is outside (Section 4.2). By this, the whole reproductive tract was described as a comprehensive entity. Which function to use is defined by the z - position of an agent, along the length of the reproductive tract. The functions describing each part of the tract are therefore "stacked" along the tract axis (result shown in Figure 8).

We divided the reproductive tract in seven different compartments, namely:

- The vagina
- The cranial vagina
- The cervix
- The uterine body
- The uterine horns
- The uterotubal junction (UTJ)
- The oviducts

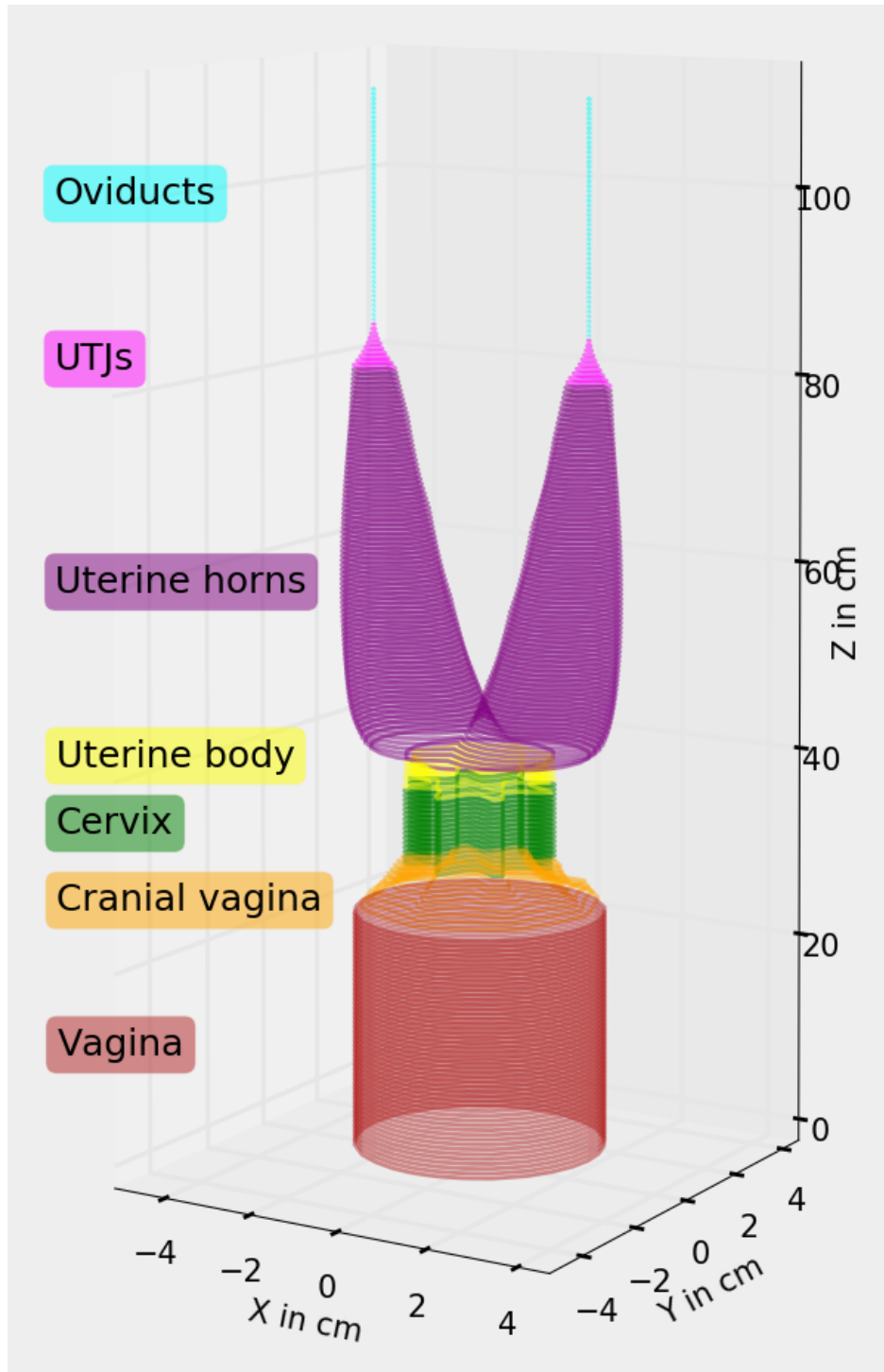


Figure 8: The reproductive tract was assembled out of seven compartments. Evaluated at different heights the lines indicate the implicit surface of the reproductive tract. The reproductive tract results from several implicit functions, stacked on top of each other in z - direction.

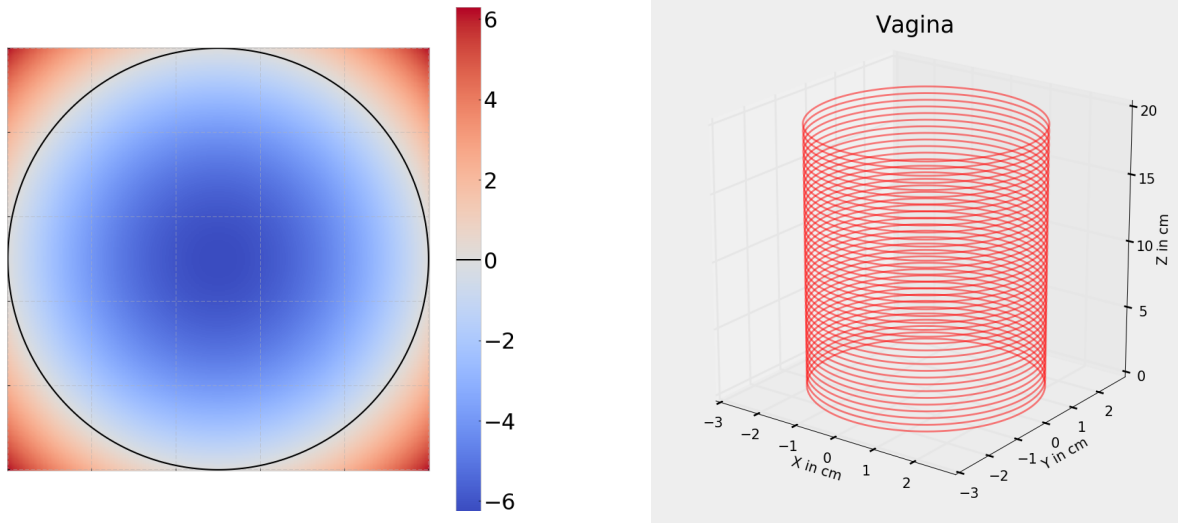


Figure 9: The vagina compartment. Left: Cross section of vagina compartment. Color indicates return value of equation 6. Negative values define the interior of the compartment. Line indicates null-cline, as seen in the color bar. Right: Three dimensional representation of bovine vagina. Lines indicate null-clines. Consequently, everything inside the shown cylinder lies inside the vagina compartment.

The z - offset of each compartment is derived from the cumulative length of the former compartments. In the following, each section and the derivation of implicit function describing its shape will be explained in detail.

5.1.1 Vagina as cylinder

The vagina is described by a cylindrical function, because it does not hold significant folds or changes of the radius.

$$f_v(x, y, z) = x^2 + y^2 - r_v^2 \quad (6)$$

Where r_v is the radius of the vagina. The position of an agent is given by x , y and z - position. The left part of Figure 9 indicates the values returned by this function. Every agent inside the circle is defined as being inside the reproductive tract. Figure 9 shows the implicit surface of the vagina described by equation 6.

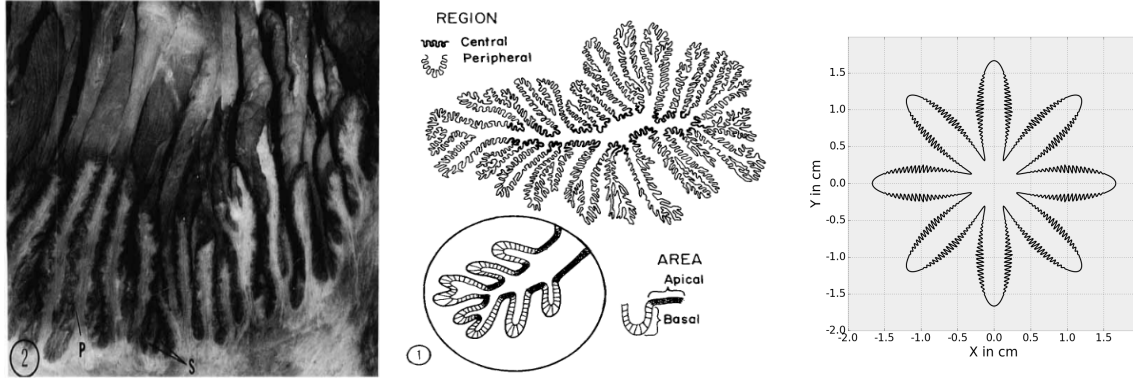


Figure 10: From biology to equation. Left: Cross section of the bovine cervix. Middle: Schematic cervical cross section depicting primary and secondary folds [41]. Right: Null-cline of the implicit function for the cervix cross section (Equation 14).

5.1.2 Cervix, cranial vagina and uterine body

The cervix possesses a far more complex surface than the vagina. It consists of several major and minor grooves, first described by Mullins and Saacke [41] (Figure 10 and Section 3.1.2). Therefore a simple, cylindrical description of the cervix would be insufficient, which is why primary and secondary folds were added. Figure 10 shows the resulting cross section.

First, the primary folds were added by altering the cervix's radius with a cosine in dependence on the angle α to the x-axis in the x, y - plane.

$$f_{cp}(x, y, z) = x^2 + y^2 - (r_c + A_{pf} \cdot \cos(\omega_{pf} \cdot \alpha))^2 \quad (7)$$

$$\alpha = \arccos\left(\frac{x}{d_0}\right) \quad (8)$$

$$d_0 = \sqrt{x^2 + y^2} \quad (9)$$

Where d_0 is the distance to the z - axis, consequently α is the angle to the x - axis in x, y - plane. ω_{pf} is the number of primary folds and A_{pf} is the amplitude of the primary folds. A_{pf} should be smaller than the cervix radius, in order to prohibit overlapping of primary folds.

An example which illustrates the difference between a shape with and without primary folds is shown in Figure 11, using the following parameters.

$$\begin{aligned}
r_c &= 1 \\
A_{pf} &= \frac{2}{3} \\
\omega_{pf} &= 8
\end{aligned}$$

As well as the following example positions of two agents: $\vec{p}_{a1} = (1.5, 0, 30)^T$ and $\vec{p}_{a2} = (0.75, 0.25, 30)^T$.

Using just a cylindrical equation, like equation 6 would yield the values: $f_v(\vec{p}_{a1}) = 1.25$ and $f_v(\vec{p}_{a2}) = -0.375$. So the agent at \vec{p}_{a1} would be outside the cervix, while the agent at \vec{p}_{a2} would be inside. Using equation 7 and the parameters above, this would yield following values: $f_{cp}(\vec{p}_{a1}) \approx -0.53$ and $f_{cp}(\vec{p}_{a2}) \approx 0.43$. Consequently, \vec{p}_{a1} would now be inside and \vec{p}_{a2} outside of the cervix (depicted in Figure 11).

In order to obtain secondary folds, a term depending on the agent's distance to the compartment center (the z - axis) was introduced into the equation. While adding the secondary grooves, caution is needed in order to prevent overlapping of the folds. Therefore, the amplitude of secondary folds (A_{sf}) was decreased with the distance to the cervix radius, so the sine has a descending amplitude (A_{sf_cur}). The distance to the cervix radius is equal to the distance to the middle of the primary grooves. Figure 12 shows by which factor the secondary folds amplitude A_{sf_cur} is decreased, with increasing distance to the middle of the primary folds. Equations 10 to 13 describe how the amplitude of secondary folds change with distance to the middle of the primary folds. d_r is the distance to the middle of the primary folds. The factor by which the secondary fold amplitude should be decreased ($F_{A_{pf}}$) is calculated in equation 11. Finally, the secondary fold amplitude A_{sf} is scaled by $F_{A_{pf}}$ (Equation 10).

$$A_{sf_cur} = A_{sf} \cdot F_{A_{pf}} \quad (10)$$

$$F_{A_{pf}} = \max\left(\frac{k_A \cdot A_{pf} - \|d_r\|}{k_A \cdot A - pf}, 0\right) \quad (11)$$

$$d_r = d_0 - r_c \quad (12)$$

$$d_0 = \sqrt{x^2 + y^2} \quad (13)$$

$F_{A_{pf}}$ is the scaling factor of the secondary fold amplitude (A_{sf}), it decreases with increasing distance to the cervix radius (r_c).

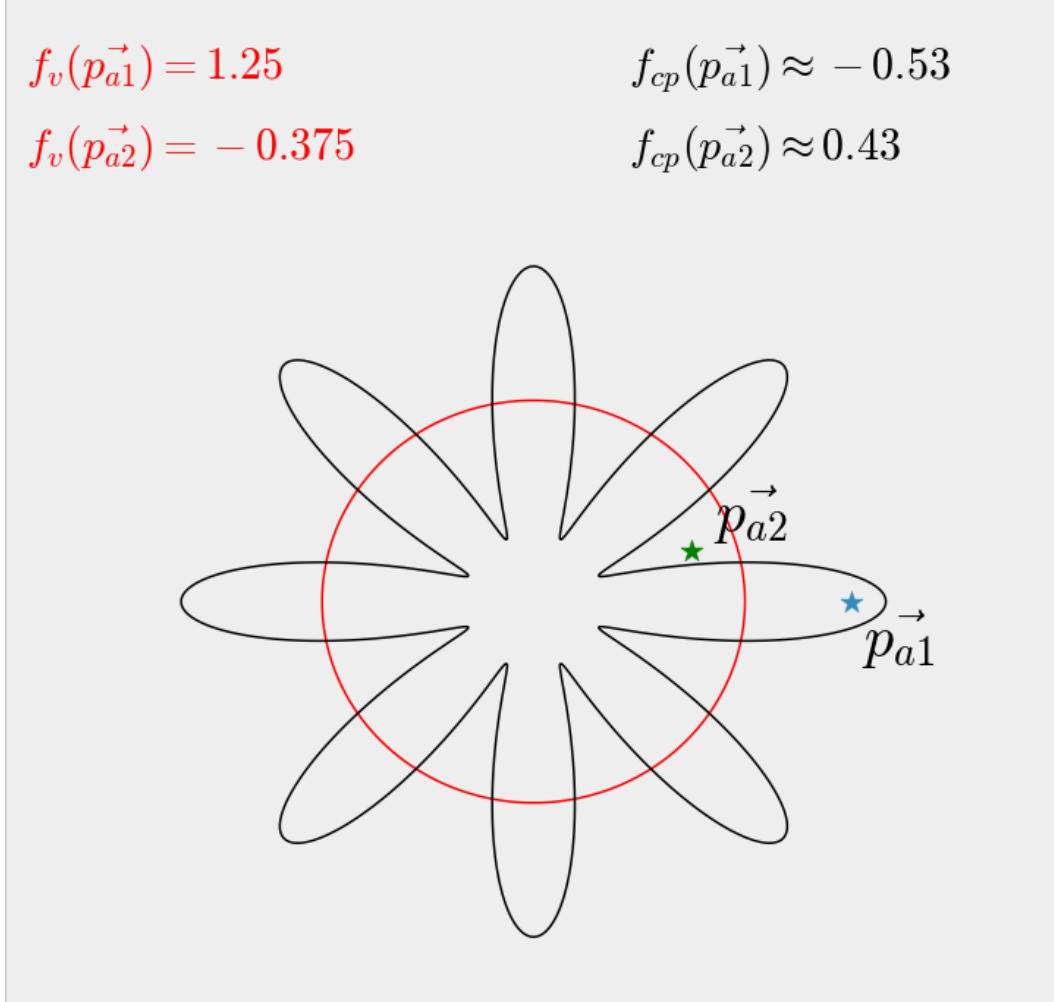


Figure 11: Comparison of cervical cross section with and without primary folds. In a cervix without folds (red) the agent at position p_{a2} would be inside the compartment, having a negative value return by function f_v (Equation 6). Considering primary folds, as described by equation 7 agent at p_{a2} would be outside the cervix. For agent 1 at position p_{a1} the opposit is the case.

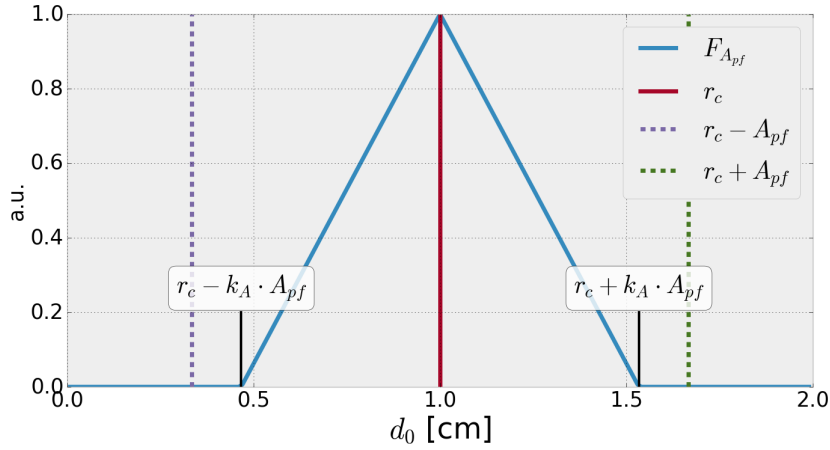


Figure 12: Alteration of the secondary fold amplitude. A_{sf} is scaled by $F_{A_{pf}}$ in equation 10 in order to obtain A_{sf_cur} . The purple and the green dashed lines indicate the inner and outer end of the primary folds, respectively. k_A is a parameter, which constrains the secondary folds to a region, where the primary folds are wide enough to hold secondary folds. This region lies inside the interval $[r - k_A \cdot A_{pf}, r + k_A \cdot A_{pf}]$, indicated by the vertical black lines. Outside this region the scaling factor for the secondary fold amplitude ($F_{A_{pf}}$) is zero (blue line).

The complete equation for the cervix is equation 14, using the description of A_{sf} from equation 10. The term $\frac{d_0 - (r - A_{pf} \cdot k_A)}{A_{pf} \cdot k_A}$ increases from 0 to 2 in the range of $r - k_A \cdot A_{pf}$ to $r + k_A \cdot A_{pf}$. The sine in this region holds ω_{sf} periods and consequently ω_{sf} secondary folds occur. k_A was chosen to be 0.8, so secondary folds do not occur in the peripheries of primary folds (Figure 13).

$$f_c(x, y, z) = x^2 + y^2 - (r_c + A_{pf} \cdot \cos(\omega_{pf} \cdot \alpha) + A_{sf} \cdot \sin(\omega_{sf} \cdot \pi \cdot \frac{d_0 - (r_c - A_{pf} \cdot k_A)}{A_{pf} \cdot k_A}))^2 \quad (14)$$

As mentioned above (Section 5.1) the model contains one compartment between the vagina and the cervix, the cranial vagina. This additional compartment is required to transit from the larger radius and smooth surface of the vagina to the smaller radius and folded surface of the cervix in a defined way. Consequently, a compartment is needed in between which accounts for adapting the radius and introducing folds. The solution is the compartment cranial vagina, described by equation 15.

$$f_{cv}(x, y, z) = x^2 + y^2 - (r_{cur} + A_{pf_cur} \cdot \cos(\omega_{pf} \cdot \alpha) + A_{sf_cur} \cdot \sin(\omega_{sf} \cdot \pi \cdot \frac{d_0 - (r_{cur} - A_{pf_cur} \cdot k_A)}{A_{pf_cur} \cdot k_A}))^2 \quad (15)$$

The radius (r_{cur}), the amplitude of primary (A_{pf_cur}) and the amplitude of secondary

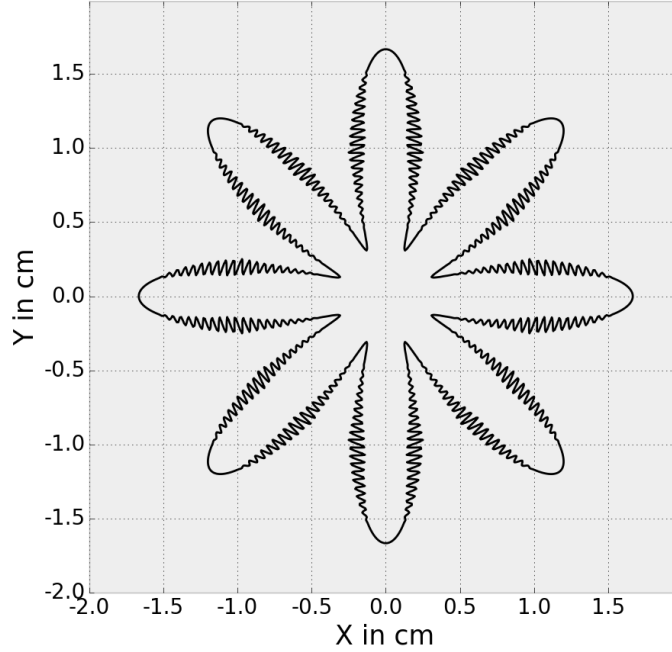


Figure 13: Cross section of cervix described by equation 14. Secondary folds do not occur in the periphery of the primary folds.

folds (A_{sf_cur}) change with z - position. The radius decreases from the vaginal radius r_v to the cervical radius r_c . Primary and secondary folds increase from 0 to their maximal value. A more detailed description is shown in the Appendix (Section A.1). The reduction in radius and the emergence of primary and secondary folds is shown in Figure 14.

Similar to the cranial vagina, the uterine body is a compartment which connects the cervix with a compartment without folds and with another radius (the uterine horns). Therefore, the radius and the fold amplitudes are altered in a very similar way. In this case the radius increases and the amplitudes of primary and secondary fold decrease. A more detailed description is given in the appendix (Section A.1). Equation 16 describes the shape of the uterine body.

$$f_{ub}(x, y, z) = x^2 + y^2 - (r_{cur} + A_{pf_cur} \cdot \cos(\omega_{pf} \cdot \alpha) + A_{sf_cur} \cdot \sin(\omega_{sf} \cdot \pi \frac{d_0 - (r_{cur} - A_{pf_cur} \cdot k_A)}{A_{pf_cur} \cdot k_A}))^2 \quad (16)$$

The shapes of the cranial vagina, the cervix and the uterine body are illustrated in Figure 15.

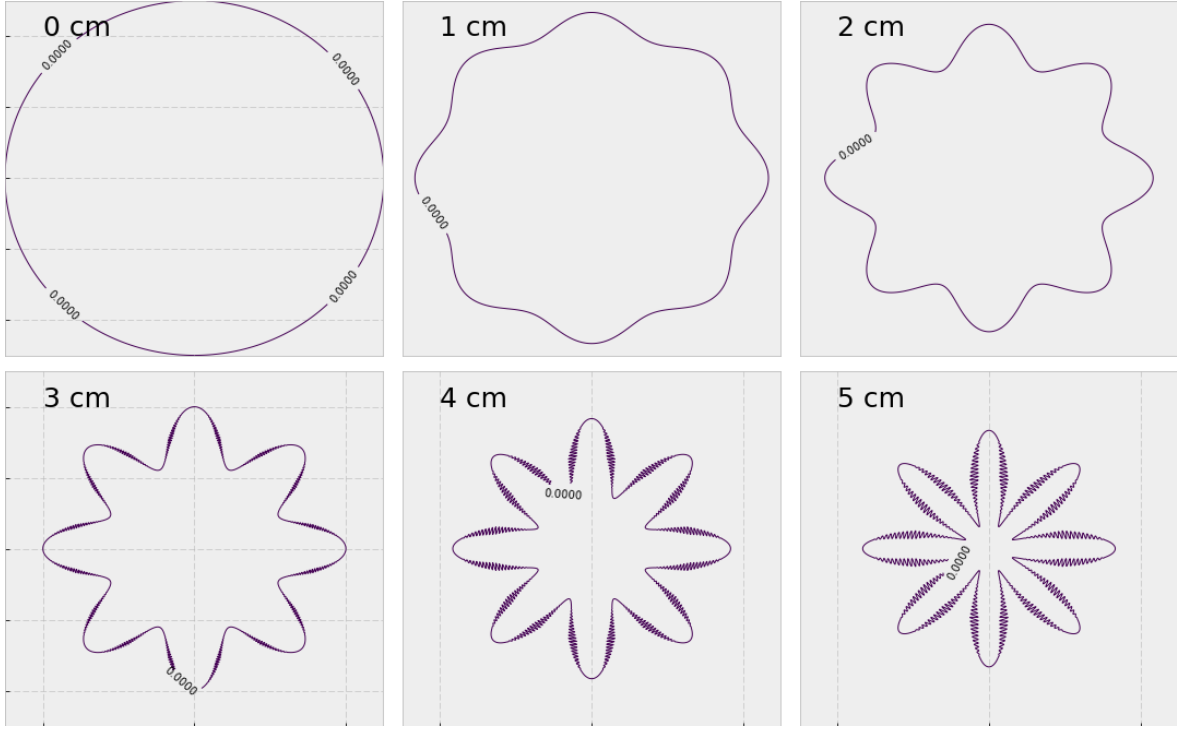


Figure 14: From vagina to cervix. Cross sections at different heights in the cranial vagina. The radius decreases from r_v to r_c . Primary fold amplitude increases with increasing z - position. When primary folds reached a critical size, secondary folds occur (Section A.1).

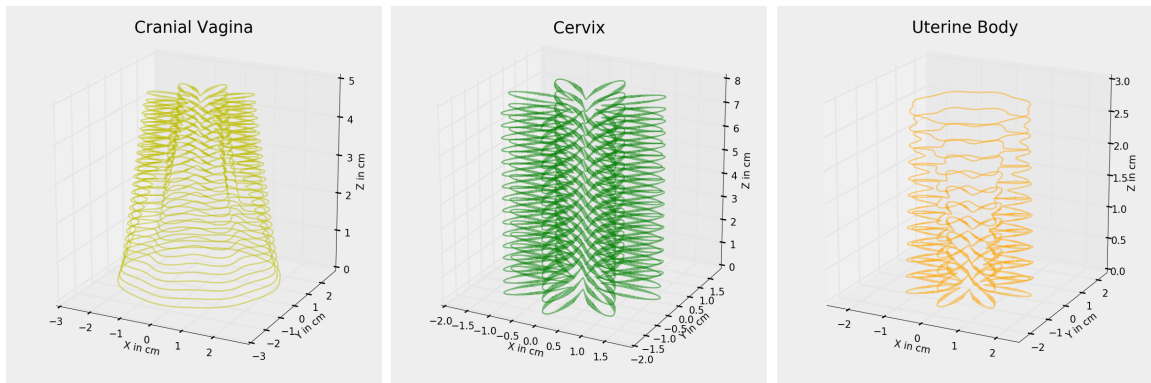


Figure 15: 3D representation of cranial vagina, cervix and uterine body. Lines indicate null-clines. Notice the different scales on the z - axis. All compartments are connected in z - direction in order to describe an enclosed entity.

5.1.3 Uterine horns to oviducts

The uterine body bifurcates into two horns, the uterine horns (Figure 1). The uterine horns need a description, which has one midpoint in the beginning and two in the end. Additionally, the diameter of each uterine horn should decrease. First, two different midpoints in dependence of the z - coordinate were calculated. Initially these midpoints should lay upon each other. As the z - coordinate increases they should drift apart. At a certain value (z_{bif}), the two horns should separate. It does not matter in which direction the midpoints drift as long as they drift apart. The diameter of both horns decreases with increasing z . Equations 17 - 19 show the functions for the uterine horns.

$$f_1(x, y, z) = x^2 + (y - y_m)^2 - r_{cur}^2 \quad (17)$$

$$f_2(x, y, z) = x^2 + (y + y_m)^2 - r_{cur}^2 \quad (18)$$

$$f_{uh}(x, y, z) = \min(f_1, f_2) \quad (19)$$

Here r_{cur} is the radius of each uterine horn in dependence of the z - position, calculated A16. Both uterine horns are described. The first one by equation 17 and the other by equation 18. The minimum of both functions is calculated with equation 19. The minimum corresponds to the union of both horns. Figure 16 shows the shape of the uterine horns compartment.

The midpoints for uterotubal junction and oviducts are calculated in the exact same way. Only the calculation of the radius r_{cur} differs for these compartments (Section A.2). The radius of the uterotubal junction decreases, with increasing z - position. In the oviducts the radius slowly increases again. These compartment are shown in Figures A3, A4 as well as in Figure 8.

On each compartment transition the two adjacent functions are identical. Consequently, the set of equations 6 - 19 and A1 - A10 represents the different compartments as an continuous entity.

5.2 Populating the reproductive tract

In the following, the simulation methodology along with some required technical details are described. The initialization of the sperm entities, their behavioral rules inside the

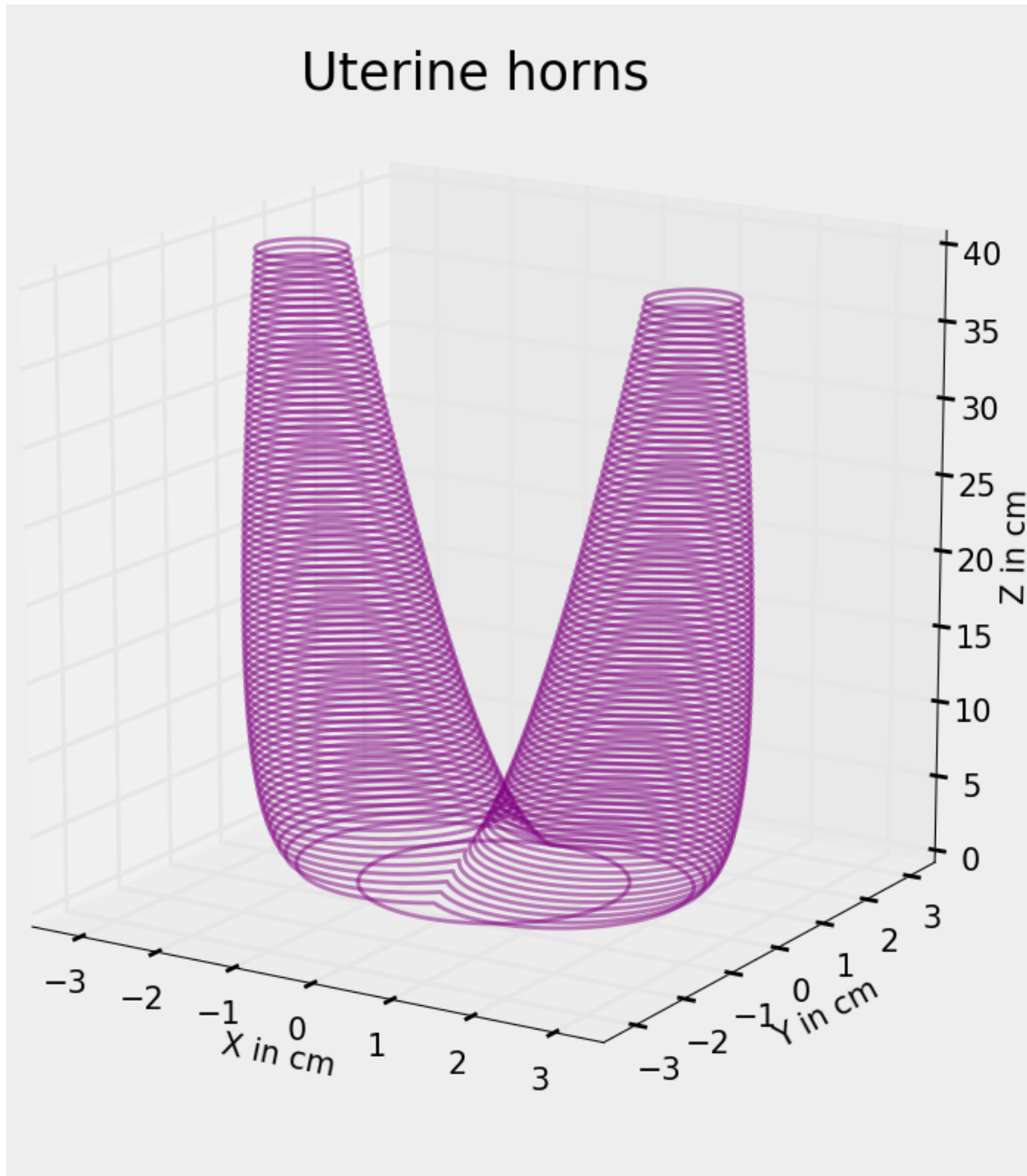


Figure 16: 3D representation of the uterine horns compartment. The compartment is described by equations 17 - 19. The uterus divides as midpoints drift apart.

reproductive tract as well as the tract itself are presented. The entire model was written in one script, holding 4 different classes and several update functions.

One class holds the simulation parameters (Table A1), e.g. how many sperms N should be modeled for which time t_s , which time step dt etc. Another class holds the compartment specific parameters (Table A3). It further holds the functions defining the different compartments, the immune response and the pH change. The third class (S_{pop}) holds general sperm parameters, like the average speed of a sperm population (Table A2). The forth and last class holds the agents. Running a simulation the cranial vagina is populated with sperms, from which those spread through the reproductive tract. When initialized each agent receives its properties, randomly chosen from probability distributions, defined by S_{pop} . Sperm speeds (\bar{s}), length (s_l) and life time (t_l) were chosen from normal distributions, with means and standard deviation shown in Table A2. For a fraction of non-motile agents/sperms ($1 - s_m$) the mean and standard deviations of the speed distribution were divided by hundred and the angle was set to 180° . Consequently, these sperms had a significantly smaller speed and their orientation changed drastically in each time step, rendering them efficiently non-motile. Initial positions (\vec{p}) were uniformly distributed in the cranial vagina compartment. Initial orientations \vec{u} were also distributed in a uniform manner.

5.3 Agents and their movement

The following sections describe how sperms move through the reproductive tract. Most of the sperm attributes are chosen from probability distributions, defined by global population parameters (Table A2). Sperms hold variables which define their interaction with the reproductive tract as well as their movement (Table 2).

5.3.1 Active swimming

In each time step (dt) the sperm positions (\vec{p}) are updated by the sperm orientations vector (\vec{u}) times sperms' current speeds (s_c , equation 20).

$$\vec{p} = \vec{p} + \vec{u} \cdot s_c \cdot dt \quad (20)$$

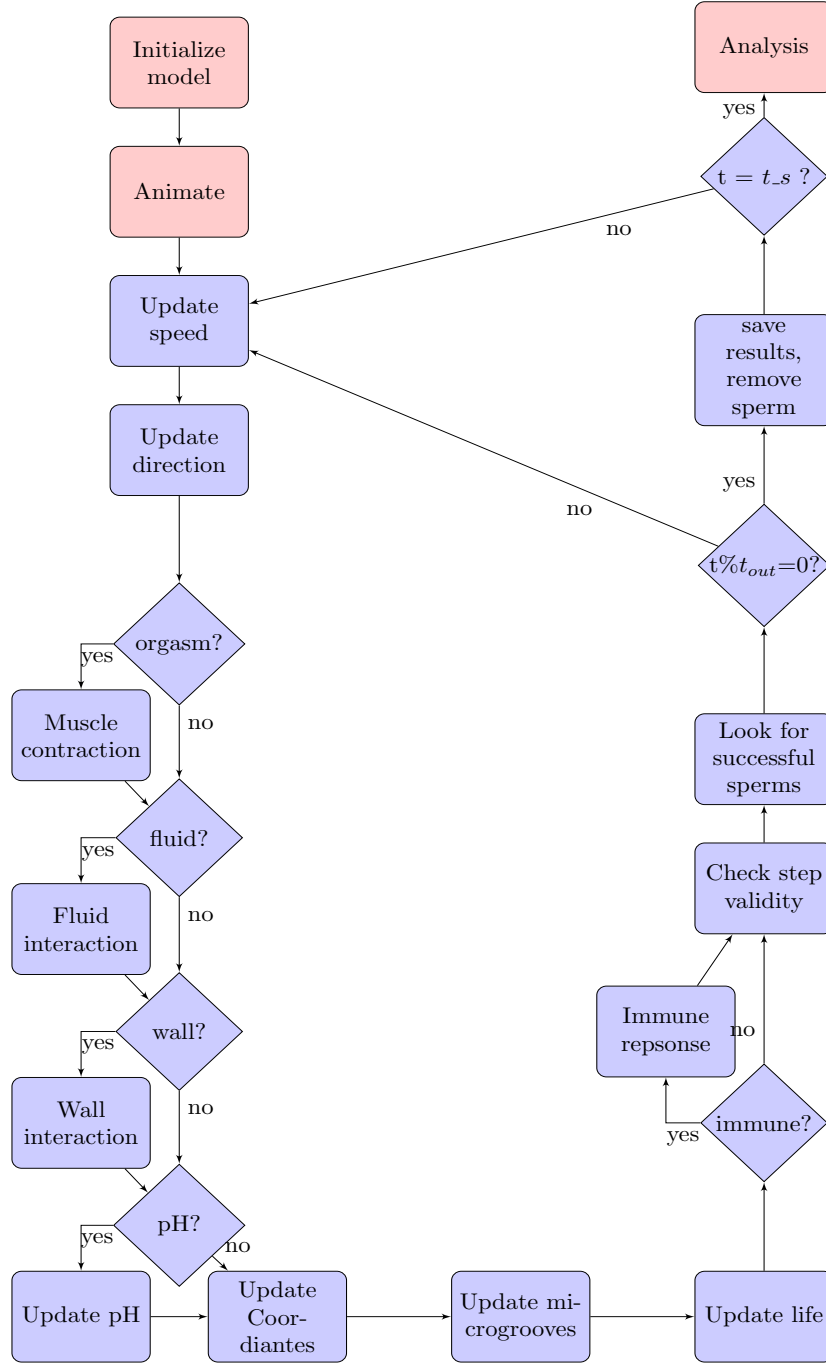


Figure 17: Model structure. First, the model is initialized and animation started. In each time step, speed and direction of sperms are updated. Diamond-shaped tiles indicate decisions. If the relevant Boolean is True muscle contraction, fluid interaction, wall interaction or pH change take place. Coordinates, microgroove state and life are updated in each time step. Immune response occurs if relevant Boolean is True. Validity of position update is evaluated. Successful sperms are recognized. If simulation time modulo t_{out} is zero, the current status of the simulation is saved. If simulation time is over data is saved for analysis.

Table 2: The most important sperm properties. Speed, length and lifetime were drawn from normal distributions with indicated means and standard deviations. Positions, orientations and angles were drawn uniformly from the given intervals. Current speeds and angles as well as fluid properties and the alignment score are calculated (calc.) entities. The motility was defined by a fraction. A fraction of p_{mot} sperms were defined to be motile.

Property	Parameter name	Determined by
speed	\bar{s}	$\mu = \overline{S_{speed}}, \sigma = \overline{S_{speed.sd}}$
length	s_l	$\mu = \overline{S_{length}}, \sigma = \overline{S_{length}}$
lifetime	t_l	$\mu = \overline{S_{lt}}, \sigma = \overline{S_{lt.sd}}$
position	\vec{p}	R^3
orientation	\vec{u}	R^3
angle	γ	$[1, 59]$
current speed	s_c	calc.
current angle	γ_c	calc.
fluid direction	\vec{u}_f	calc.
fluid velocity	s_f	calc.
alignment score	a	calc.
motility	s_m	p_{mot}

The current speed of a sperm is drawn from a normal distribution, with mean \bar{s} and standard deviation $\bar{s}/S_{speed.\sigma}$ in each time step dt . Before updating the sperm position, which describes the movement through the reproductive tract the orientation of the sperm as well as their current velocity have to be determined.

The orientation vector is drawn randomly from a predefined cone around the sperm's former orientation, prohibiting unphysiological orientation changes. The cone is defined by the sperm's movement angle γ_c with respect to its orientation \vec{u} (Table 2, Figure 26). This process can be considered as a random walk, but is not the only factor which affects the update of sperm orientations. Sperms also align to the wall ([81]) and orient into a fluid flow ([45]).

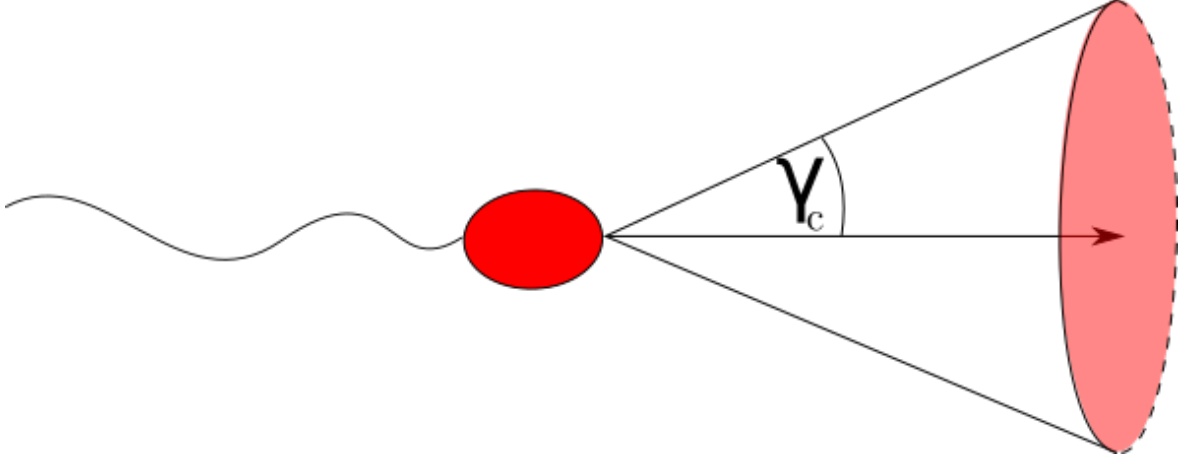


Figure 18: Illustration of sperm orientation update. The cone indicates the feasible space of orientations that can be selected in the next iteration step. Angle γ_c describes the standard deviation of a normal distribution, from which the deflection angle β is chosen.

To choose a new vector out of a cone of feasible directions the orientation vector is deflected \vec{u} by a random angle β , which is chosen from a normal distribution around zero with standard deviation γ_c . In order to choose angle β independently of the time-step, the *Euler-Maruyama method* is applied, resulting in a multiplication of the angle by the square-root of the time-step dt [82][83]. The vector is always deflected in the same direction. That is justifiable, because the resulting deflected vector (\vec{v}) is then turned around its original orientation \vec{u} by a uniformly chosen angle from the interval $[0, 2\pi[$.

5.3.1.1 Vector deflection

As described above (Section 5.3.1) the orientation is always deflected in the same direction, which is away from the z - axis. First the orientation vector \vec{u} is transformed from Cartesian to polar coordinates.

$$\begin{pmatrix} u_x \\ u_y \\ u_z \end{pmatrix} = \begin{pmatrix} r \cdot \sin \theta \cdot \cos \phi \\ r \cdot \sin \theta \cdot \sin \phi \\ r \cdot \cos \theta \end{pmatrix} \quad (21)$$

Where:

$$\theta = \arccos\left(\frac{u_z}{r}\right) \quad (22)$$

$$\phi = \begin{cases} \arccos\left(\frac{u_x}{r \cdot \sin \theta}\right) & , u_y \geq 0 \\ -\arccos\left(\frac{u_x}{r \cdot \sin \theta}\right) & , u_y < 0 \end{cases} \quad (23)$$

with r being the length of the vector, which is 1 because \vec{u} is normalized.

In order to obtain the deflected vector \vec{v} from the sperm orientation \vec{u} by angle $\beta \cdot \sqrt{dt}$, θ was increased by $\beta \cdot \sqrt{dt}$.

$$\begin{pmatrix} v_x \\ v_y \\ v_z \end{pmatrix} = \begin{pmatrix} r \cdot \sin(\theta + \beta \cdot \sqrt{dt}) \cdot \cos(\phi) \\ r \cdot \sin(\theta + \beta \cdot \sqrt{dt}) \cdot \sin(\phi) \\ r \cdot \cos(\theta + \beta \cdot \sqrt{dt}) \end{pmatrix} \quad (24)$$

Equation 24 provides the deflected vector. Subsequently this vector \vec{v} is turned around the former sperm orientation vector \vec{u} .

5.3.1.2 Vector rotation

Rotation matrix R_u turns a vector (e.g. \vec{v}) around an arbitrary axis (e.g. \vec{u}) by angle α . α is uniformly chosen from the interval $[0, 2\pi[$.

$$R_u = \begin{bmatrix} \cos \alpha + u_x^2 \cdot (1 - \cos \alpha) & u_x u_y \cdot (1 - \cos \alpha) - u_z \sin \alpha & u_x u_z \cdot (1 - \cos \alpha) + u_y \sin \alpha \\ u_x u_y \cdot (1 - \cos \alpha) + u_z \sin \alpha & \cos \alpha + u_y^2 \cdot (1 - \cos \alpha) & u_y u_z \cdot (1 - \cos \alpha) - u_x \sin \alpha \\ u_x u_z \cdot (1 - \cos \alpha) - u_y \sin \alpha & u_y u_z \cdot (1 - \cos \alpha) + u_x \sin \alpha & \cos \alpha + u_z^2 \cdot (1 - \cos \alpha) \end{bmatrix} \quad (25)$$

The new orientation is consequently given by equation 26.

$$\vec{u} = R_u \cdot \vec{v} \quad (26)$$

The derivation of the rotation matrix is shown in the Appendix (Section A.4).

5.3.2 Alignment to the epithelium

As argued in Section 3.1.2 sperms can be classified as hydrodynamic pushers, i.e. pushing fluid to the front and to the back, while it is replenished from the sides. Coming close to a wall, the replenishment only takes place from one side and the sperm is pushed and aligned to the wall (Figure 2, [46]).

Having no fluid dynamics in the model, this alignment has to be approximated. In order to align a sperm's orientation to the closest compartment wall, the closest point on the wall as well as the wall's orientation at this point have to be known. This is realized by defining 14 uniformly distributed points around the sperm position \vec{p} . For each of these points it is investigated if it lies inside or outside of the reproductive tract. If a point lies outside of the reproductive tract, the compartment wall is between that point and the sperm. From all vectors which point to the outside, the average vector is calculated and used as the normal vector of a plane. This plane should be approximately parallel to the compartment wall. Afterwards the projection of the sperm orientation on the plane is determined. This projection is used to update the orientation by calculating the average of the projection and the orientation (Figure 19). Figure 19 shows a two dimensional simplification of this process.

5.3.2.1 Choosing verification vectors around the sperm position

The same vectors, covering all spatial directions (Equation 27), are used for each sperm in order to investigate, if the sperm is near a compartment wall. These vectors are named *checking directions* (\vec{cd}).

$$\vec{cd} = \left[\begin{pmatrix} 1 \\ 0 \\ 0 \end{pmatrix} \begin{pmatrix} 0 \\ 1 \\ 0 \end{pmatrix} \begin{pmatrix} 0 \\ 0 \\ 1 \end{pmatrix} \begin{pmatrix} -1 \\ 0 \\ 0 \end{pmatrix} \begin{pmatrix} 0 \\ -1 \\ 0 \end{pmatrix} \begin{pmatrix} 0 \\ 0 \\ -1 \end{pmatrix} \begin{pmatrix} 1 \\ 1 \\ 1 \end{pmatrix} \begin{pmatrix} 1 \\ 1 \\ -1 \end{pmatrix} \begin{pmatrix} 1 \\ -1 \\ 1 \end{pmatrix} \begin{pmatrix} -1 \\ 1 \\ 1 \end{pmatrix} \begin{pmatrix} 1 \\ -1 \\ -1 \end{pmatrix} \begin{pmatrix} -1 \\ 1 \\ -1 \end{pmatrix} \begin{pmatrix} -1 \\ -1 \\ 1 \end{pmatrix} \begin{pmatrix} -1 \\ -1 \\ -1 \end{pmatrix} \right] \quad (27)$$

These vectors are normalized and then scaled by (i) their scalar product with the sperm orientation vector \vec{u} and (ii) with half of the length of the sperm s_l . Scaling with the scalar product of the sperm orientation has an interesting effect. Vectors from the *checking directions*, which point in approximately the same direction as the sperm, become longer than those being nearly perpendicular to the sperm orientation. This gives the sperms an ellipsoidal "sensing" volume (Figures 19 and 20), which depends in the sperm's length s_l . Consequently sperms sense walls in front of them earlier than walls on their sides. Also, the length of the sperm plays a role, since longer sperms begin to align earlier.

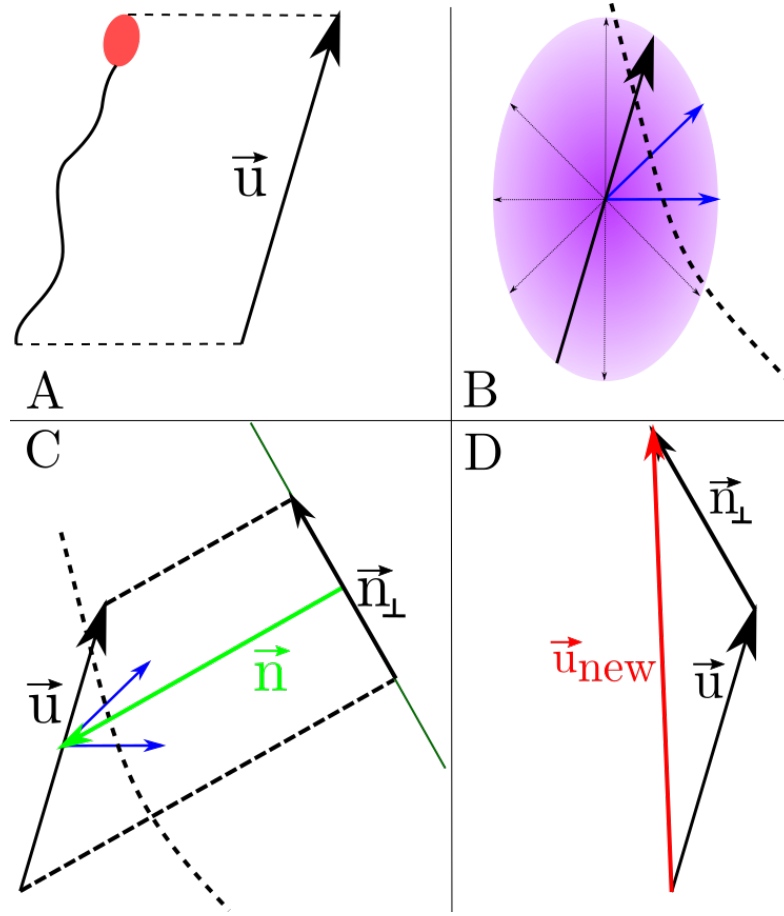


Figure 19: **A:** Sperm orientation is defined by its orientation vector \vec{u} . Vector \vec{u} has the length 1. **B:** The *checking directions* are scaled by the scalar product of themselves with the sperm orientation vector \vec{u} . The solid black vector indicates sperm orientation. Smaller black and blue arrows indicate the scaled *checking directions*. The scaling provokes an ellipsoidal shape, indicated by the magenta colored ellipse. The dashed black line mimics a compartment wall. The two blue colored arrows, point outside the compartment and are characterized as *outliers*. The magenta colored ellipse corresponds to the ellipsoid in Figure 20. **C:** The average of the *outliers* defines the normal vector of a plane. *Outliers* are shown in blue. Sperm orientation as solid black arrow with label \vec{u} . Green arrow indicates resulting normal vector \vec{n} . For representational reason it was inverted and enlarged. This normal vector describes a plane, shown in dark green. \vec{n}_\perp depicts the projection from \vec{u} onto the plane defined by \vec{n} . **D:** The new sperm orientation \vec{u}_{new} vector is shown in red. It results from the sum of the former direction vector and the projection onto the plane. Subsequently the new orientation vector is normalized.

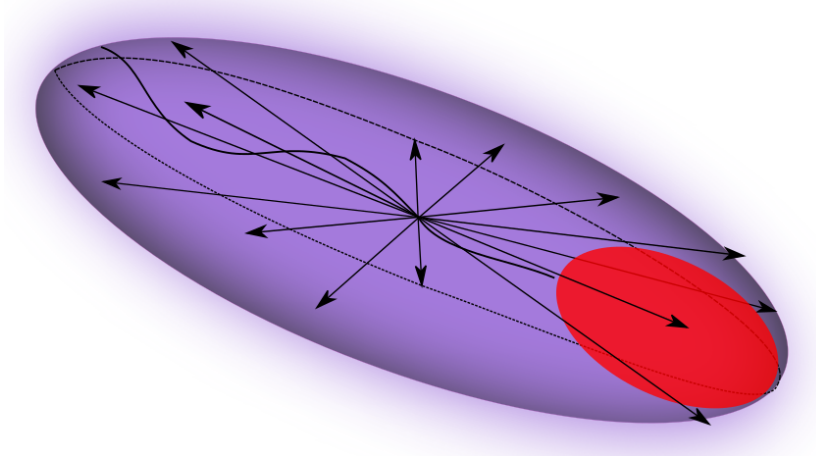


Figure 20: The 14 points resulting from the *checking directions* give the agents an approximately ellipsoidal shape.

5.3.2.2 Find outliers

Each sperm has a set of 14 individual scaled vectors for which it should be checked, whether the sum of each vector with the sperm's position would lie outside the reproductive tract. This is done by adding the sperm position vector \vec{p} to the individual *checking directions*, obtaining a set of *checking positions* around the sperm. For each of these positions the return value of the compartment function (described in equations 6 - 19 and A1 - A10, according to the position's z-value) is calculated and thus positions, which are outside the reproductive tract, are identified. The corresponding vectors (the *checking directions* to the *checking positions*) are termed *outliers*. These *outliers* are now averaged and normalized. The resulting vector (\vec{n}) is used as the normal vector of a plane, which is approximately parallel to the compartment wall (Figure 19). The next step is to calculate the projection (\vec{n}_{\perp}) of the sperm's orientation on this plane (Equation 28).

$$\vec{n}_{\perp} = \vec{u} - \vec{n} \cdot (\vec{n} \cdot \vec{u}) \quad (28)$$

The new sperm orientation is calculated by the sum of the former orientation vector \vec{u} and the projection \vec{n}_{\perp} , scaled by the time step dt (Equation 29).

$$\vec{u} = \vec{u} + \vec{n}_{\perp} \cdot dt \quad (29)$$

Before the orientation \vec{u} is updated, the sperm's alignment score a is calculated by

the scalar product of the sperm orientation and the projection on the wall:

$$a = \vec{u}_s \cdot \vec{n}_\perp \quad (30)$$

This alignment score a defines the angle γ_c , which is used as standard deviation for the random deflection (Section 5.3.1.1), by equation 31.

$$\gamma_c = \gamma \cdot e^{-\frac{S_{ar}}{a}} \quad (31)$$

S_{ar} is a global parameter (Table A2). Sperms aligned to a wall are deflected by a smaller angle. This increases the chance to swim parallel to the surface, which mimics the decreased angle expected from a hydrodynamic pusher near a wall (Section 3.1.2).

5.3.3 Reaction to fluid flow

As mentioned in Section 3.1.2, smooth fluid flows exist within the cervix [41] exist. Sperms tend to align into fluid flows of a certain velocity (Section 3.1.2). The following section describes how the direction and velocity of the fluid flow is approximated in vagina, cranial vagina, cervix and uterine body.

5.3.3.1 Approximation of fluid flow

Each compartment possessing a fluid flow holds a function for calculating fluid direction \vec{u}_f and speed s_f . The speed of fluid declines along the compartment radius with increasing distance to the compartment center, the z - axis. The flow direction in vagina and cervix points down the z -axis, having cylindrical and cylindrical-like shape. Fluid directions in cranial vagina and uterine body were more difficult to approximate, due to the conical shape, primary- and secondary folds. For simplicity, secondary folds were neglected for fluid direction approximation. Being of conical shape, both cranial vagina and uterine body can be extrapolated to a center (or tip). These center points are not part of the mathematically described reproductive tract, because they lie below and above the z -intercept for the uterine body and cranial vagina, respectively. Nevertheless, they can be calculated with help of the second intercept theorem, if secondary folds are neglected.

The right picture in Figure 21 shows the lines needed for the calculation of the center of cranial vagina. The midpoint in x, y - plane is $(0, 0)$. So only the z - coordinate of

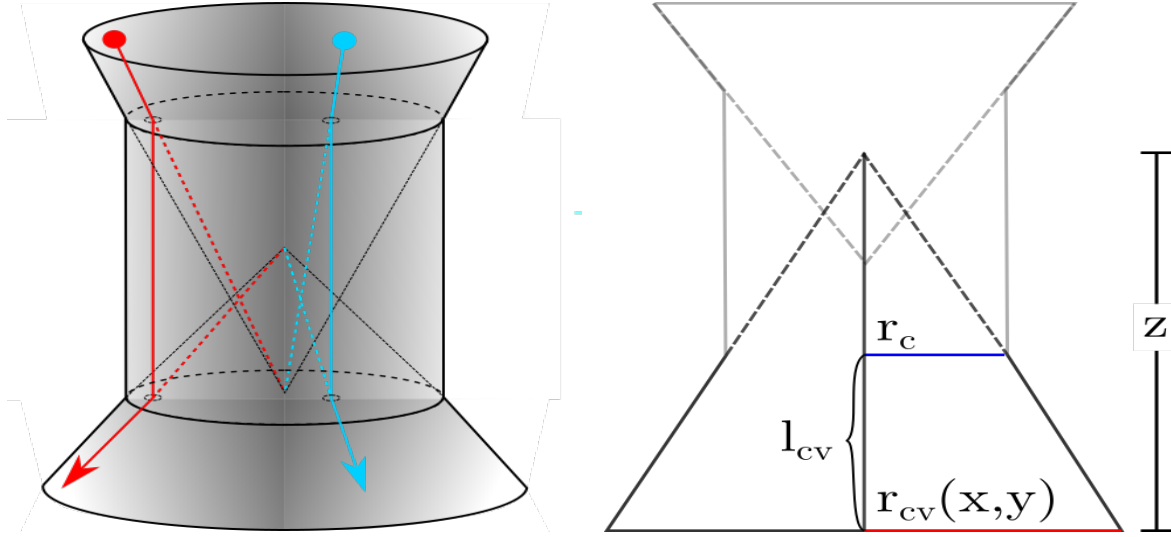


Figure 21: Fluid flow approximation. Left: 3D - sketch of uterine body, cervix and cranial vagina (from top to bottom). The red and cyan solid lines indicate the fluid directions. The colored dashed lines show how the fluid flow is approximated. Being in the uterine body, the fluid flow is directed towards the compartment tip. In the cervix the fluid direction is parallel to the z - axis. In the cranial vagina, the fluid direction points away from the compartment center/tip. Shading indicates the fluid velocity, being maximal in the compartment center and declining towards the periphery. The solid colored lines show the final fluid flow through the 3 compartments. Right: 2D sketch of the compartments, indicating how the tip of the cranial vagina is calculated. Via the second intercept theorem z_{center} can be derived from $r_c(x, y)$, r_v and l_{cv} (Equation 32).

the center (z_{center}) has to be calculated. The second intercept theorem yields equation 32, with the requirement that $r_c(\alpha)$ is strictly smaller than r_v . This requirement is fulfilled by the used parameter set (Table A3).

$$\frac{r_v}{r_c(\alpha)} = \frac{z_{center}}{z_{center} - l_{cv}} \quad (32)$$

$$r_c(\alpha) = r_c + A_{pf} \cdot \cos(\omega_{sf}\alpha) \quad (33)$$

α is defined by equation A7. After some transformation z_{center} is given by:

$$z_{center} = \frac{R_i \cdot l_{cv}}{R_i - 1} \quad (34)$$

$$R_i = \frac{r_v}{r_{cv}(\alpha)} \quad (35)$$

The surrounding fluid flow is an agent attribute and always calculated at the agent positions. Having an agent in the cranial vagina, the fluid direction is described such that the fluid flows from the compartment center (\vec{c}) to the agent's position (\vec{p}).

The fluid direction is consequently calculated by $\vec{u}_f = \vec{p} - \vec{c}$. z_{center} is the distance from the z - offset of cranial vagina (z_{cv}) to its center. The position of the center, regarding the whole reproductive tract, is therefore $\vec{c} = (0, 0, z_{cv} + z_{center})^T$. The fluid flow direction is then given by:

$$\vec{u}_f = \vec{p} - \vec{c} \quad (36)$$

$$= (x_a, y_a, z_a - z_{cv} - z_{center})^T \quad (37)$$

With x_a , y_a and z_a being the coordinates of the agent. The fluid direction vector is then normalized, because it's length is later defined by the fluid speed. In the uterine body calculation of the compartment center and therefore calculation of the fluid flow becomes slightly more complicated, but the principle remains the same (Section A.3). Figure 21, indicates the fluid direction in the uterine body, cervix and cranial vagina.

The velocity of the fluid flow depends on the agent's distance to the compartment center (Equation 38, Figure 22) and on the cervix radius (r_c , for cranial vagina, cervix and uterine body) or the vagina radius (r_v , for vagina), respectively. This implementation yields a maximal fluid velocity in the middle of the compartment and a decreasing velocity towards the compartment peripheries.

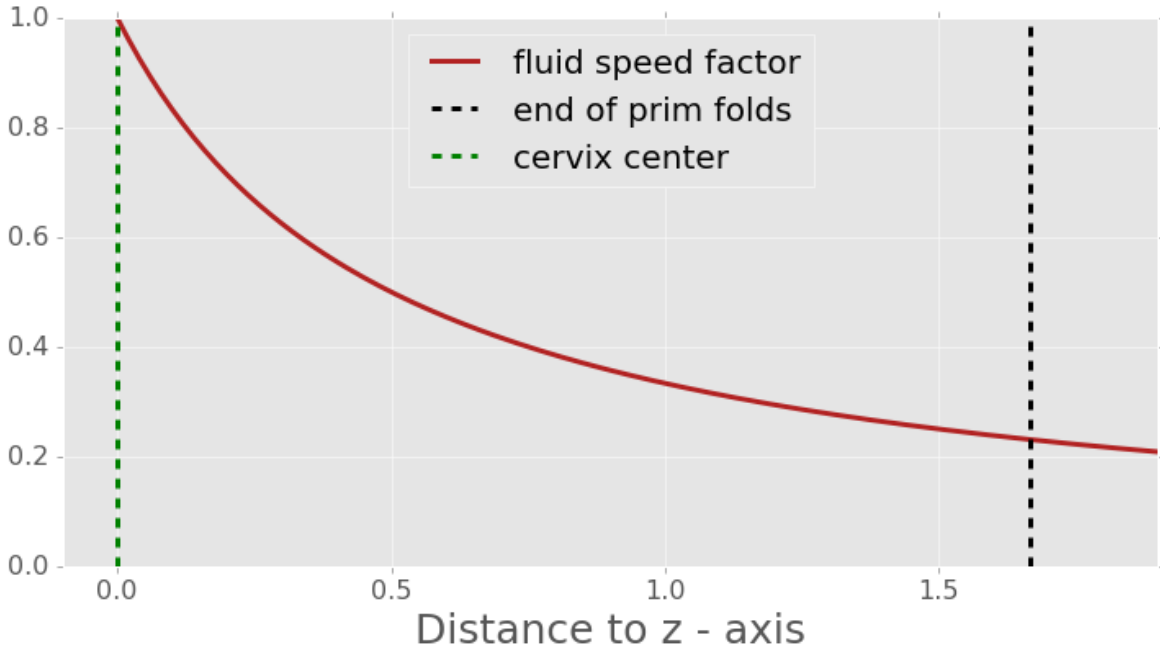


Figure 22: Fluid speed scaling factor in dependence of distance to center of the cervix.

Described the fraction in equation 38. Where S_{fluid} is the maximal fluid speed at the z - axis.

$$\vec{s}_f = \frac{0.5 \cdot r}{0.5 \cdot r + d_0} \cdot S_{fluid} \quad (38)$$

with S_{fluid} being the maximal fluid speed (Table A3) and d_0 being the euclidean distance to the z - axis (Equation A9). The decline of the fluid speed with increasing distance to the z - axis is depicted in Figure 22.

5.3.3.2 Orientation into fluid flow

Exposed to the fluid flow, sperms undergo positive rheotaxis. In the model, the sperms hold all, the variables for their orientation (\vec{u}), for the fluid direction (\vec{u}_f) as well as the corresponding speeds (\bar{s} and s_f). The faster a sperm, the faster it should orient itself into the flow, because more collision events with the fluid molecules occur with increased speed. In addition, the faster the fluid, the faster sperm should align, for the same reason. Therefore, sperm orientation is updated by equation 39.

$$\vec{u} = \vec{u} \cdot \frac{\overline{S_{speed}}}{s} - \vec{u}_f \cdot \frac{s_f}{S_{fluid}} \quad (39)$$

with $\overline{S_{speed}}$ being the mean of the standard deviations of speed over the sperm population.

5.3.4 Muscle contractions

Muscle contractions, for example following an orgasm, are hypothesized to assist sperm migration (Section 3.1.3). They were modelled by a sperm displacement in z - direction. In each time-step (dt), this displacement took place with declining probability. The probability of a muscle contraction declines with equation 40:

$$P_{org} = \left(1 - \frac{t^{n_{org}}}{t_{org}^{n_{org}} + t^{n_{org}}}\right) \cdot P_{org_max} \cdot \sqrt{dt} \quad (40)$$

P_{org_max} is the maximal contraction probability, t_{org} is the time of half-maximal P_{org_max} and n_{org} is the Hill coefficient of the probability decline. To avoid time-step dependence the probability is scaled with \sqrt{dt} (*Euler Maruyama method*)[82].

If a muscle contraction takes place, a random z - position inside the cranial vagina is chosen. All sperms in an interval contraction center (c_{center}) are displaced by a number chosen from a normal distribution with mean $\overline{cw_{org}}$ and a standard deviation of cw_{org_sd} .

5.3.5 Modeling of pH and immune system

The vaginal pH and the immune response are modeled as time-dependent deterministic functions. The vaginal pH reduces the speed of sperms located inside the vagina (Section 3.1.1). The response of sperm motility in dependence on pH is sigmoidal [84] and after insemination pH decreases, in the model from 7.5 to around 4.5 (Equation 41). In dependence of equation 42 the pH defines the current speed s_c of the sperms in the vagina and the cranial vagina.

$$pH = pH_v + (pH_s - pH_v) \cdot e^{\frac{-t}{\lambda_{pH}}} \quad (41)$$

$$\gamma_c = \gamma_c \cdot \frac{pH^{n_{pH}}}{Km_{pH}^{n_{pH}} + pH^{n_{pH}}} \quad (42)$$

where λ_{pH} defines the rate of pH decrease.

The invasion of neutrophilic granulocytes into the reproductive tract is a response to semen deposition during the first hours after insemination [85]. In the model this immune response is represented by an accelerated decrease in the sperm's life time t_l . The immune response takes place in all compartments, except for the oviducts. The

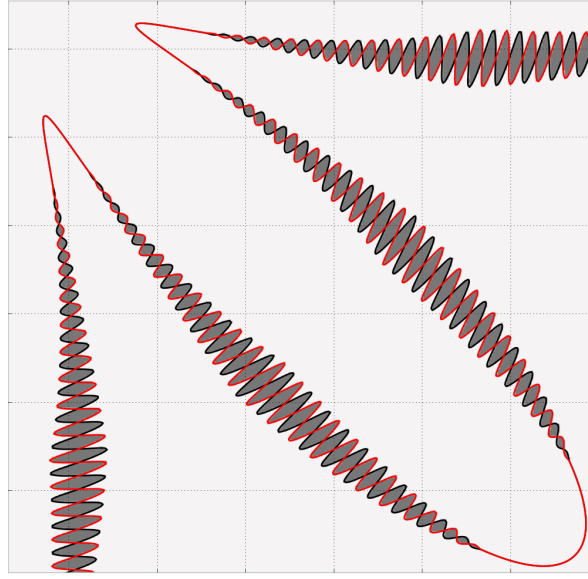


Figure 23: Identification of microgrooves. Black and red lines show cervix cross section with original and inverted secondary folds. Shaded regions are defined as microgrooves.

level of immune response (IR) is described by equation 43 and the life time t_l decreased by equation 44, where C_{is} is the strength of the immune response.

$$IR = \frac{t^{n_{IR}}}{Km_{IR}^{n_{IR}} + t^{n_{IR}}} \quad (43)$$

$$t_l = t_l - IR \cdot C_{is} \cdot dt \quad (44)$$

5.3.6 Environment of the microgrooves

Sperms located in microgrooves are most likely protected from the immune response [41]. The additional life time (t_l) reduction (equation 44) is therefore only applied to sperms not located in a microgroove. It is difficult to describe the region of microgrooves analytically. Therefore, the compartment region belonging to the microgrooves was described by inverting the secondary fold amplitude A_{sf} . Sperms which are located outside this "inverted" reproductive tract are considered to be in a microgroove (Figure 23).

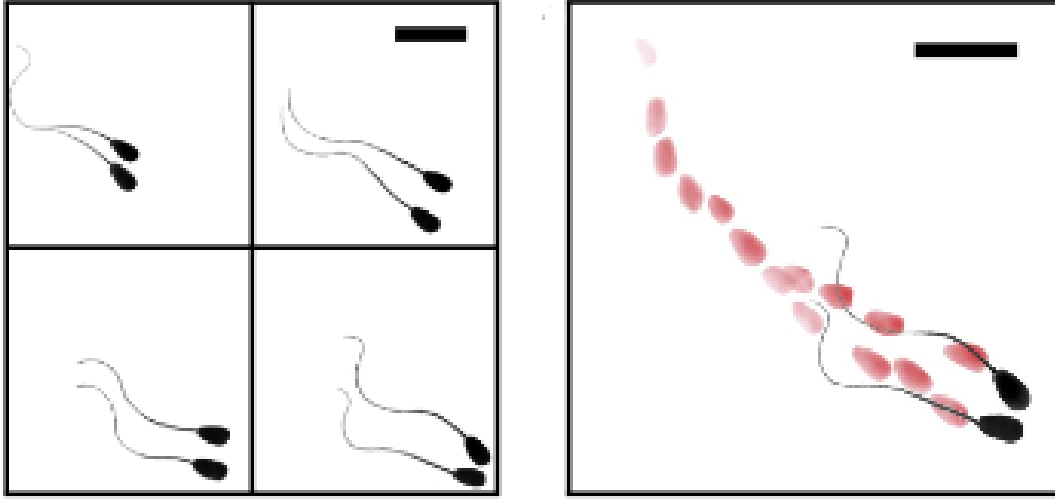


Figure 24: Bull sperms synchronize their movement. Scale bars are $20\mu m$ long. Left: Sequence showing adaptation of beating frequency and flagellar waveform. Right: Overlaid trajectories. Figure adapted from reference [81].

5.3.7 Interaction with neighbors

TIRF (Total internal reflection fluorescence) microscopy has been used to image swimming trajectories of bull sperm [81]. It was shown that bull sperms tend to synchronize their flagellar beating frequency as well as their flagellar waveform (Figure 24), when they come close to each other.

To model interactions between sperms, the k closest neighbors of each sperm ought to be found. To do so, the KDTree (k dimensional tree) algorithm [86] is used. It splits the data along the dimension medians into cubes until the cubes hold k neighbors. Only for these neighbors the distance is calculated. In *Python* this algorithm is already implemented in the *scipy* package [87]. According to the distance a score is calculated, which defines the strength of the influence the neighbors have on each other (Equation 45).

$$F_{int} = \frac{k_d^{n_d}}{k_d^{n_d} + D^{n_d}} \quad (45)$$

where F_{int} is the interaction strength, D the distance to the neighbor, k_d the distance at which F_{int} is half maximal and n_d defines the steepness of the response curve.

Depending on this interaction strength, the weighted average of the neighbor's orientations was calculated, which was used to update the sperm's orientation.

5.4 Removing agents

The model does not include the binding to the epithelium in the oviducts, capacitation or the movement from the sperm storage site to the oocyte (Section 3.1.5). Sperms which reached one of the oviducts are therefore termed as *successful* and removed from the simulation, decreasing the number of agents and therefore increasing simulation speed. Sperms are also removed from the simulation if their lifetime or their z - position becomes negative, standing for sperm death and sperm exclusion from the female body, respectively.

5.5 Simulation results

While simulating the model, the interactions (Sections 5.3.2 - 5.3.5) which should be considered can be switched on and off, with help of 5 Boolean parameters.

To test the capabilities of the model and to quantify the effects of the implemented interactions on the sperm success rate, the model was simulated with eleven different parameter settings. Table 3 shows the naming of these model runs, the corresponding parameter setting.

Other parameters can be looked up in tables A1 - A3. Simulation time was set to 8 hours for all runs. For runs *All_True_sF* and *O_False_sF* the parameter for maximal fluid speed s_f was increased from $18 \mu\text{ms}^{-1}$ to $100 \mu\text{ms}^{-1}$. $18 \mu\text{ms}^{-1}$ is the measured fluid speed in mouse oviducts (Section 3.1.2). $100 \mu\text{ms}^{-1}$ was chosen as stronger fluid flow, being in the same order of magnitude as the sperm velocities. The simulation run *no_lin* is a special run. It had the exact same setting as *All_True*, but a modified version of sperm alignment to the wall, in which the sperm alignment has no influence on the deflection angle. This run is further described in the discussion (Section 6).

Figure 25 and table 3 show the percentage of sperms which would reach the oviducts, with indicated parameter sets. In order to present the results, three kinds of graphical representations are used. Those three illustration instruments are first introduced and described for the simulation run *All_False*. Primarily the z - positions of the agents are analyzed, because this the entity depicts how successful a sperm was on its journey through the reproductive tract.

Table 3: Different settings of simulation runs. Parameters starting with B are Boolean switches for pH, immune response, muscle contractions, wall interactions and fluid flows. T is true, F is false. N is the number of simulated agents per parameter setting. N_{suc} is the number of successful sperms and t_f the time point at which the first successful sperm was recognized. P_{suc} is the percentage of successful sperms.

Simulation name	B_{pH}	B_{ir}	B_{org}	B_w	B_f	N [10^6]	N_{suc}	$P_{suc}[\%]$	t_f [min]
<i>All_False</i>	F	F	F	F	F	9.275	0	0	<i>NaN</i>
<i>All_True</i>	T	T	T	T	T	1.95	3489	0.1789	60
<i>F_False</i>	T	T	T	T	F	0.9	50	$5.6 \cdot 10^{-3}$	60
<i>FO_False</i>	T	T	F	T	F	1.95	48	$2.5 \cdot 10^{-3}$	70
<i>W_False</i>	T	T	T	F	T	2.0	0	0	<i>NaN</i>
<i>O_False</i>	T	T	F	T	T	0.95	1643	0.1729	60
<i>pH_False</i>	F	T	T	T	T	1.8	3278	0.1821	60
<i>All_True_sF</i>	T	T	T	T	T	0.95	1548	0.1629	60
<i>O_False_sF</i>	T	T	F	T	T	1.0	1581	0.1581	60
<i>WFO_False</i>	T	T	F	F	F	1.9	0	0	<i>NaN</i>
<i>no_lin</i>	T	T	T	T	T	1.925	1788	0.0929	60

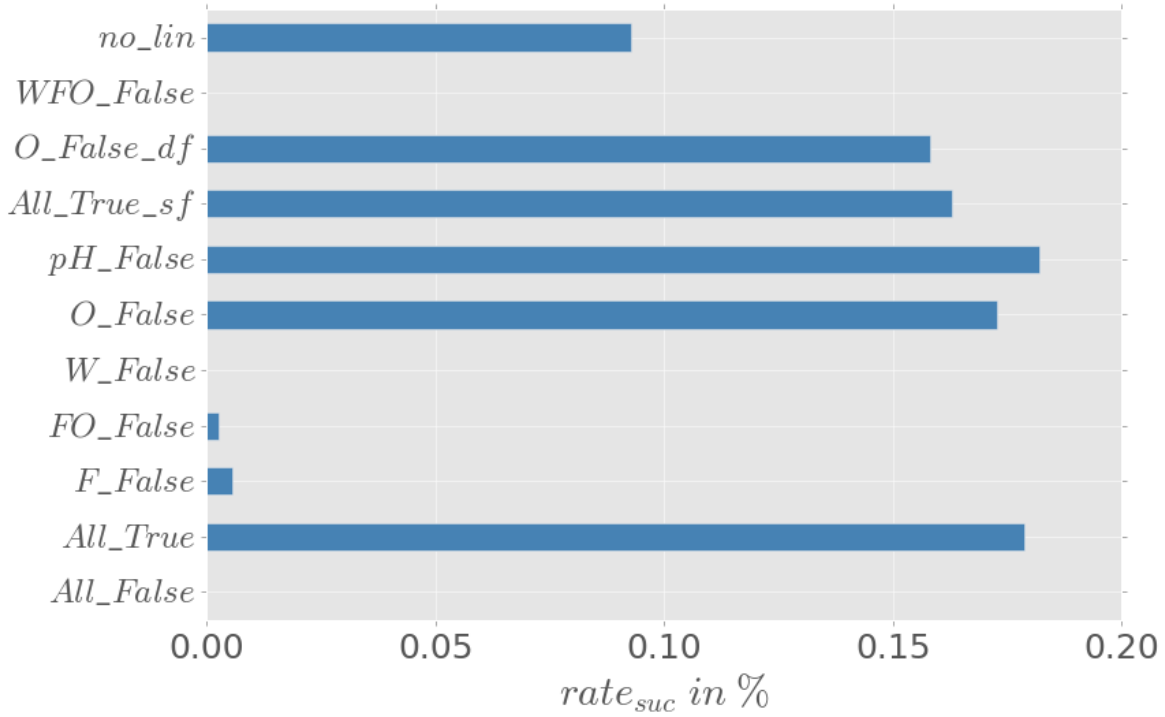


Figure 25: Percentages of sperms which reached the oviduct per simulation setting.

5.5.1 Parameter setting *All_False*

In Figure 26 the time-evolving population densities for simulation run *All_False* are shown. In this simulation the sperm movement was only spatially restricted due to the reproductive tract geometry, without wall alignment, fluid interaction, muscle contraction, pH change and immune response. Sperms spread throughout the reproductive tract, reaching the end of the vagina within 30 minutes. The maximal z - positions continuously increases over time. After 6 hours some sperm manage to reach the uterotubal junction, but they are not able to pass it within the simulation time (Figure 26, Table 3). Within the simulation time approximately 40000 sperms are removed from the system. Figure 27 shows the number of sperms per compartment over time.

The time resolution in Figure 27 is higher than in Figure 26 (10 minutes) and it becomes visible that sperms begin to enter the uterotubal junction after 5 hours and 20 minutes. Another additional information, which can be drawn from Figure 27, is the relative number of sperms located in each compartment. The majority of sperms stays in the cranial vagina that can be seen in both Figures 26 and 27. Approximately every millionth sperm was in the uterotubal junction at the last time point (Figure

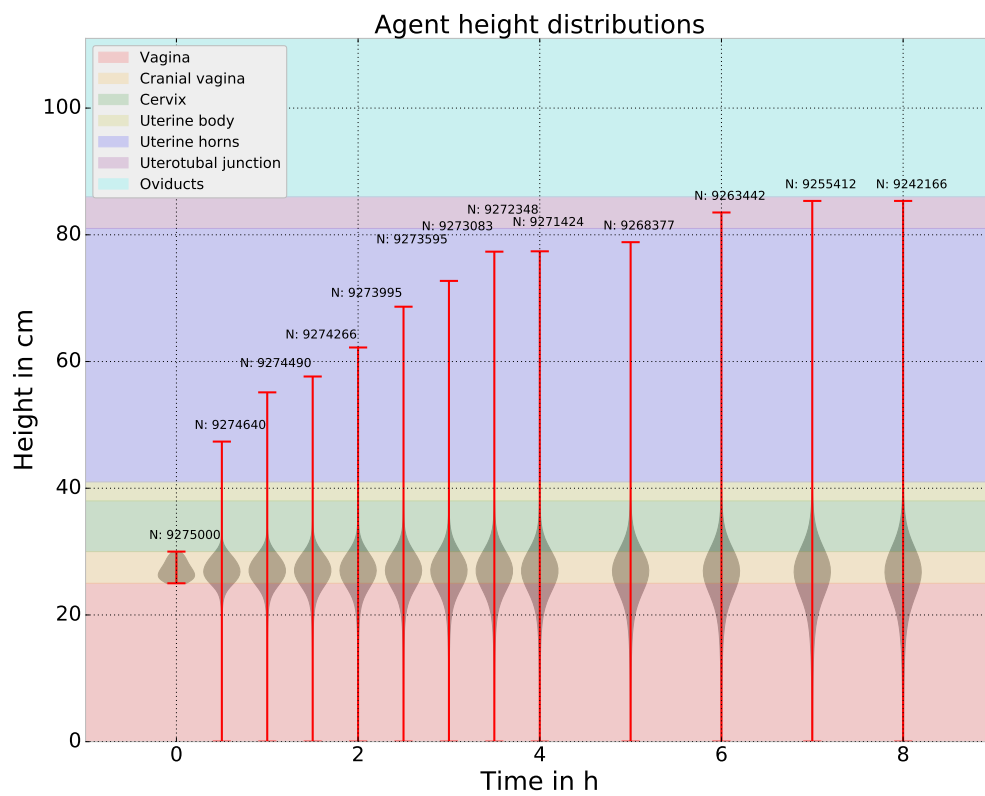


Figure 26: Population propagation over time of run *All_False*. Violins represent density distributions of agent z - positions at several time points. Red whiskers represent minimal and maximal z - position. Number above violin indicates the number of agents in the system. Background color represents the compartment.

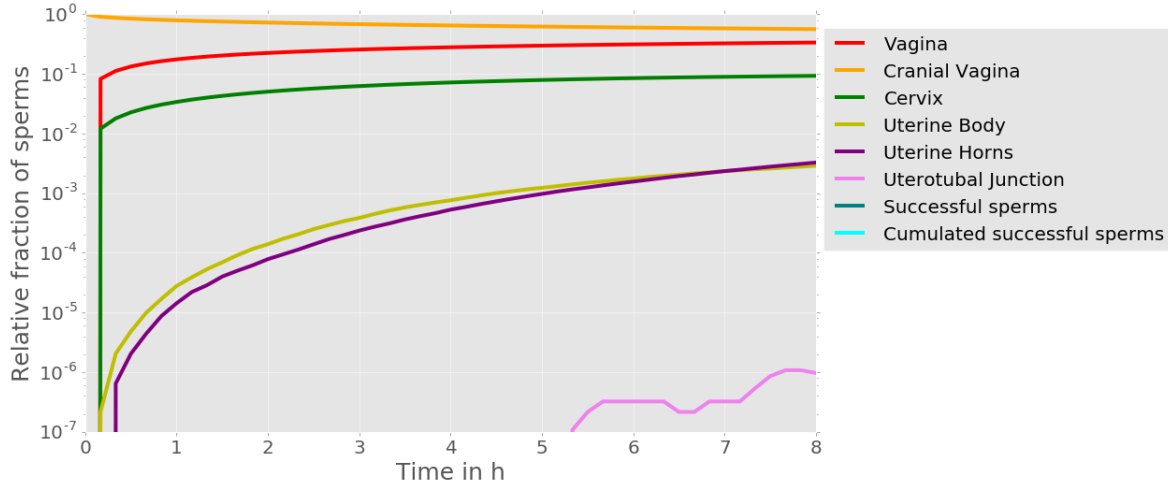


Figure 27: Relative number of sperm per compartment over time with log - scaled y - axis. Relative sperm number means relative to the number of sperm which entered the simulation, not relative to the number of sperm at each time point. Sperm were initially positioned in the cranial vagina. From there they spread through the reproductive tract. After more than 5 hours the first sperm enter the uterotubal junction.

27). A third type of Figure is the sperm height distribution at a certain time point, with additional information about the angles sperm have in dependence of their height (Figure 28).

Initial angles γ were uniformly distributed in the interval from $1 - 59^\circ$ (Table A2). Sperm located in the cranial vagina show angles from the entire interval, while sperm reaching the uterine horns have smaller angles (Figure 28).

5.5.2 Results with fluid flow, orgasm, wall interaction, pH change and immune response

Figure 29 shows the time dependent distribution of sperm for the run *AllTrue*. In this simulation run the sperm were able to align to the compartment wall, interacted with the fluid flow, were potentially displaced by muscle contractions, had to withstand the immune response and were possibly immobilized by the pH change. Two findings attract attention: First, the maximal height of sperm rapidly decreases after 4 hours. Second, sperm reach the oviducts after approximately one hour. Distribution maximum soon shifts into the uterine horns. Also the shape of the distributions varies

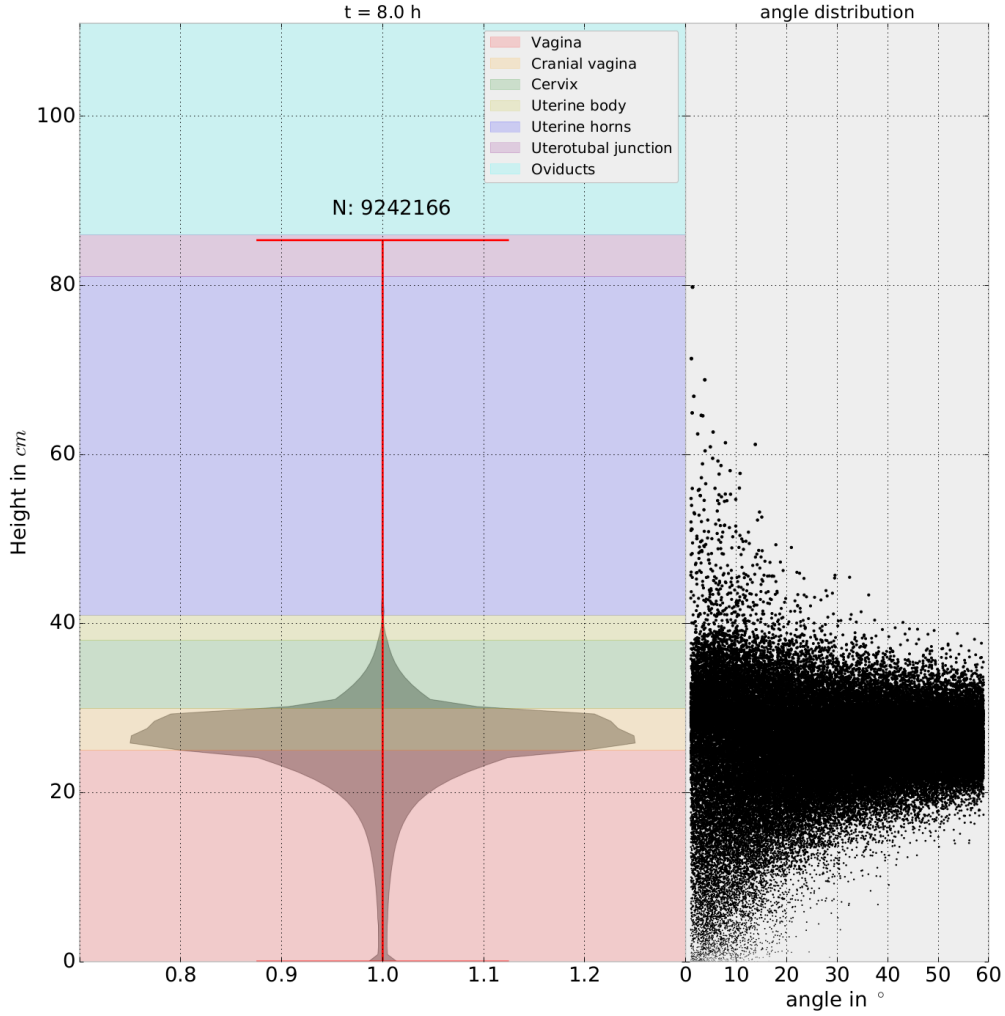


Figure 28: Left: Sperm z - position distribution density of run *All_False* after 8 hours of simulation. N indicates the number of sperms inside the reproductive tract 8 hours after insemination. Right: z - positions in dependence of the sperm angles γ . Due to graphical reasons not all $9.24 \cdot 10^6$ sperm are depicted, but a random subset of 10^5 sperms. Sperms with smaller angles advance further into the reproductive tract. The dot size is scaled by the z - position.

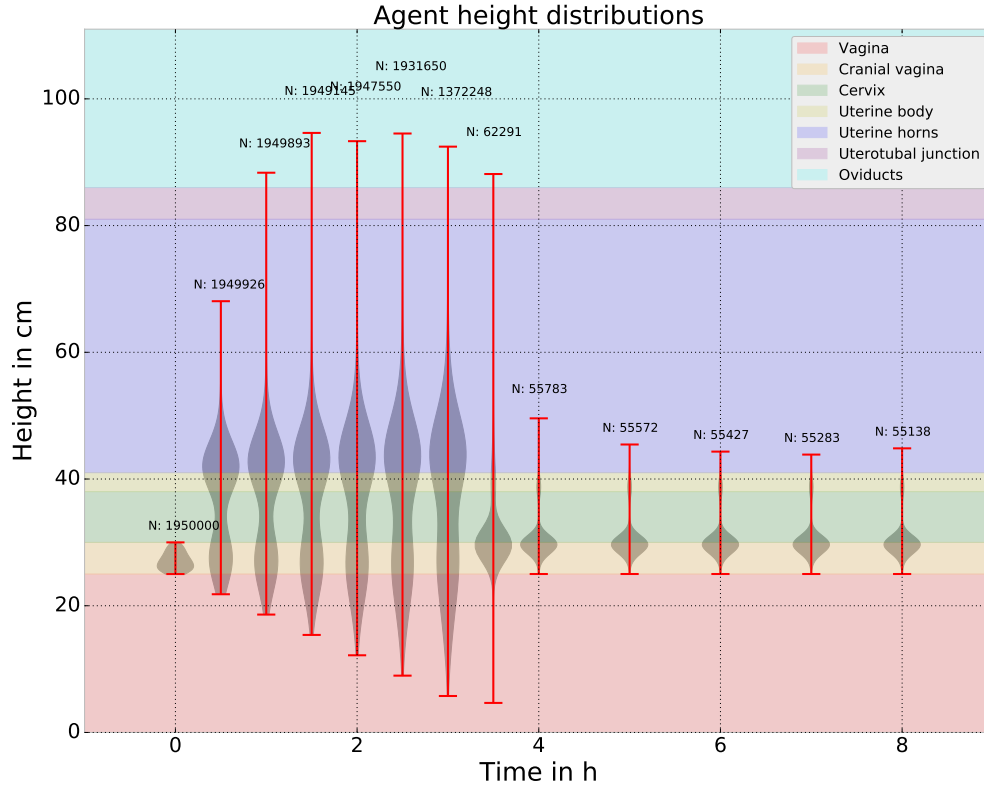


Figure 29: Dynamics of population density distribution for run *All_True*. Shaded regions indicate density distribution per time point. Red whiskers show minimal and maximal z - position of the sperms. N indicate the number of sperms in the reproductive tract at given time point. Number of sperms significantly decreases after 3.5 hours. Sperms rapidly bypass cervix and uterine body and reach oviducts one hour after insemination.

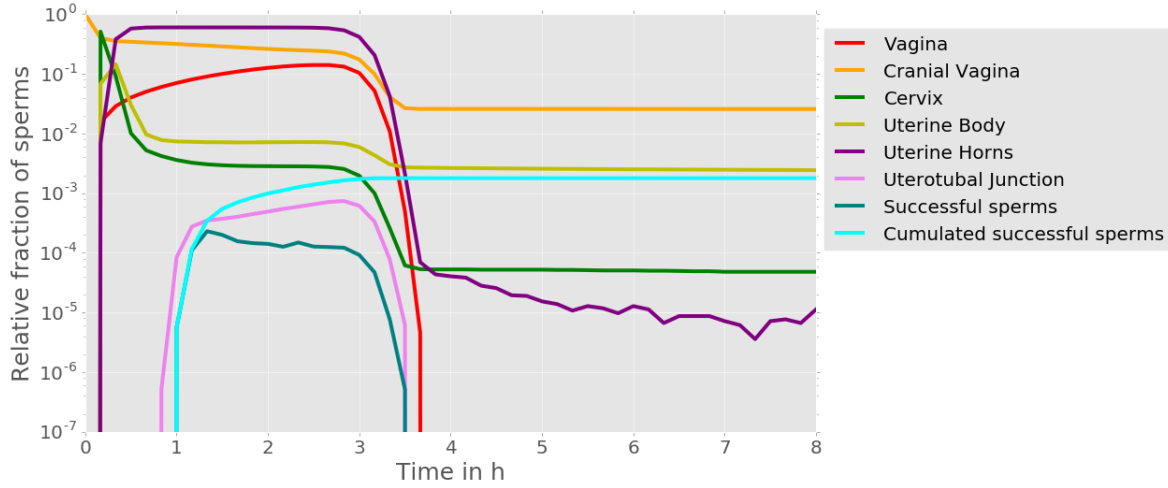


Figure 30: Number of sperms per compartment over time for run *All_True*. Time resolution: 10 minutes. It is important to notice that successful sperms are removed after each output step. So the line *Successful sperms* indicates how many sperms reached the oviducts per 10 minutes. The trace *Cumulated successful sperms* shows how many sperms were successful until the given time.

significantly with respect to the distributions from run *All_False*. Table 3 shows that 0.18% of sperms reach one of the oviducts. Figure 30 indicates that 0.01% of sperms reach the oviduct per 10 minutes, between hour 1 and 3. This rate stays constant until the immune response removes sperms from the system. The value of the "successful sperms" - trace is a rate, because successful sperms are removed from the simulation.

As in run *All_False*, the angle distribution over the population at a certain time point is shown (Figure 31). In contrast to the former run, the number of agents significantly declines after 3.5 hours (Figures 29 and 30). Therefore, the angle distribution after 3 hours was chosen to be analyzed (Figure 31).

In Figure 31 two interesting results occur. One, there are no sperms located in the middle of the cervix. Two, the minimal z - position is not dependent on the sperm angles, as it was in run *All_False* (Figure 28). Further, some sperms with an angle below approximately 25° stay in the uterine body.

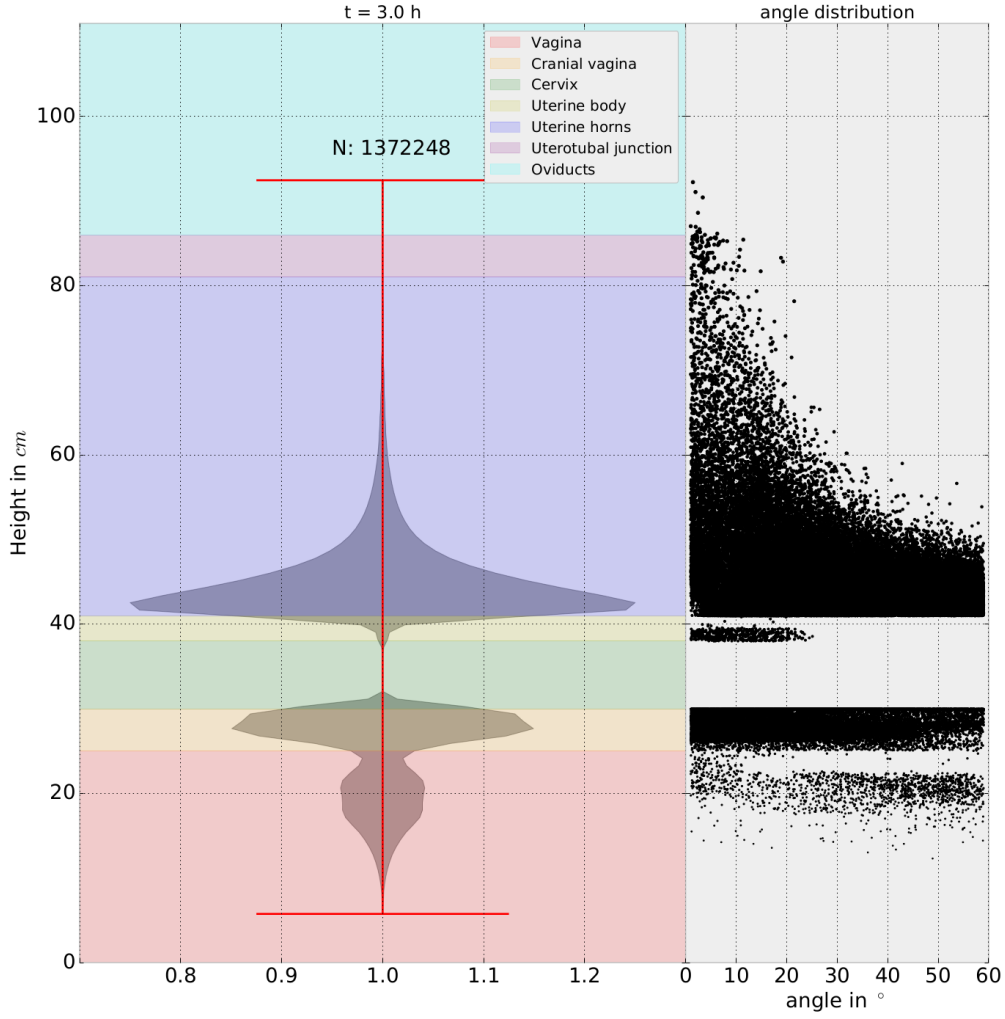


Figure 31: Distribution of angles after 3 hours in run *All_True*. Left: Sperm population's z - position distribution. N is the number of sperms inside the tract after 3 hours. Right: z - positions in dependence on sperm angles. Sperms with smaller deflection angles propagate further in the reproductive tract. Only a random subset of 10^5 sperms is depicted. The dot size is scaled by the z - position.

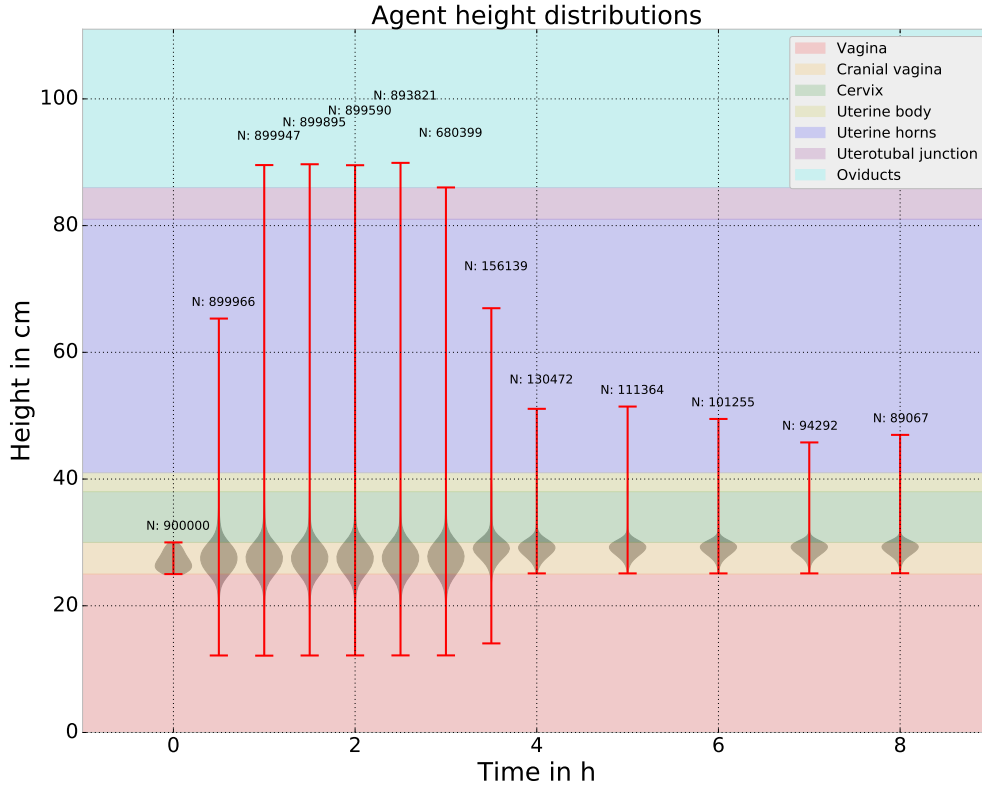


Figure 32: Dynamics of sperm z - positions distribution in the reproductive tract over time, in a simulation run without fluid flow (run *F_False*). Shaded region: sperm z - position distribution. Red whiskers: minimal and maximal z - positions. Background indicates the compartments of the reproductive tract. The majority of sperms does not leave the cranial vagina without fluid flow. Nevertheless, some sperms reach the oviducts one hour after insemination.

5.5.3 Results without fluid flow

For run *F_False* the fluid flow was turned off ($B_f = False$). Figure 32 shows the resulting sperms distributions.

Removing the fluid flow significantly changed the system's behavior. Only $56 \cdot 10^{-4}\%$ of the sperms reach the oviducts within the simulation time, compared to 0.18% in the former run *All_True*. However, the time until the first sperm reaches the oviduct is within the same ten minutes as for the simulation with fluid flow (Table 3, Figure 33). The majority of sperms does not leave the cranial vagina at all. The number of sperms reaching the uterine body and uterine horns is significantly lower compared to the run

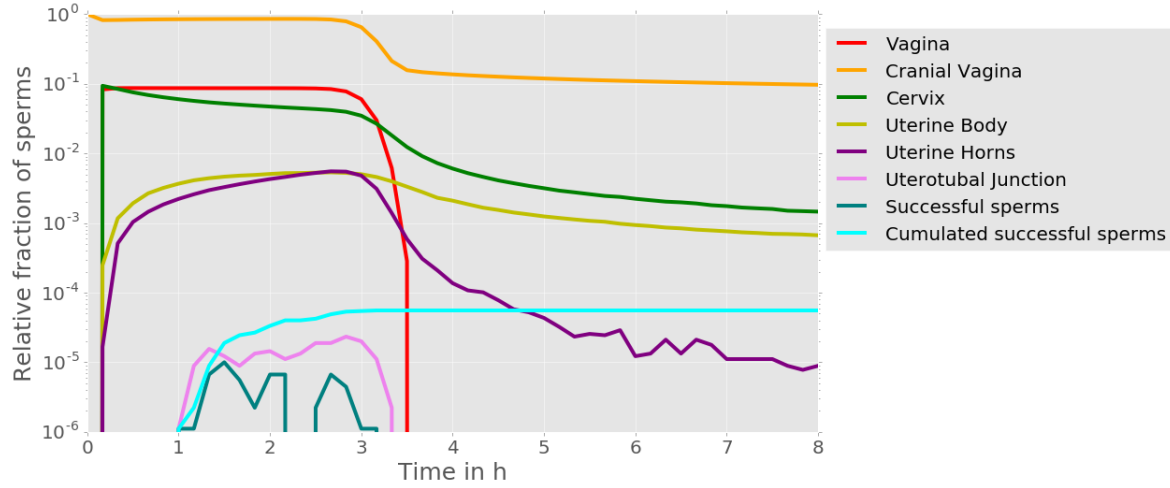


Figure 33: Sperms per compartment over time. Run *F_False*. After 1 hour sperms enter the uterotubal junction and the oviducts. Sperms in the oviducts are indicated by the successful sperms. Without fluid flow the uterine horns are rarely populated.

with fluid flow, comparing Figures 30 and 33. After three hours, approximately 60% of the sperms are in the uterine horns in run *All_True*. Removing the fluid flow decreases that fraction to approximately 0.5%. Additionally, more sperms stay in the cervix, which is best visible in Figure 34.

5.5.4 Results without wall interaction

Next, interaction between sperms and the compartment wall was removed, while the fluid flow was restored. No sperms were able to reach the oviducts within simulation time. On the first view, the distribution over time of *F_False* and *All_True* looks similar (Figures 29 and 35). The major difference is that sperms do not exceed the uterotubal junction without wall interaction (run *W_False*). However, comparing the results of *W_False* to the run without fluid flow (*F_False*), far more sperms reach the uterine body and uterine horns (Figures 32, 33, 35 and 36).

5.5.5 Results with strong fluid flow

Increasing the fluid flow speed s_f has no significant effect on the numbers of sperms reaching the oviducts (Table 3). However, the distribution of the sperm z - positions broadened and sperms were swept out of the vagina (Figure 37).

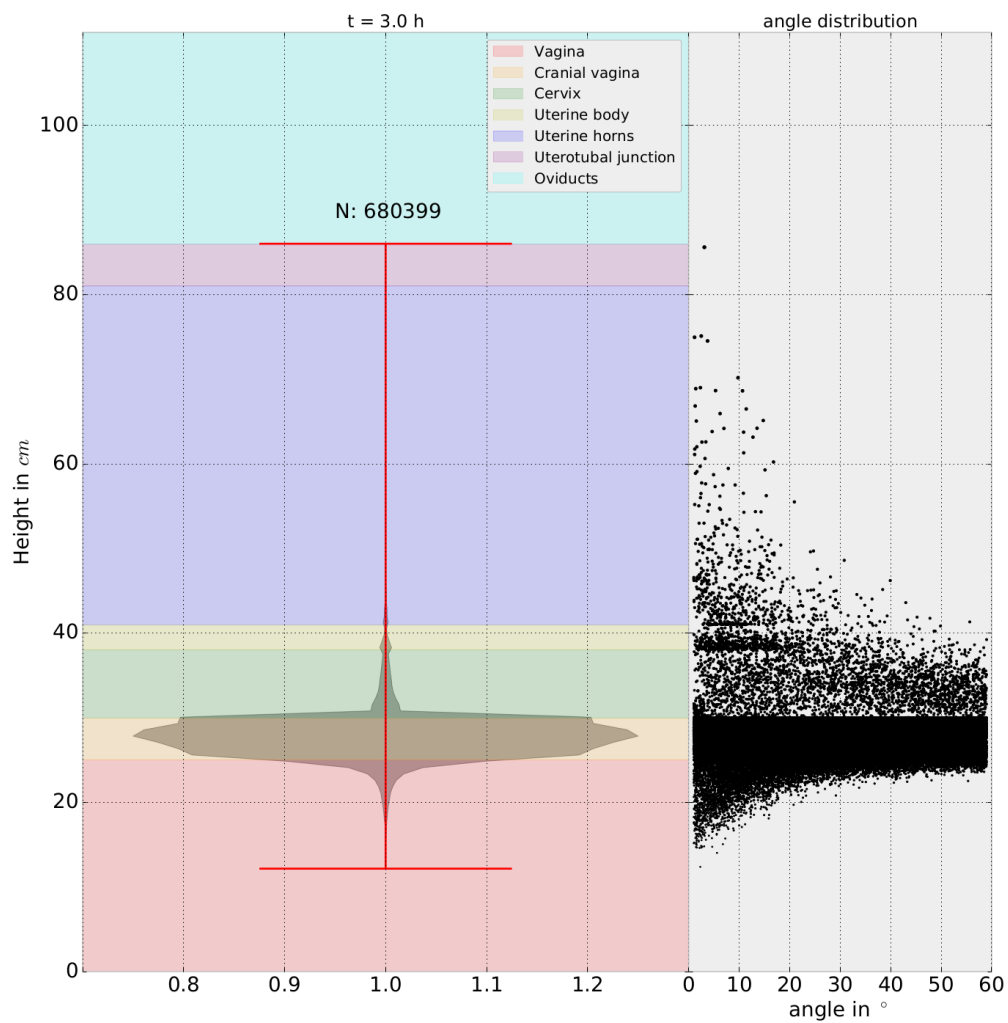


Figure 34: Sperm z - position distribution after 3 hours (run *F_False*). Left: Distribution of sperm z -positions after 3 hours. N is the number of sperm. Background indicates the compartments. Right: z - positions in dependence of the sperm angles. Sperm populate the cervix. The dot size is scaled by the z - position.

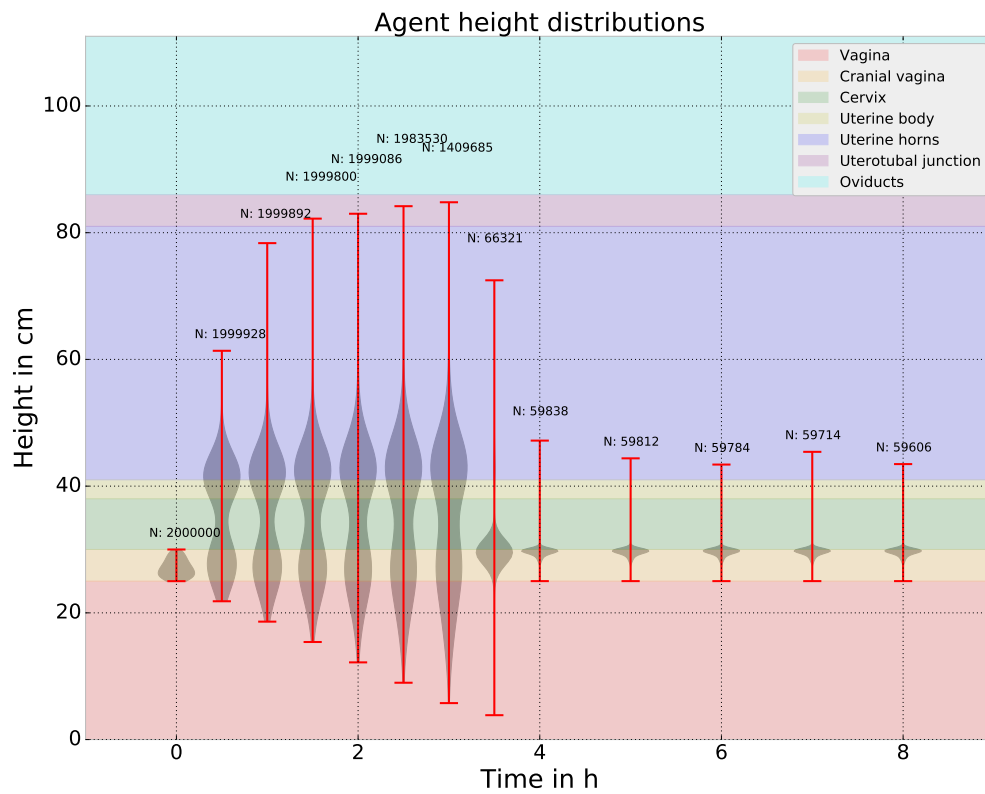


Figure 35: Sperm z - position distribution over time (run W_False). Shaded regions indicate z - position distribution. Maximal and minimal z - positions are indicated by red whiskers. N indicates the number of sperms in the tract at given time point. No sperms were able to reach the oviducts without wall interaction W_False , albeit many sperms reached the uterine horns.

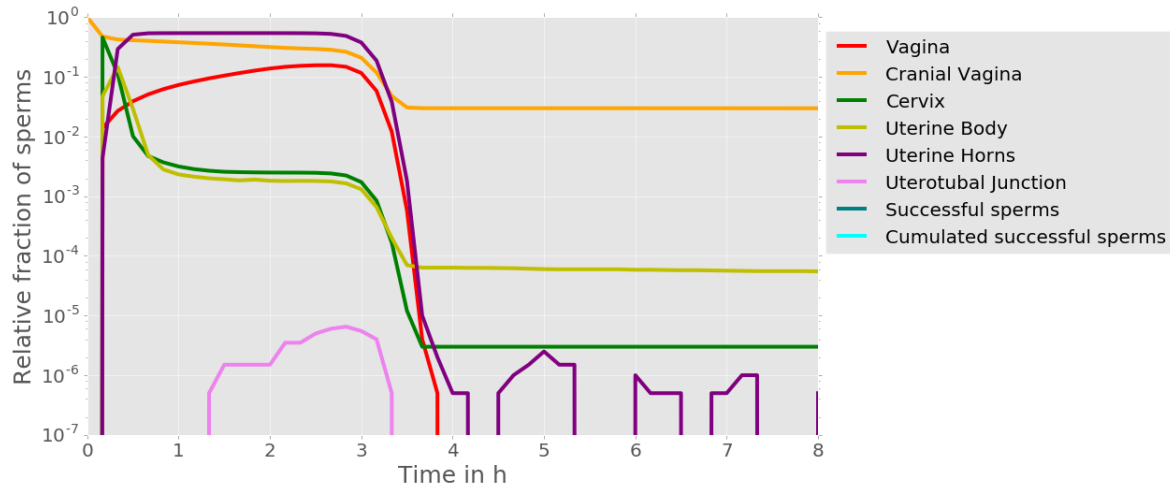


Figure 36: Relative number of sperms per compartment over time. After 80 minutes sperms enter the uterotubal junction. No sperm enters one of the oviducts. Run without wall interaction *W_False*.

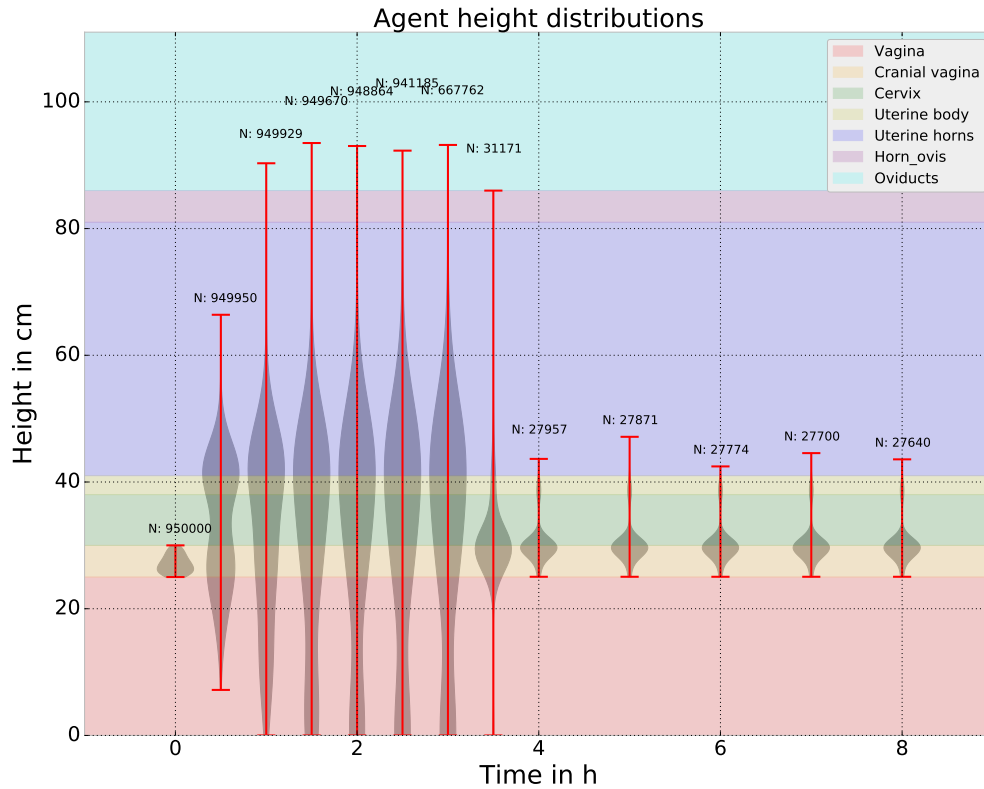


Figure 37: Sperm z - position distributions over time in run *All_True_sF*. Sperms are swept outside the vagina due to stronger fluid speed.

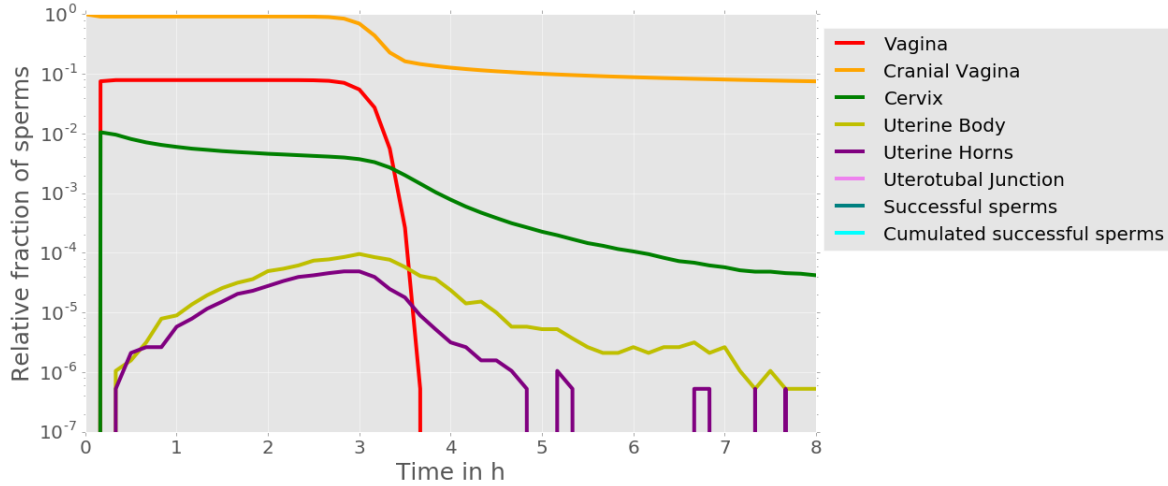


Figure 38: Relative number of sperms per compartment over time. Run without wall interaction, fluid flow and orgasm (*WFO_False*). Only a minority of sperms is able to leave the cranial vagina. No sperm is able to reach the oviducts.

5.5.6 Runs *WFO_False* and *FO_False*

The influence of the wall interaction in absence of fluid flow and muscle contractions was investigated. Simulations *WFO_False* and *FO_False* have been performed in order to tackle this question. Figures 38 and 39 show the resulting time courses of sperms per compartment.

Figure 38 shows that only a small fraction of sperms reaches the uterine body and horns. Turning on wall interaction increases this fraction significantly (Figure 39).

5.5.7 Interaction of sperm - proof of concept

In none of the mentioned simulations the implemented sperm-sperm interactions were considered. As a proof of concept, sperm movement was simulated in a shallow box and visualized with *paraview*[78]. The resulting videos confirmed that sperms aligned to neighbors in their proximity. Figures 40 and 41 shown snapshots from the visualizations. The pictures were taken from small movies. Figure 40 a larger section of a sperm population is shown, but no groups of sperm could be identified. A group of sperms would indicate sperm interactions. In Figure 41 many of those groups occur, highlighted by red circles. Consequently, the implementation of sperm-sperm interaction was successful. However, these interactions prolonged the simulation time drastically

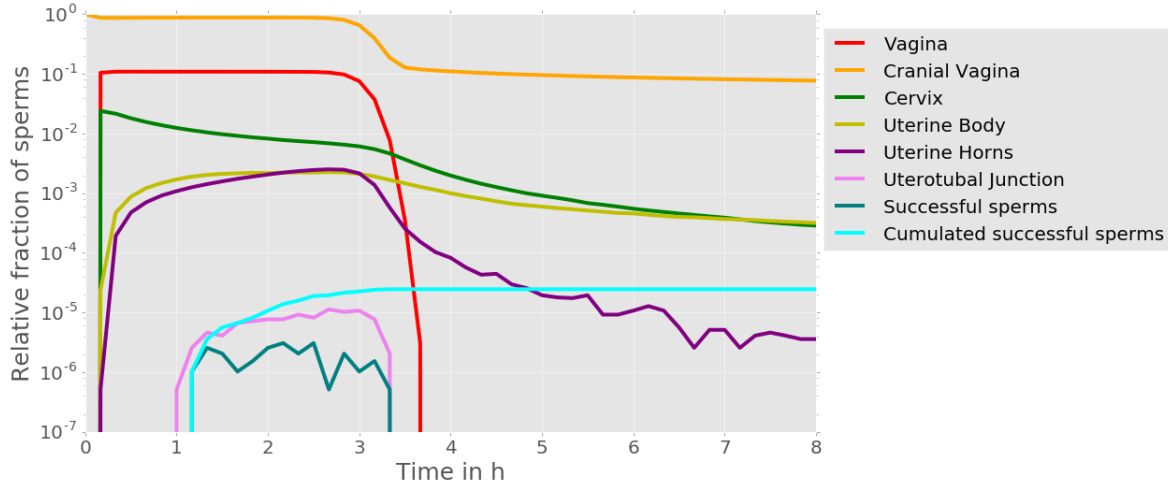


Figure 39: Relative number of sperms per compartment over time. Run without fluid flow and orgasm (*FO_False*). The majority of sperms stays in the cranial vagina. Nevertheless, some sperms reach the oviducts 70 minutes after insemination.

and were therefore not included in the current analysis.

6 Discussion

The presented results are discussed below. Therefore, two numbers will be introduced: First, in human approximately 1 out of a million sperms reaches the oviducts [16]. Second, the number of spermatozoa is reduced by a factor of 1000 during the transit from the vagina to the oviduct [1]. These numbers strongly contradict each other and illustrate the uncertainty in the analysis of sperm propagation. All simulation runs except those without wall interaction exceed the first value by at least one order of magnitude (Table 3). However, the model does not include the flow back of seminal plasma, which occurs in 94% of copulations and removes in average 35% of sperms. Another factor which would reduce the number of sperms reaching the oviducts is the higher viscosity of cervical mucus compared to that of water. The average sperm velocity of $133\mu m s^{-1}$ was measured in low-viscosity aqueous medium [45]. The results are difficult to compare with data from the literature. Nevertheless, comparing them among themselves, determines which interaction types have the largest influence on successful sperm propagation.

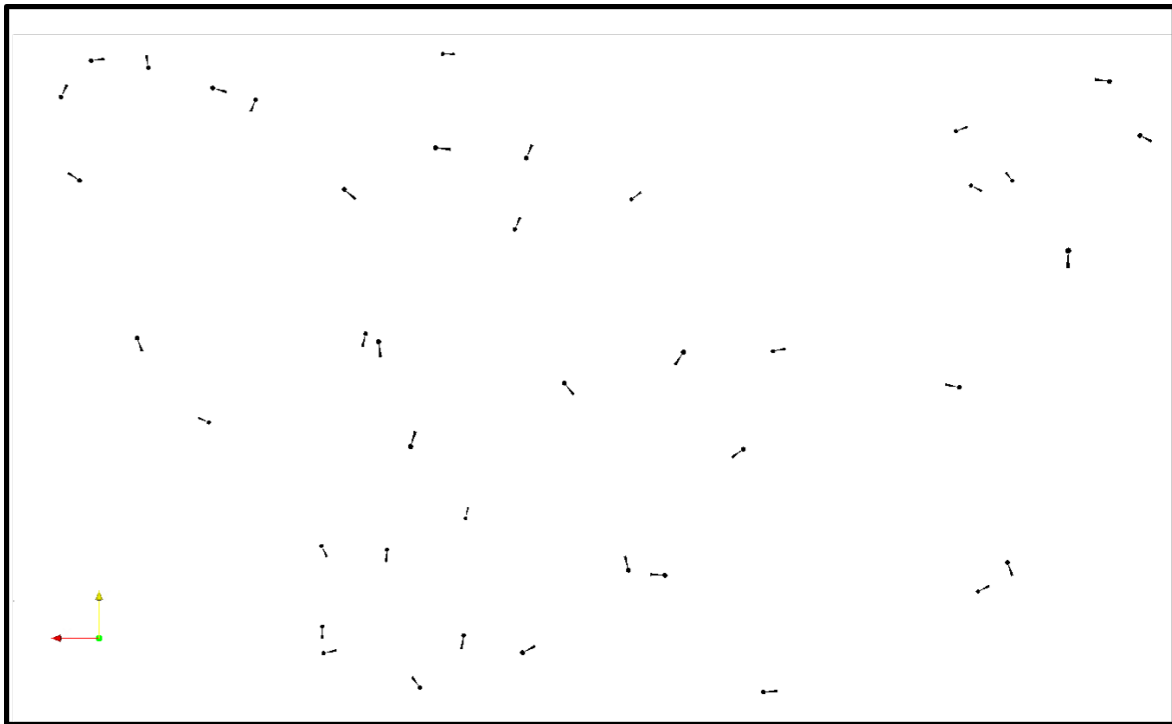


Figure 40: Snapshot from simulation of sperms in a box without sperm-sperm interaction. Sperms do not interact with each other.



Figure 41: Snapshot from simulation of sperms in a box with sperm-sperm interaction. Sperms tend to align their swimming directions.

6.1 Sperm swimming in a linear fashion are more likely to reach oviducts

Independently of the simulation setting sperms with a smaller deflection angle travelled further in the reproductive tract (Figures 28, 31 and 34). In the first run (*All_False*) no interactions with the reproductive tract took place, so the movement of sperm was a random walk in the reproductive tract. Even with nearly 10 million simulated sperms none of them reached the oviducts. This indicates that interactions of spermatozoa with the reproductive tract are essential for successful fertilization.

6.2 Fluid flow fuels sperm passage through cervix

Simulations with and without fluid flow show that the distribution of sperms in the reproductive tract differed significantly between these simulations. Without flow sperms have difficulties to pass the cervix (Figure 32). The number of sperms, which reached the oviducts dropped from 0.18% in run *All_True* to $5.6 \cdot 10^{-3}\%$ in run *F_False*. This reduction must be due to an effect in the cervix, because the number of sperms in the uterine horns decreased more than a hundredfold (from 60% to 0.5%) when removing the fluid flow (Section 5.5.3). The flow directs sperm towards the uterus and therefore strongly increases the number of sperms in the uterine cavity. Another interaction, which could orient sperm in direction of the uterus is the alignment to the wall. A comparison of the runs *WFO_False* and *FO_False*, the first without wall interaction and both runs without fluid flow and orgasm, shows that wall interactions are able to promote passage through cervix. The number of sperms reaching the uterine body increases by more than a factor of ten, when adding alignment to the wall (Figures 38 and 39).

Nonetheless, fluid flow remains by far the most important factor affecting cervix transition, which is evident comparing the population densities of the run without wall interaction and the run without fluid flows (Figures 32 and 35).

6.3 Wall interaction assists journey through the uterus

As fluid flow is the motor for guidance of sperm into the uterine body, wall interactions seem to be indispensable to navigate sperms towards the oviducts. In each simulation run lacking wall interaction no sperm reached the oviducts. In total $13 \cdot 10^6$ sperms were simulated in runs without wall interaction. The importance of wall interaction becomes clear in Figures 29, 32 and 35. After 30 minutes the sperm distribution in *All_True* and *W_False* are similar (Figures 29 and 35). The fraction of sperms reaching the uterine horns is similar (Figures 27 and 36). Despite this similar starting condition, sperms rapidly enter and pass through the uterotubal junction, when aligning to the wall. Without wall interaction (run *W_False*) sperms reach the uterotubal junction later and struggle with the enclosing compartment walls, which prevents them from entering the oviducts before the immune response removes them from the system. Even in absence of fluid flows, which leads to a significantly lower number of sperms in the uterine body (Section 6.2), sperms are able to reach the oviducts within 60 minutes when aligning to the wall (Table 3 and Figure 32).

In the model, alignment to the wall increases sperm linearity (Section 5.3.2). In order to investigate, if this increase in linearity or the alignment to the wall is the factor which enables sperms to find the entrance to the oviducts, another simulation was started. The current angle γ_c was set to angle γ in each time step, instead of updating the current angle depending of the alignment score (Equation 31). As a consequence, sperms still align to the wall, but their deflection angle is not decreased due to their alignment. So the alignment to the wall does not lead to a more linear movement. Table 3 shows that the number of sperms which reached the oviducts was reduced by factor 2. Alignment, without increasing the linearity of sperm movement, still led to a large fraction of successful sperm. So both, the more linear movement as well as the alignment itself play an important role in passing through the uterotubal junction and reaching the oviducts. As mentioned in Section 3.1.4, hamster sperms swimming in a linear fashion were shown to be more successful in passing the uterotubal junction [54]. The model results represent this finding (e.g. Figure 28), as sperms with a smaller angle are more likely to reach the oviduct. Anyway, at least in the model this

difference arises from the fact that sperms with smaller angles swim more directed and therefore reach the oviducts faster. This could also be the case for the experiment in hamsters. In this experiment, uncapacitated and capacitated sperms were inseminated in the uterus and the number of sperms recovered from the oviducts was determined. Thus, the result that more uncapacitated sperms reached the oviduct might solely rely on the faster propagation of uncapacitated sperms independent of the uterotubal junction.

6.4 Influence of orgasm and pH

The effects of muscle contractions and pH change were minor compared to the factors mentioned above. Comparing the number of successful sperm from table 3 it becomes evident that the differences between the runs *All_True*, *O_False* and *pH_False* are negligible.

The orgasm seems to play a larger role when fluid flow is missing, comparing run *F_False* with run *FO_False*. Without the fluid flow the system is lacking the mechanism, which is mainly responsible for the passage of sperm through the vagina. Muscle contractions on the other hand displaces on average the same number of sperms into the uterine cavity. Therefore, only the percentage share of sperms displaced to the uterus increases, when the simulation runs without the fluid flows. The influence of orgasms on the fertilization rate controversial. It was shown that orgasms lead to muscle contractions which transport sperm through the reproductive tract, but there is a lack of evidence that absence of orgasms decreases conception rates [88]. The model predicts only an infinitesimal increase in sperms reaching the oviducts comparing runs with and without orgasm. Possibly the effect of an orgasm on the conception rate is just insufficient in order to be observed *in vivo*.

The vaginal pH in cows is not acidic (pH 7.35 [89]). Thus, sperm would not be immobilized in a cow's vagina. Anyway, in the model run without a change in pH, the number of sperm reaching the oviducts did not change significantly, because the pH only affect sperms in the vagina and the cranial vagina. Consequently, the acidic environment in the human vagina is most likely only important as a microbial defense mechanism and has no influence on the fertilization rate.

6.5 Sperms get stuck in microgrooves

In all simulations with immune response some sperms survived. These sperms are most likely stuck in the microgrooves, where immune response has no influence on them. That is an artifact of the way the model was implemented. If a sperm is orientated perpendicular to a compartment wall, it is not aligned to it. Further, if it is close enough the random movement is not sufficient to release the sperm. A sperm only moves forwards if it stays inside the reproductive tract. Thus, a sperm close to the wall with an orientation perpendicular to it would always try to swim outside the compartment. Consequently, they do not move anymore. The fact that they survive is due to the missing immune response in microgrooves. How the entrapment of sperms influences the simulation results and in which dimension such influence is biological feasible remains to be investigated. It is not inconceivable that sperms get stuck in microgrooves. Motile sperms were recovered from human cervical mucus 5 days after insemination [90]. So either these sperm survived inside the cervical mucus or they somehow withstood the immune response in the uterus and reentered the cervix.

6.6 Drawing random angles

As described in Section 5.3 the angles by which the sperm orientations are deflected is drawn from a normal distribution. Drawing an angle, which is a circular entity from a normal distribution, which is not defined on a circle is mathematically questionable. The *von Mises* distribution is an approximation of the wrapped normal distribution, which is defined on a circle. This approximation is often used in spatial modeling [91]. For this model usage of a normal distribution is reasonable, since the standard deviation is very small. Even three standard deviations do not exceed 180° . Further, using a normal distribution is more intuitive, because the standard deviation is an angle and therefore has a biological analogue. The shape of the *von Mises* distribution depends on a concentration parameter. For large concentration parameters the distribution limits in a normal distribution, if this parameter is zero the distribution is uniform. Sperms would hold this concentration parameter instead of the deflection angle and therefore, it would be much more difficult to estimate the resulting turning angle.

7 Conclusion

In this work the first 3D agent-based model which covers the journey of sperm from insemination to the oviducts is presented. The model is able to analyze the contribution of various proposed mechanism of sperm selection to the system's behavior. Interactions with the compartment walls and orientation into fluid flows were identified as the most important factors in sperm propagation.

The reproductive tract was described with a set of three dimensional equations (Section 5.1). Describing the reproductive tract by these equations has two major advantages compared to represent it on a three dimensional grid, which would be another option to describe the reproductive tract. First, the spatial solution of the tract and therefore of the sperm movement is infinite. Second, holding a set of equations instead of a enormous grid is far less expensive in terms of computational costs. Describing the reproductive tract with a grid, would lead to a storage size up to a Terabyte.

The model predicts that the alignment to surfaces and the reaction to fluid flows are the most important regulating factors for guidance of sperm to the oviducts. Without these mechanism the percentage of sperms passing the uterotubal junctions decreased significantly or even vanished. The alignment into fluid flows helps the sperm travelling through the cervix into the uterine body and the alignment to the compartment walls guides it towards the oviducts.

According to the model, sperm propagation is thus largely determined by two basic physical properties: alignment to the walls of the oviduct and inclusion into a fluid flow.

Those mechanism are studied *in vitro* and therefore are well described biologically and physically. Chemo- and thermotaxis most likely play an important role inside the oviduct, but the model assumes that those are not necessary in order to populate the oviducts.

The first 3D ABM about sperm propagation inside the oviducts was published previously [92]. This model contains an elegant description of a mouse oviduct, but unfortunately does not provide any results. Otherwise, the idea of connecting the two 3D models would have been tempting, because they are complementary in their scope.

8 Outlook

While the results presented here are biologically relevant, the model is easily extendable. The following section presents suggestions for further use, modification and extension of the model. One aim should be to quantify the effects of wall interaction and fluid flows more reliable. This could be done by parameter scans. Additionally, the influence of sperm-sperm interactions, which are already implemented, could be studied. The model already contains the description of the oviducts, which are momentarily set as the end of the journey of sperms. Using the already existing oviduct to add an oocyte and define it as the new goal could be easily done. Thereafter, interactions with the oviductal epithelium, i.e. binding, capacitation and hyperactivation could be added. This could be realized by giving each sperm a binding and a unbinding probability in the oviducts. This probability could be coupled to the number of *checking directions* which point outside. Capacitation could be modeled as an increase in unbinding probability and the facilitation for chemotaxis. After unbinding the sperms could then move towards the oocyte by chemotaxis. In order to add a chemo-attractant to the model, partial differential equations (PDEs) could be used.

In order to describe a more physiological immune response, the leukocytes could be introduced as another agent species. This addition makes it possible to determine sperm-leukocyte interaction. Although leukocytes internalize many sperms, interaction with leukocytes can also prolong sperm life time [93]. So the immune response and the invasion of leukocytes could actually have a bi-variant influence on the system.

Summarizing, this work described the first 3D ABM of the entire female reproductive tract. The use of implicit functions makes it computationally cheap and flexible. The model is able to identify important system properties and is easily extendable.

9 Acknowledgements

I would like to express my gratitude to Edda Klipp for supervising my project, for motivating inspiration and for her warm guidance of the entire group. I want to address my gratitude to Karin Müller and the Leibniz-Institut für Zoo- und Wildtierforschung (IZW) for the idea for this project, the trust and for great collaboration.

Many thanks belong to Karin Müller and Jens Hahn for many helpful discussions, an immense amount of enthusiasm and their omnipresence.

I cannot thank Katja Tummler, Judith Wodke, Josch Pauling, Severin Ehret and again Karin Müller and Jens Hahn enough for incredible constructive advice during the writing process.

Great thanks go to Wolfgang Giese, Björn Goldenbogen and Andrea Auconi for mathematical discussions. I wish to thank Marie Hemmen for inspiring lunch breaks and for introducing me to the complicated library system.

I want to thank the entire group of tbp for your support, for your ideas concerning my project and for being as you are. I'm incredibly happy to be part of this group.

Finally, I desire to thank my parents, my friends and Virginia Waitschies for their wonderful support throughout my studies.

References

- [1] Karine Reynaud, Zeev Schuss, Nathalie Rouach, and David Holcman. Why so many sperm cells? *Communicative & integrative biology*, 8(3):e1017156, 2015.
- [2] Patrick Abbot and Antonis Rokas. Mammalian pregnancy. *Current Biology*, 27(4):R127–R128, 2017.
- [3] Lawrence L. Espey. *Knobil and Neill’s Physiology of Reproduction*, volume 1. 2006.
- [4] C. R. AUSTIN and A. W. H. BRADEN. Polyspermy in Mammals. *Nature*, 172(4367):82–83, jul 1953.
- [5] Deborah E McFadden, Ruby Jiang, Sylvie Langlois, and Wendy P Robinson. Dispermy–origin of diandric triploidy: brief communication. *Human reproduction (Oxford, England)*, 17(12):3037–8, dec 2002.
- [6] Pilar Coy and Manuel Aviles. What controls polyspermy in mammals, the oviduct or the oocyte? *Biological Reviews*, 85(3):593–605, dec 2010.
- [7] M. S. Kupka, T. D’Hooghe, A. P. Ferraretti, J. De Mouzon, K. Erb, J. A. Castilla, C. Calhaz-Jorge, Ch De Geyter, and V. Goossens. Assisted reproductive technology in Europe, 2011: Results generated from European registers by ESHRE. *Human Reproduction*, 31(2):233–248, mar 2015.
- [8] Pierre Comizzoli, Nucharin Songsasen, and David E. Wildt. Protecting and extending fertility for females of wild and endangered mammals. *Cancer Treatment and Research*, 156:87–100, 2010.
- [9] M. Rolland, J. Le Moal, V. Wagner, D. Royère, and J. De Mouzon. Decline in semen concentration and morphology in a sample of 26 609 men close to general population between 1989 and 2005 in France. *Human Reproduction*, 28(2):462–470, feb 2013.
- [10] Trevor G. Cooper, Elizabeth Noonan, Sigrid von Eckardstein, Jacques Auger, H. W Gordon Baker, Hermann M. Behre, Trine B. Haugen, Thinus Kruger,

- Christina Wang, Michael T. Mbizvo, and Kirsten M. Vogelsong. World Health Organization reference values for human semen characteristics. *Human Reproduction Update*, 16(3):231–245, may 2009.
- [11] Susan S. Suarez. Mammalian sperm interactions with the female reproductive tract. *Cell and Tissue Research*, 363(1):185–194, jan 2016.
- [12] S. S. Suarez and A. A. Pacey. Sperm transport in the female reproductive tract. *Human Reproduction Update*, 12(1):23–37, aug 2006.
- [13] William V. Holt and Alireza Fazeli. Do sperm possess a molecular passport? Mechanistic insights into sperm selection in the female reproductive tract. *Molecular Human Reproduction*, 21(6):491–501, jun 2015.
- [14] W. V. Holt and A. Fazeli. Sperm selection in the female mammalian reproductive tract. Focus on the oviduct: Hypotheses, mechanisms, and new opportunities. *Theriogenology*, 85(1):105–112, 2016.
- [15] John L. Fitzpatrick and Stefan Lüpold. Sexual selection and the evolution of sperm quality. *Molecular Human Reproduction*, 20(12):1180–1189, dec 2014.
- [16] Michael Eisenbach and Laura C. Giojalas. Sperm guidance in mammals — an unpaved road to the egg. *Nature Reviews Molecular Cell Biology*, 7(4):276–285, apr 2006.
- [17] Francisco Alberto García-Vázquez, Iván Hernández-Caravaca, Carmen Matás, Cristina Soriano-Úbeda, Silvia Abril-Sánchez, and María José Izquierdo-Rico. Morphological study of boar sperm during their passage through the female genital tract. *The Journal of reproduction and development*, 61(5):407–13, 2015.
- [18] Edda Klipp, Wolfram Liebermeister, Christoph Wierling, Axel Kowald, Hans Lehrach, and Ralf Herwig. *Systems Biology: A Textbook*. 2009.
- [19] Gary An, Qi Mi, Joyeeta Dutta-Moscato, and Yoram Vodovotz. Agent-based models in translational systems biology. *Wiley Interdisciplinary Reviews: Systems Biology and Medicine*, 1(2):159–171, 2009.

- [20] Stefan Kallenberger and Stefan Legewie. Modeling formalisms in systems biology of apoptosis. *Systems Biology of Apoptosis*, 1:1–32, dec 2013.
- [21] Busch and Waberski. *Künstliche Besamung bei Haus- und Nutztieren*. Schattauer, 2007.
- [22] Maximiliano Tourmente, Montserrat Gomendio, and Eduardo RS Roldan. Sperm competition and the evolution of sperm design in mammals. *BMC Evolutionary Biology*, 11(1):12, jan 2011.
- [23] S T Mortimer and D Mortimer. Kinematics of human spermatozoa incubated under capacitating conditions. *Journal of andrology*, 11(3):195–203, may 1990.
- [24] E. Sloter, T. E. Schmid, F. Marchetti, B. Eskenazi, J. Nath, and A. J. Wyrobek. Quantitative effects of male age on sperm motion. *Human Reproduction*, 21(11):2868–2875, sep 2006.
- [25] J. M. Cummins and P. F. Woodall. On mammalian sperm dimensions. *Reproduction*, 75(1):153–175, sep 1985.
- [26] I. G F Goovaerts, G. G. Hoflack, A. Van Soom, J. Dewulf, M. Nichi, A. de Kruif, and P. E J Bols. Evaluation of epididymal semen quality using the Hamilton-Thorne analyser indicates variation between the two caudae epididymides of the same bull. *Theriogenology*, 66(2):323–330, jul 2006.
- [27] P. Vyt, D. Maes, T. Rijsselaere, E. Dejonckheere, F. Castryck, and A. Van Soom. Motility assessment of porcine spermatozoa: A comparison of methods. *Reproduction in Domestic Animals*, 39(6):447–453, dec 2004.
- [28] A. Darszon, T. Nishigaki, C. Beltran, and C. L. Trevino. Calcium Channels in the Development, Maturation, and Function of Spermatozoa. *Physiological Reviews*, 91(4):1305–1355, 2011.
- [29] William V. Holt. Mechanisms of sperm storage in the female reproductive tract: An interspecies comparison. *Reproduction in Domestic Animals*, 46(SUPPL. 2):68–74, sep 2011.

- [30] T. R. BIRKHEAD and A. P. MOLLER. Sexual selection and the temporal separation of reproductive events: sperm storage data from reptiles, birds and mammals. *Biological Journal of the Linnean Society*, 50(4):295–311, dec 1993.
- [31] E R Boskey, R A Cone, K J Whaley, and T R Moench. Origins of vaginal acidity: high D/L lactate ratio is consistent with bacteria being the primary source. *Hum Reprod*, 16(9):1809–1813, sep 2001.
- [32] Elizabeth A. Miller, De Anna E. Beasley, Robert R. Dunn, and Elizabeth A. Archie. Lactobacilli dominance and vaginal pH: Why is the human vaginal microbiome unique? *Frontiers in Microbiology*, 7(DEC):1936, 2016.
- [33] J. Ravel, P. Gajer, Z. Abdo, G. M. Schneider, S. S. K. Koenig, S. L. McCulle, S. Karlebach, R. Gorle, J. Russell, C. O. Tacket, R. M. Brotman, C. C. Davis, K. Ault, L. Peralta, and L. J. Forney. Vaginal microbiome of reproductive-age women. *Proceedings of the National Academy of Sciences*, 108(Supplement_1):4680–4687, mar 2011.
- [34] T. S. Acott. Inhibition of bovine spermatozoa by caudal epididymal fluid: II. Interaction of pH and a quiescence factor. *Biology of Reproduction*, 30(4):926–935, may 1984.
- [35] D W Carr, M C Usselman, and T S Acott. Effects of pH, lactate, and viscoelastic drag on sperm motility: a species comparison. *Biology of reproduction*, 33(3):588–595, oct 1985.
- [36] S. Olatunbosun Banjoko and Fasiu O. Adeseolu. Seminal plasma pH, inorganic phosphate, total and ionized calcium concentrations in the assessment of human spermatozoa function. *Journal of Clinical and Diagnostic Research*, 7(11):2483–2486, nov 2013.
- [37] David M. Phillips and Susan Mahler. Leukocyte emigration and migration in the vagina following mating in the rabbit. *The Anatomical Record*, 189(1):45–59, sep 1977.

- [38] R. K. Zimmer and J. A. Riffell. Sperm chemotaxis, fluid shear, and the evolution of sexual reproduction. *Proceedings of the National Academy of Sciences*, 108(32):13200–13205, may 2011.
- [39] D. F. Katz, D. A. Slade, and S. T. Nakajima. Analysis of pre-ovulatory changes in cervical mucus hydration and sperm penetrability. *Advances in Contraception*, 13(2-3):143–151, 1997.
- [40] Emma Lorenzen, Frank Follmann, Gregers Jungersen, and Jorgen S. Agerholm. A review of the human vs. porcine female genital tract and associated immune system in the perspective of using minipigs as a model of human genital Chlamydia infection. *Veterinary Research*, 46(1):116, sep 2015.
- [41] K. June Mullins and R. G. Saacke. Study of the functional anatomy of bovine cervical mucosa with special reference to mucus secretion and sperm transport. *The Anatomical Record*, 225(2):106–117, oct 1989.
- [42] P. Denissenko, V. Kantsler, D. J. Smith, and J. Kirkman-Brown. Human spermatozoa migration in microchannels reveals boundary-following navigation. *Proceedings of the National Academy of Sciences*, 109(21):8007–8010, may 2012.
- [43] Kiyoshi Miki and David E. Clapham. Rheotaxis guides mammalian sperm. *Current Biology*, 23(6):443–452, mar 2013.
- [44] Chih-kuan Tung, Florencia Ardon, Alyssa G. Fiore, Susan S. Suarez, and Mingming Wu. Cooperative roles of biological flow and surface topography in guiding sperm migration revealed by a microfluidic model. *Lab Chip*, 14(7):1348–1356, apr 2014.
- [45] Chih-kuan Tung, Lian Hu, Alyssa G. Fiore, Florencia Ardon, Dillon G. Hickman, Robert O. Gilbert, Susan S. Suarez, and Mingming Wu. Microgrooves and fluid flows provide preferential passageways for sperm over pathogen *Tritrichomonas foetus*. *Proceedings of the National Academy of Sciences*, 112(17):5431–5436, apr 2015.

- [46] Luis Alvarez, Benjamin M. Friedrich, Gerhard Gompper, and U. Benjamin Kaupp. The computational sperm cell. *Trends in Cell Biology*, 24(3):198–207, 2014.
- [47] Jens Elgeti and Gerhard Gompper. Microswimmers near surfaces. *European Physical Journal: Special Topics*, 225(11-12):2333–2352, nov 2016.
- [48] Richard S J Felleisen. Host-parasite interaction in bovine infection with *Tritrichomonas foetus*. *Microbes and Infection*, 1(10):807–816, aug 1999.
- [49] S T Mortimer and M a Swan. Kinematics of capacitating human spermatozoa analysed at 60 Hz. *Human reproduction (Oxford, England)*, 10(4):873–9, apr 1995.
- [50] G Kunz, D Beil, H Deininger, L Wildt, and G Leyendecker. The dynamics of rapid sperm transport through the female genital tract: evidence from vaginal sonography of uterine peristalsis and hysterosalpingoscintigraphy. *Human reproduction (Oxford, England)*, 11(3):627–632, mar 1996.
- [51] L H Crane and L Martin. Postcopulatory myometrial activity in the rat as seen by video-laparoscopy. *Reproduction, fertility, and development*, 3(6):685–698, 1991.
- [52] Karl Heinz Wrobel, Richard Kujat, and Gilbert Fehle. The bovine tubouterine junction: general organization and surface morphology. *Cell and Tissue Research*, 271(2):227–239, feb 1993.
- [53] S. J. Hook and E. S E Hafez. A Comparative anatomical study of the mammalian uterotubal junction. *Journal of Morphology*, 125(2):159–184, jun 1968.
- [54] T Timothy, R Shalgi, T T Smith, and R Yanagimachi. A quantitative comparison of the passage of capacitated and uncapacitated hamster spermatozoa through the uterotubal junction. *Biology of reproduction*, 46(3):419–424, mar 1992.
- [55] Hitoshi Nishimura, Ekyune Kim, Tomoko Nakanishi, and Tadashi Baba. Possible function of the ADAM1a/ADAM2 fertilin complex in the appearance of ADAM3 on the sperm surface. *Journal of Biological Chemistry*, 279(33):34957–34962, aug 2004.

- [56] Kazuo Yamagata, Tomoko Nakanishi, Masahito Ikawa, Ryou Yamaguchi, Stuart B. Moss, and Masaru Okabe. Sperm from the calmegin-deficient mouse have normal abilities for binding and fusion to the egg plasma membrane. *Developmental Biology*, 250(2):348–357, oct 2002.
- [57] D S Settlage, M Motoshima, and D R Tredway. Sperm transport from the external cervical os to the fallopian tubes in women: a time and quantitation study. *Fertility and Sterility*, 24(9):655–661., sep 1973.
- [58] H. Rodriguez-Martinez, L. Nicander, S. Viring, S. Einarsson, and K. Larsson. Ultrastructure of the Uterotubal Junction in Preovulatory Pigs. *Anatomia, Histologia, Embryologia*, 19(1):16–36, mar 1990.
- [59] M E Kervancioglu, O Djahanbakhch, and R J Aitken. Epithelial cell coculture and the induction of sperm capacitation. *Fertility & Sterility.*, 61(6):1103–1108, jun 1994.
- [60] J W Pollard, C Plante, W A King, P J Hansen, K J Betteridge, and S S Suarez. Fertilizing capacity of bovine sperm may be maintained by binding of oviductal epithelial cells. *Biology of reproduction*, 44(1):102–107, jan 1991.
- [61] Ri-Cheng Chian and Marc-André Sirard. Fertilizing Ability of Bovine Spermatozoa Cocultured with Oviduct Epithelial Cells1. *Biology of Reproduction*, 52(1):156–162, jan 1995.
- [62] S S Suarez, I Revah, M Lo, and S Kölle. Bull sperm binding to oviductal epithelium is mediated by a Ca^{2+} -dependent lectin on sperm that recognizes Lewis-a trisaccharide. *Biology of reproduction*, 59(1):39–44, jul 1998.
- [63] A. Stephen Georgiou, Ambrosius P.L. Snijders, Editia Sostaric, Reza Aflatoonian, Jose L. Vazquez, Juan M. Vazquez, Jordi Roca, Emilio A. Martinez, Phillip C. Wright, and Alireza Fazeli. Modulation of the oviductal environment by gametes. *Journal of Proteome Research*, 6(12):4656–4666, dec 2007.
- [64] Roslyn M A Elliott, Rhiannon E. Lloyd, Alireza Fazeli, Editia Sostaric, A. Stephen Georgiou, Nana Satake, Paul F. Watson, and William V. Holt. Effects of HSPA8,

- an evolutionarily conserved oviductal protein, on boar and bull spermatozoa. *Reproduction*, 137(2):191–203, feb 2009.
- [65] Susan S. Suarez and H. C. Ho. Hyperactivated motility in sperm. *Reproduction in Domestic Animals*, 38(2):119–124, apr 2003.
- [66] R Lefebvre, P J Chenoweth, M Drost, C T LeClear, M MacCubbin, J T Dutton, and S S Suarez. Characterization of the oviductal sperm reservoir in cattle. *Biology of reproduction*, 53(5):1066–1074, nov 1995.
- [67] Fei Sun, Anat Bahat, Anna Gakamsky, Eliezer Girsh, Nathan Katz, Laura C. Giojalas, Ilan Tur-Kaspa, and Michael Eisenbach. Human sperm chemotaxis: Both the oocyte and its surrounding cumulus cells secrete sperm chemoattractants. *Human Reproduction*, 20(3):761–767, feb 2005.
- [68] Anat Bahat, Michael Eisenbach, and Ilan Tur-Kaspa. Periovulatory increase in temperature difference within the rabbit oviduct. *Human Reproduction*, 20(8):2118–2121, apr 2005.
- [69] Anat Bahat, S. Roy Caplan, and Michael Eisenbach. Thermotaxis of human sperm cells in extraordinarily shallow temperature gradients over a wide range. *PLoS ONE*, 7(7):e41915, 2012.
- [70] P. Coy, F. A. Garcia-Vazquez, P. E. Visconti, and M. Aviles. Roles of the oviduct in mammalian fertilization. *Reproduction*, 144(6):649–660, dec 2012.
- [71] E. Bonabeau. Agent-based modeling: Methods and techniques for simulating human systems. *Proceedings of the National Academy of Sciences*, 99(Supplement 3):7280–7287, may 2002.
- [72] Craig W. Reynolds. Flocks, herds and schools: A distributed behavioral model. In *ACM SIGGRAPH Computer Graphics*, volume 21, pages 25–34, New York, New York, USA, 1987. ACM Press.
- [73] Jules Bloomenthal. Polygonization of implicit surfaces. *Computer Aided Geometric Design*, 5(4):341–355, nov 1988.

- [74] Kenneth Salisbury and Christopher Tarr. Haptic rendering of surfaces defined by implicit functions. *ASME Dynamic Systems and Control*, 61(November):61–67, 1997.
- [75] Python. <https://www.python.org/>.
- [76] John D. Hunter. Matplotlib: A 2D graphics environment. *Computing in Science and Engineering*, 9(3):99–104, 2007.
- [77] W. Schroeder K. Marti and B.Lorensen. *The Visualization Toolkit: An Object Oriented Approach to 3D Graphics*. Kitware, 2006.
- [78] Amy Henderson. *The ParaView Guide: A Parallel Visualization Application*. Kitware, Inc., USA, 2004.
- [79] VTK Logo. <http://www.vtk.org/download/>.
- [80] Python Logo. <https://www.python.org/community/logos/>.
- [81] Reza Nosrati, Amine Driouchi, Christopher M. Yip, and David Sinton. Two-dimensional slither swimming of sperm within a micrometre of a surface. *Nature Communications*, 6:8703, nov 2015.
- [82] P E Kloeden and E Platen. *Numerical Solution of Stochastic Differential Equations*. Springer Berlin Heidelberg, Berlin, Heidelberg, 1992.
- [83] Andre Longtin. Stochastic dynamical systems. *Scholarpedia*, 5(4):1619, 2010.
- [84] D W Carr, M C Usselman, and T S Acott. Effects of pH, lactate, and viscoelastic drag on sperm motility: a species comparison. *Biology of reproduction*, 33(3):588–595, oct 1985.
- [85] H. J. Schuberth, U. Taylor, H. Zerbe, D. Waberski, R. Hunter, and D. Rath. Immunological responses to semen in the female genital tract. *Theriogenology*, 70(8):1174–1181, 2008.
- [86] Jon Louis Bentley. Multidimensional binary search trees used for associative searching. *Communications of the ACM*, 18(9):509–517, sep 1975.

- [87] Travis E Oliphant. SciPy: Open source scientific tools for Python. *Computing in Science and Engineering*, 9:10–20, 2007.
- [88] John R Wheatley and David A. Puts. Evolutionary Science of Female Orgasm. In *The Evolution of Sexuality*, pages 123–148. Springer International Publishing, 2015.
- [89] B. Beckwith-Cohen, O. Koren, S. Blum, and D. Elad. 55 Variations in Vaginal pH in Dairy Cattle. *Israel Journal of Veterinary Medicine*, 67(1), 2012.
- [90] J. E. Gould, J W Overstreet, and F W Hanson. Assessment of human sperm function after recovery from the female reproductive tract. *Biology of reproduction*, 31(5):888–94, dec 1984.
- [91] Jonathan R. Potts, Karl Mokross, and Mark A. Lewis. A unifying framework for quantifying the nature of animal interactions. *Journal of The Royal Society Interface*, 11(96), 2014.
- [92] M. Burkitt, D. Walker, D. M. Romano, and A. Fazeli. Using computational modeling to investigate sperm navigation and behavior in the female reproductive tract. *Theriogenology*, 77(4):703–716, mar 2012.
- [93] U. Taylor, D. Rath, H. Zerbe, and H. J. Schuberth. Interaction of intact porcine spermatozoa with epithelial cells and neutrophilic granulocytes during uterine passage. *Reproduction in Domestic Animals*, 43(2):166–175, apr 2008.

Glossary

A_{pf_cur} Altered primary fold amplitude. 25, 87, 88

A_{pf} Amplitude of primary folds. 22, 87, 88, 103

A_{sf_cur} Altered amplitude of secondary folds. 23, 25, 26, 88

A_{sf} Amplitude of secondary folds. 23, 25, 43, 87, 103

All_False Setting with all Boolean False. iv, 45–48, 50, 52, 62, 85

All_True Setting with all Boolean True. 45, 46, 49, 51–55, 62–64, 85, 86

All_True_sF Setting with all Boolean True and strong fluid flow. 45, 46, 58, 86

B_f Switch for fluid flow. 46, 54, 101

B_{ir} Switch for immune response. 46, 101

B_{org} Switch for muscle contractions. 46, 101

B_{pH} Switch for pH change. 46, 101

B_w Switch for wall interaction. 46, 101

C_{is} Strength of immune response. 43, 103

FO_False Setting with fluid and orgasm Boolean False. iv, 46, 59, 60, 62, 64, 86

F_False Setting with fluid Boolean False. 46, 54–56, 62, 64, 86

F_z Scaling factor for secondary fold amplitude in dependence on z - axis in cranial vagina and uterine body, respectively. 88

$F_{A_{pf_cur}}$ Scaling factor for secondary fold amplitude in dependence on distance to the variable radius in cranial vagina and uterine body, respectively. 88

$F_{A_{pf}}$ Scaling factor for secondary fold amplitude in dependence on distance to cervix radius. 23, 25

- IR Level of immune response. 43
- Km_{IR} Time of half-maximal immune response.. 101
- Km_{pH} pH of half-maximal speed of sperms. 103
- N Number of agents/sperms. 30, 101
- O_False Setting with orgasm Boolean False. 46, 64, 86, 98
- O_False_sF Setting with all Boolean True and strong fluid flow. 45, 46
- P_{org_max} Maximal probability for muscle contraction. 42, 101
- R_u Rotation matrix around an arbitrary axis. 34
- S_{fluid} maximal fluid velocity. 41, 103
- S_{pop} Class which holds general parameters of a sperm population.. 30
- $S_{speed_σ}$ Factor by which standard deviation is smaller than mean, for choosing current speeds of sperms. 102
- Sim_{steps} Simulation steps. 101
- T_l Length of reproduction tract. 3
- WFO_False Setting with wall,fluid and orgasm Boolean False. iv, 46, 59, 62, 86
- W_False Setting with wall Boolean False. 46, 55, 57, 58, 63, 86
- \bar{s} Mean speed of one sperm. 30, 32, 41
- γ Standard deviation of angle. 32, 49, 50, 63
- γ_c Standard deviation of current angle. 32, 33, 38, 63
- λ_γ Decay rate for decreasing maximal turning angle in dependence of sperm alignment scores. 102
- λ_{pH} Conversion rate of semen pH to vagina pH. 42, 103
- ω_{pf} Number of primary folds. 22

ω_{sf} Number of secondary folds per primary fold side. 25, 103

$\overline{S_{angle}}$ mean of maximal turning angle distribution. 102

$\overline{S_{length_sd}}$ Standard deviation of sperm length distribution. 102

$\overline{S_{length}}$ Mean of sperm length distribution. 32, 102

$\overline{S_{lt_sd}}$ Standard deviation of sperm lifetime distribution. 32, 102

$\overline{S_{lt}}$ Mean of sperm lifetime distribution. 32, 102

$\overline{S_{speed_sd}}$ Standard deviation of $\overline{S_{speed}}$. 32, 102

$\overline{S_{speed}}$ Mean standard deviation of speed of sperm population. 32, 41, 81, 102

$\overline{cw_{org}}$ Mean z displacement due to muscle contraction. 42, 101

\vec{cd} Checking directions for wall interaction. 35

\vec{c} Center of cranial vagina or uterine body. 40, 90

\vec{n}_{\perp} Projection of sperm orientation on approximated wall. 37

\vec{n} Normal vector of approximated wall. 37

\vec{p} Sperm position vector. 30, 32, 35, 37, 40

\vec{u}_f Fluid flow direction. 38, 40, 41

\vec{u}_f Fluid flow direction at sperm's position. 32

\vec{u} Sperm orientation vector. 30, 32–37, 41

\vec{v} Vector resulting from deflecting the sperm orientation vector. 33, 34

a Sperm alignment score. 32, 37, 38

c_{center} Contraction center. 42

cw_{org_sd} Standard deviation of z displacement due to muscle contraction. 42, 101

cw_{org} Width of window for muscle contraction. 101

- dt Simulation time step. 30, 32, 33, 37, 42, 101
- k_A Fraction which defines range in primary folds in which secondary folds occur. 25, 103
- k_B Defines range on z-axis where secondary folds occur in cranial vagina and uterus body. 103
- k_z Fraction of primary fold depth to maximal primary fold depth at which secondary folds occur.. 88
- l_c Length of cervix. 103
- l_o Length of oviducts. 103
- l_v Length of vagina. 103
- l_{cv} Length of cranial vagina. 87, 103
- l_{ub} Length of uterine body. 103
- l_{uh} Length of uterine horns. 103
- l_{utj} Length of uterotubal junction. 103
- n_{IR} Hill coefficient of immune response.. 101
- n_{org} Hill coefficient of muscle contraction probability decline. 42, 101
- n_{pH} Hill coefficient of sperm response to pH. 103
- no_lin Setting with all Boolean True, but no decrease in current angle due to wall alignment. 45, 46
- pH_False Setting with pH Boolean False. 46, 64
- pH_{semen} pH of seminal plasma. 103
- pH_{vagina} pH of vagina. 103
- p_{mot} fraction of motile sperms. 32, 102

r_c Cervix radius. 23, 26, 27, 40, 87, 103

$r_c(\alpha)$ Cervix radius, including primary grooves. 40, 89

r_v Vagina radius. 21, 26, 27, 40, 87, 103

r_{o1} Lower radius of oviducts. 103

r_{o2} Upper radius of oviducts. 103

r_{uh1} Lower radius of uterine horns. 89

r_{uh1} Start radius of uterine horns.. 103

r_{uh2} Upper radius of uterine horns. 103

r_{z_bif} Radius of each uterine horn when they divide. 89, 103

s_c Current speed of one sperm. 30, 32, 42

s_f Fluid flow speed. 38, 41, 45, 55

s_f Fluid flow speed at sperm's position. 32

s_l Length of spermatozoa. 3, 30, 32, 35

s_m Sperm motility. 30, 32

s_{speed} Speed of spermatozoa. 3

t_l Lifetime of sperm. 30, 32, 42, 43

t_s Simulation time. 30, 101

t_{org} Time of half-maximal contraction probability. 42, 101

t_{out} Time intervals between outputs. 31, 101

w_{pf} Number of primary folds. 103

z_c z - offset of the cervix compartment. 87, 103

z_{bif} z - distance in uterine horns, where they bifurcate. 28, 89, 103

z_{cv} z - offset of cranial vagina. 87, 103

z_o z - offset of oviducts. 103

z_{ub} z - offset of uterine body. 103

z_{uh} z - offset of uterine horns. 103

z_{utj} z - offset of uterotubal junction. 103

z_v z - offset of vagina. 103

ABM Agent-based modeling. 2, 3, 14, 66, 67

HIV human immunodeficiency virus. 5

IVF *in vitro* fertilization. 1, 2

IZW Leibniz-Institut für Zoo-und Wildtierforschung. 3

KDTree k dimensional tree. 44

ODE Ordinary differential equation. 2

PDE Partial differential equations. 67

UTJ Uterotubal junction. 10

[title=List of Abbreviations]

List of Figures

1	Comparison of bovine and human female reproductive tract.	4
2	The sperm - a hydrodynamic pusher	7
3	Bull sperms swim against fluid flow	8
4	Bovine sperms in the oviductal sperm storage site	12
5	Site of Fertilization	13
6	An example for an implicit function	16
7	Simulation workflow	18
8	Modeled reproductive tract	20
9	The vagina compartment	21
10	From biology to equation	22
11	Adding primary folds	24
12	Alteration of the secondary fold amplitude	25
13	Modeled cervical cross section	26
14	From vagina to cervix	27
15	3D representation of cranial vagina, cervix and uterine body	27
16	3D representation of the uterine horns	29
17	Model structure	31
18	Sperm orientation update	33
19	Wall alignment step by step	36
20	Ellipsiodal shape of sperm	37
21	Fluid flow approximation	39
22	Fluid velocity	41
23	Identification of microgrooves	43
24	Bull sperms synchronize their movement	44
25	Percentages of successful sperms	47
26	Population dynamics of <i>All_False</i>	48
27	Sperms per compartment <i>All_False</i>	49
28	Angle distribution <i>All_False</i>	50
29	Population dynamics <i>All_True</i>	51

30	Number of sperms per compartment <i>All_True</i>	52
31	Angle distribution <i>All_True</i>	53
32	Dynamics of sperm population <i>F_False</i>	54
33	Sperm per compartment <i>F_False</i>	55
34	Angle distribution <i>F_False</i>	56
35	Population dynamics <i>W_False</i>	57
36	Sperms per compartment <i>W_False</i>	58
37	Population dynamics <i>All_True_sF</i>	58
38	Sperms per compartment <i>WFO_False</i>	59
39	Sperms per compartment <i>FO_False</i>	60
40	Sperm movement without interaction.	61
41	Sperm movement with interaction.	61
A1	Sperms per compartment <i>O_False</i>	98
A2	Wall alignment	99
A3	Mathematical representation of the uterotubal junctions	100
A4	Mathematical representation of the oviducts	100

List of Tables

1	Dimension of mammalian reproduction	3
2	Most important sperm properties	32
3	Different settings of simulation runs	46
A1	Simulation parameters	101
A2	Sperm parameters	102
A3	Compartment parameter	103

A Appendix

A.1 Description of cranial vagina and uterine body

The solution is the compartment cranial vagina, described by equation A1.

$$f_{cv}(x, y, z) = x^2 + y^2 - (r_{cur} + A_{pf_cur} \cdot \cos(\omega_{pf} \cdot \alpha) + A_{sf_cur} \cdot \sin(\omega_{sf} \cdot \pi \cdot \frac{d_0 - (r_{cur} - A_{pf_cur} \cdot k_A)}{A_{pf_cur} \cdot k_A}))^2 \quad (A1)$$

Where:

$$r_{cur} = \frac{z - z_{c_v}}{l_{c_v}} \cdot (r_c - r_v) + r_v \quad (A2)$$

$$A_{pf_cur} = A_{pf} \cdot \frac{z - z_{c_v}}{l_{c_v}} \quad (A3)$$

$$A_{sf_cur} = A_{sf} \cdot F_{A_{pf_cur}} \cdot F_z \quad (A4)$$

$$F_{A_{pf_cur}} = \max\left(\frac{k_A \cdot A_{pf_cur} - \|d_r\|}{k_A \cdot A_{pf_cur}}, 0\right) \quad (A5)$$

$$F_z = \max\left(\frac{(z - z_{c_v}) - l_{c_v} \cdot k_z}{l_{c_v} - l_{c_v} \cdot k_z}, 0\right) \quad (A6)$$

$$\alpha = \arccos\left(\frac{x}{d_0}\right) \quad (A7)$$

$$d_r = d_0 - r_c \quad (A8)$$

$$d_0 = \sqrt{(x^2 + y^2)} \quad (A9)$$

Three entities change in dependence of the z - coordinate and each other. First, the radius (r_{cur}):

z_{cv} is the z - position at which the vagina ends and the cranial vagina starts. So if the z - position is equal to z_{cv} , r_{cur} will be r_v . A z - position at the upper end of the cranial vagina ($z_{cv} + l_{cv}$) would lead to an r_{cur} of r_c .

Second, the amplitude of primary folds (A_{pf_cur}):

In general A_{pf} is some fraction of r_c . On the way through the cranial vagina (from z_{cv} to z_c) A_{pf_cur} should rise from 0 to A_{pf} . That is done by equation A3.

Third, the amplitude of secondary folds (A_{sf}):

The secondary folds, as discussed above (Figure 12), only occur in a specified region in primary folds to avoid overlapping. When primary folds begin to occur, secondary

folds are initially inadmissible (A_{sf_cur} should be 0). Therefore, A_{sf_cur} is defined by equation A4, where $F_{A_{pf_cur}}$ constrains secondary folds to the mid region of primary folds (A_{pf_cur}) and F_z only allows secondary folds, if primary folds reached a certain fraction (k_z) of their maximal value A_{pf} . If k_z is equal 0.5, it would limit the occurrence of secondary folds to that part of the cranial vagina, in which the current amplitude of primary folds (A_{pf_cur}) is larger than $A_{pf} \cdot k_z$. A value of 0.5 for k_z would lead to occurrence of secondary folds only in the upper half of the cranial vagina. More precise, given a z - value in the middle of the cranial vagina ($z_m = z_{cv} + l_{cv} \cdot 0.5$), F_z and A_{pf_cur} can be calculated with equations A3 and A6. F_z would be zero, so secondary folds will occur if $z > z_m$. A_{pf_cur} would be $0.5 \cdot A_{pf}$, so with k_z equals 0.5 secondary folds are constraint to (i) the upper half of the cranial vagina and (ii) to primary folds with an amplitude higher than 0.5. These two are actually equivalents.

Similar to the cranial vagina, the uterine body is a compartment which connects the cervix with a compartment without folds and with another radius (the uterine horns), therefore the radius and the fold amplitudes are altered in a very similar way:

$$f_{ub}(x, y, z) = x^2 + y^2 - (r_{cur} + A_{pf_cur} \cdot \cos(\omega_{pf} \cdot \alpha) + A_{sf_cur} \cdot \sin(\omega_{sf} \cdot \pi \frac{d_0 - (r_{cur} - A_{pf_cur} \cdot k_A)}{A_{pf_cur} \cdot k_A}))^2 \quad (A10)$$

Where:

$$r_{cur} = \frac{r_{uh1} - r_c}{l_{ub}} \cdot (z - z_{ub}) + r_c \quad (A11)$$

$$A_{pf_cur} = A_{pf} \cdot \frac{r_{uh1} - r_c}{l_{ub}} \quad (A12)$$

$$A_{sf_cur} = A_{sf} \cdot F_{A_{pf_cur}} \cdot F_z \quad (A13)$$

$$F_{A_{pf_cur}} = \max(\frac{k_A \cdot A_{pf_cur} - \|d_r\|}{k_A \cdot A_{pf_cur}}, 0) \quad (A14)$$

$$F_z = \max(\frac{k_B \cdot l_{ub} - (z - z_{ub})}{k_B \cdot l_{ub}}, 0) \quad (A15)$$

α , d_r and d_0 are calculated with equations A7 - A9. The resulting shapes are illustrated in Figure 15.

A.2 Description of uterine horns, uterotubal junction and oviducts

$$r_{cur} = \frac{r_{uh2} - r_{uh1}}{l_{uh}} \cdot (z - z_{uh}) + r_{uh1} \quad (A16)$$

$$y_m = \sqrt[4]{\frac{z - z_{uh}}{z_{bif}}} \cdot r_{z_bif} \quad (A17)$$

$$f_1(x, y, z) = x^2 + (y - y_m)^2 - r_{cur}^2 \quad (A18)$$

$$f_2(x, y, z) = x^2 + (y + y_m)^2 - r_{cur}^2 \quad (A19)$$

$$f_{uh}(x, y, z) = \min(f_1, f_2) \quad (A20)$$

With

$$r_{z_bif} = \frac{r_{uh2} - r_{uh1}}{l_{uh}} \cdot z_{bif} + r_{uh1} \quad (A21)$$

r_{z_bif} is the r_{cur} at z_{bif} . At an altitude of z_{bif} the y - coordinates of the midpoints (equations A17 - A19) have drifted apart by $2 \cdot r_{z_bif}$.

r_{cur} for the uterotubal junction:

$$r_{cur} = \frac{r_{o1} - r_{uh2}}{l_{utj}} \cdot (z - z_{utj}) + r_{uh2} \quad (A22)$$

r_{cur} for the oviducts:

$$r_{cur} = \frac{r_{o2} - r_{o1}}{l_o} \cdot (z - z_o) + r_{o1} \quad (A23)$$

A.3 Fluid flow in uterine body

Approximating the fluid direction in the uterine body compartment is mote difficult, than in the cranial vagina. That is because, $r_c(\alpha)$ can exceed r_{uh1} , so according to the second intercept theorem one obtains either equation A24a or A24b.

$$\frac{z_{center}}{z_{center} - l_{ub}} = \begin{cases} \frac{r_{uh1}}{r_c(\alpha)}, & \text{if } r_{uh1} > r_c(\alpha) \\ \frac{r_c(\alpha)}{r_{uh1}}, & \text{if } r_{uh1} < r_c(\alpha) \end{cases} \quad (A24a)$$

$$(A24b)$$

Setting:

$$R_i := \frac{r_{uh1}}{r_c(\alpha)} \quad (\text{A25})$$

one obtains:

$$z_{center} = \begin{cases} \frac{R_i - l_{ub}}{R_i - 1}, & \text{if } r_{uh1} > r_c(\alpha) \\ \frac{l_{ub}}{1 - R_i}, & \text{if } r_{uh1} < r_c(\alpha) \end{cases} \quad (\text{A26a})$$

$$(\text{A26b})$$

In case one (Equations A24a and A26a) the center is calculated by $\vec{c} = (0, 0, z_{uh} - z_{center})^T$, while in case two (Equations A24b and A26b) $\vec{c} = (0, 0, z_{ub} + z_{center})^T$. In order to obtain a downstream fluid flow its direction is calculated as shown below (Equations A27a and A27b).

$$\vec{u}_f = \begin{cases} \vec{c} - \vec{p}_a = (-x_a, -y_a, z_{uh} - z_a - z_{center})^T, & \text{if } r_{uh1} > r_c(\alpha) \\ \vec{p}_a - \vec{c} = (x_a, y_a, z_a - z_{ub} - z_{center})^T, & \text{if } r_{uh1} < r_c(\alpha) \end{cases} \quad (\text{A27a})$$

$$(\text{A27b})$$

A.4 Derivation of rotation matrix

For agent-based modelling it can be useful to give an agent a direction vector, e.g. for movement. If this movement underlies random direction changes, one has to find a way to update the direction vector \vec{u} .

In two dimension this is easily done:

A vector \vec{u} with angle γ to the x-axis, should be turned by angle β . Vector \vec{u} has the coordinates:

$$\vec{u} = \begin{pmatrix} x \\ y \end{pmatrix} = \begin{pmatrix} r \cdot \cos \gamma \\ r \cdot \sin \gamma \end{pmatrix}$$

Let's call the vector after being turned by α vector \vec{v} . Logically it will be:

$$\vec{v} = \begin{pmatrix} x' \\ y' \end{pmatrix} = \begin{pmatrix} r \cdot \cos(\gamma + \beta) \\ r \cdot \sin(\gamma + \beta) \end{pmatrix} = \begin{pmatrix} r \cdot \cos \gamma \cos \beta - r \sin \gamma \sin \beta \\ r \sin \gamma \cos \beta + r \cos \gamma \sin \beta \end{pmatrix} = \begin{pmatrix} x \cos \beta - y \sin \beta \\ y \cos \beta + x \sin \beta \end{pmatrix}$$

So a vector can be easily turned by an angle β .

Here I give the constraint that the updated vector should lay in a cone around \vec{u} .

This could be done by deflecting the vector by an angle β in order to obtain vector \vec{v} and afterwards turn \vec{v} around \vec{u} by an angle between 0 and 2π . How to realize these two steps is described below.

A.5 Vector Deflection

Having vector \vec{u} it is first deflected by α . With $\vec{u} = \begin{pmatrix} u_x \\ u_y \\ u_z \end{pmatrix}$.

To deflect the vector I use polar coordinates.

$$\begin{pmatrix} u_x \\ u_y \\ u_z \end{pmatrix} = \begin{pmatrix} r \cdot \sin \theta \cdot \cos \phi \\ r \cdot \sin \theta \cdot \sin \phi \\ r \cdot \cos \theta \end{pmatrix}$$

Deflect \vec{u} by β :

$$\begin{pmatrix} v_x \\ v_y \\ v_z \end{pmatrix} = \begin{pmatrix} r \cdot \sin(\theta + \beta) \cdot \cos(\phi) \\ r \cdot \sin(\theta + \beta) \cdot \sin(\phi) \\ r \cdot \cos(\theta + \beta) \end{pmatrix}$$

So one has the problem that v_x, v_y and v_z depend on θ and ϕ . Those can be calculated by x,y and z:

$$\theta = \arccos\left(\frac{z}{r}\right)$$

$$\phi = \begin{cases} \arccos\left(\frac{x}{r \cdot \sin \theta}\right) & y \geq 0 \\ -\arccos\left(\frac{x}{r \cdot \sin \theta}\right) & y < 0 \end{cases}$$

Vector \vec{u} can be deflected by β yielding the deflected vector \vec{v} . Subsequent the deflected vector \vec{v} has to be turned around \vec{u} by a random angle.

A.6 Vector Rotation

A vector can be turned around an arbitrary axis (\vec{u}) by angle α using the rotation matrix R_u :

$$R_u = \begin{bmatrix} \cos \alpha + u_x^2 \cdot (1 - \cos \alpha) & u_x u_y \cdot (1 - \cos \alpha) - u_z \sin \alpha & u_x u_z \cdot (1 - \cos \alpha) + u_y \sin \alpha \\ u_x u_y \cdot (1 - \cos \alpha) + u_z \sin \alpha & \cos \alpha + u_y^2 \cdot (1 - \cos \alpha) & u_y u_z \cdot (1 - \cos \alpha) - u_x \sin \alpha \\ u_x u_z \cdot (1 - \cos \alpha) - u_y \sin \alpha & u_y u_z \cdot (1 - \cos \alpha) + u_x \sin \alpha & \cos \alpha + u_z^2 \cdot (1 - \cos \alpha) \end{bmatrix}$$

The derivation of R_u is shown below. To turn around the normalized vector one has to do five different steps:

1. Rotate around z-axis into x-z-plane
2. Rotate around y-axis into z-axis
3. Rotate around z-axis by angle α
4. Inverse of 2.
5. Inverse of 1.

The rotation matrices around z (R_z) and y-axis (R_y) are needed:

$$R_z(\beta) = \begin{bmatrix} \cos \beta & -\sin \beta & 0 \\ \sin \beta & \cos \beta & 0 \\ 0 & 0 & 1 \end{bmatrix}$$

$$R_y(\gamma) = \begin{bmatrix} \cos \gamma & 0 & \sin \gamma \\ 0 & 1 & 0 \\ -\sin \gamma & 0 & \cos \gamma \end{bmatrix}$$

A.6.1 Rotation in xz-plane

$$\vec{u} = \begin{pmatrix} u_x \\ u_y \\ u_z \end{pmatrix} = \begin{pmatrix} r \cdot \sin \theta \cdot \cos \phi \\ r \cdot \sin \theta \cdot \sin \phi \\ r \cdot \cos \theta \end{pmatrix}$$

With $r = 1$. Vector \vec{u} is turned into xz-plane, by turning it around the z-axis by angle

$-\phi$.

$$R_z(-\phi) = \begin{bmatrix} \cos -\phi & -\sin -\phi & 0 \\ \sin -\phi & \cos -\phi & 0 \\ 0 & 0 & 1 \end{bmatrix} = \begin{bmatrix} \cos \phi & \sin \phi & 0 \\ -\sin \phi & \cos \phi & 0 \\ 0 & 0 & 1 \end{bmatrix} = \begin{bmatrix} \frac{u_x}{a} & \frac{u_y}{a} & 0 \\ -\frac{u_y}{a} & \frac{u_x}{a} & 0 \\ 0 & 0 & 1 \end{bmatrix}$$

With $a = \sqrt{u_x^2 + u_y^2}$.

A.6.2 Rotation in z-axis

Subsequent it is turned into z-axis by turning it around the y-axis by $-\theta$.

$$R_y(-\theta) = \begin{bmatrix} \cos -\theta & 0 & \sin -\theta \\ 0 & 1 & 0 \\ -\sin -\theta & 0 & \cos -\theta \end{bmatrix} = \begin{bmatrix} \cos \theta & 0 & -\sin \theta \\ 0 & 1 & 0 \\ \sin \theta & 0 & \cos \theta \end{bmatrix} = \begin{bmatrix} u_z & 0 & -a \\ 0 & 1 & 0 \\ a & 0 & u_z \end{bmatrix}$$

A.6.3 Rotate around z-axis

Next turning it by α around z-axis.

$$R_z(\alpha) = \begin{bmatrix} \cos \alpha & -\sin \alpha & 0 \\ \sin \alpha & \cos \alpha & 0 \\ 0 & 0 & 1 \end{bmatrix}$$

A.6.4 Inverse of rotation into z-axis

$$R_y(\theta) = \begin{bmatrix} u_z & 0 & a \\ 0 & 1 & 0 \\ -a & 0 & u_z \end{bmatrix}$$

A.6.5 Inverse of rotation in xz-plane

$$R_z(\phi) = \begin{bmatrix} \frac{u_x}{a} & -\frac{u_y}{a} & 0 \\ \frac{u_y}{a} & \frac{u_x}{a} & 0 \\ 0 & 0 & 1 \end{bmatrix}$$

A.6.6 Putting it all together

In order to turn \vec{v} around \vec{u} by angle α steps 2.1-2.5 are applied one after another on \vec{v} .

$$\vec{v}' = R_z(\theta)R_y(\phi)R_z(\alpha)R_y(-\phi)R_z(-\theta) \cdot \vec{v} = R_u(\alpha)\vec{v}$$

To find the expression for R_u one has to multiply all the matrices from steps 2.1-2.5 .

$$R_u = R_z(\theta)R_y(\phi)R_z(\alpha)R_y(-\phi)R_z(-\theta)$$

$$\begin{aligned} R1 &= R_y(-\phi) \cdot R_z(-\theta) = \begin{bmatrix} \frac{u_x}{a} & \frac{u_y}{a} & 0 \\ -\frac{u_y}{a} & \frac{u_x}{a} & 0 \\ 0 & 0 & 1 \end{bmatrix} \cdot \begin{bmatrix} u_z & 0 & -a \\ 0 & 1 & 0 \\ a & 0 & u_z \end{bmatrix} = \begin{bmatrix} \frac{u_x u_z}{a} & \frac{u_y u_z}{a} & -a \\ -\frac{u_y}{a} & \frac{u_x}{a} & 0 \\ u_x & u_y & u_z \end{bmatrix} \\ R2 &= R_z(\alpha) \cdot R1 = \begin{bmatrix} \cos \alpha & -\sin \alpha & 0 \\ \sin \alpha & \cos \alpha & 0 \\ 0 & 0 & 1 \end{bmatrix} \cdot \begin{bmatrix} \frac{u_x u_z}{a} & \frac{u_y u_z}{a} & -a \\ -\frac{u_y}{a} & \frac{u_x}{a} & 0 \\ u_x & u_y & u_z \end{bmatrix} = \begin{bmatrix} \frac{u_x u_z \cos \alpha + u_y \sin \alpha}{a} & \frac{u_y u_z \cos \alpha - u_x \sin \alpha}{a} & -a \cos \alpha \\ \frac{u_x u_z \sin \alpha - u_y \cos \alpha}{a} & \frac{u_y u_z \sin \alpha + u_x \cos \alpha}{a} & -a \sin \alpha \\ u_x & u_y & u_z \end{bmatrix} \\ R3 &= R_y(\phi) \cdot R2 = \begin{bmatrix} u_z & 0 & a \\ 0 & 1 & 0 \\ -a & 0 & u_z \end{bmatrix} \cdot \begin{bmatrix} \frac{u_x u_z \cos \alpha + u_y \sin \alpha}{a} & \frac{u_y u_z \cos \alpha - u_x \sin \alpha}{a} & -a \cos \alpha \\ \frac{u_x u_z \sin \alpha - u_y \cos \alpha}{a} & \frac{u_y u_z \sin \alpha + u_x \cos \alpha}{a} & -a \sin \alpha \\ u_x & u_y & u_z \end{bmatrix} \\ &= \begin{bmatrix} \frac{u_x u_z^2 \cos \alpha + u_y u_z \sin \alpha}{a} + a u_x & \frac{u_y u_z^2 \cos \alpha - u_x u_z \sin \alpha}{a} + a u_y & -a u_z \cos \alpha + a u_z \\ \frac{u_x u_z \sin \alpha - u_y \cos \alpha}{a} & \frac{u_y u_z \sin \alpha + u_x \cos \alpha}{a} & -a \sin \alpha \\ -u_x u_z \cos \alpha - u_y \sin \alpha + u_x u_z & -u_y u_z \cos \alpha + u_x \sin \alpha + u_y u_z & a^2 \cos \alpha + u_z^2 \end{bmatrix} \end{aligned}$$

$$R_u(\alpha) = R_z(\theta) \cdot R3 = \begin{bmatrix} \frac{u_x}{a} & -\frac{u_y}{a} & 0 \\ \frac{u_y}{a} & \frac{u_x}{a} & 0 \\ 0 & 0 & 1 \end{bmatrix} \cdot \begin{bmatrix} \frac{u_x u_z^2 \cos \alpha + u_y u_z \sin \alpha}{a} + a u_x & \frac{u_y u_z^2 \cos \alpha - u_x u_z \sin \alpha}{a} + a u_y & -a u_z \cos \alpha + a u_z \\ \frac{u_x u_z \sin \alpha - u_y \cos \alpha}{a} & \frac{u_y u_z \sin \alpha + u_x \cos \alpha}{a} & -a \sin \alpha \\ -u_x u_z \cos \alpha - u_y \sin \alpha + u_x u_z & -u_y u_z \cos \alpha + u_x \sin \alpha + u_y u_z & a^2 \cos \alpha + u_z^2 \end{bmatrix}$$

$$= \begin{bmatrix} \frac{\frac{u_x^2 u_z^2 \cos \alpha + u_x u_y u_z \sin \alpha}{a^2} + u_x^2 - \frac{u_x u_y u_z \sin \alpha - u_y^2 \cos \alpha}{a^2} & \frac{u_x u_y u_z^2 \cos \alpha - u_x^2 u_z \sin \alpha}{a^2} + u_x u_y - \frac{u_y^2 u_z \sin \alpha + u_x u_y \cos \alpha}{a^2} & -u_x u_z \cos \alpha + u_x u_z + u_y \sin \alpha \\ \frac{u_x u_y u_z^2 \cos \alpha + u_y^2 u_z \sin \alpha}{a^2} + u_x u_y + \frac{u_x^2 u_z \sin \alpha - u_x u_y \cos \alpha}{a^2} & \frac{u_y^2 u_z^2 \cos \alpha - u_x u_y u_z \sin \alpha}{a^2} + u_y^2 + \frac{u_x u_y u_z \sin \alpha + u_x^2 \cos \alpha}{a^2} & -u_y u_z \cos \alpha + u_y u_z - u_x \sin \alpha \\ u_x u_z (1 - \cos \alpha) - u_y \sin \alpha & u_y u_z (1 - \cos \alpha) + u_x \sin \alpha & a^2 \cos \alpha + u_z^2 \end{bmatrix}$$

$$= \begin{bmatrix} \frac{\cos \alpha (u_x^2 u_z^2 + u_y^2)}{u_x^2 u_y^2} + u_x^2 & \frac{\cos \alpha (u_x u_y u_z^2 - u_x u_y) - \sin \alpha (u_x^2 u_z + u_y^2 u_z)}{u_x^2 u_y^2} + u_x u_y & u_x u_z (1 - \cos \alpha) + u_y \sin \alpha \\ \frac{\cos \alpha (u_x u_y u_z^2 - u_x u_y) + \sin \alpha (u_y^2 u_z + u_x^2 u_z)}{u_x^2 + u_y^2} + u_x u_y & \frac{\cos \alpha (u_y^2 u_z^2 + u_x^2)}{u_x^2 u_y^2} + u_y^2 & u_y u_z (1 - \cos \alpha) - u_x \sin \alpha \\ u_x u_z (1 - \cos \alpha) - u_y \sin \alpha & u_y u_z (1 - \cos \alpha) + u_x \sin \alpha & (u_x^2 u_y^2) \cos \alpha + u_z^2 \end{bmatrix}$$

$$= \begin{bmatrix} \frac{\cos \alpha (u_x^2 u_z^2 + u_y^2)}{u_x^2 u_y^2} + u_x^2 + u_x^2 \cos \alpha - u_x^2 \cos \alpha & \frac{\cos \alpha (u_x u_y u_z^2 - u_x u_y) - \sin \alpha u_z (u_x^2 + u_y^2)}{u_x^2 u_y^2} + u_x u_y + u_x u_y \cos \alpha - u_x u_y \cos \alpha & u_x u_z (1 - \cos \alpha) + u_y \sin \alpha \\ \frac{\cos \alpha (u_x u_y u_z^2 - u_x u_y) + \sin \alpha u_z (u_x^2 + u_y^2)}{u_x^2 + u_y^2} + u_x u_y + u_x u_y \cos \alpha - u_x u_y \cos \alpha & \frac{\cos \alpha (u_y^2 u_z^2 + u_x^2)}{u_x^2 u_y^2} + u_y^2 + u_y^2 \cos \alpha - u_y^2 \cos \alpha & u_y u_z (1 - \cos \alpha) - u_x \sin \alpha \\ u_x u_z (1 - \cos \alpha) - u_y \sin \alpha & u_y u_z (1 - \cos \alpha) + u_x \sin \alpha & (u_x^2 u_y^2) \cos \alpha + u_z^2 + u_z^2 \cos \alpha - u_z^2 \cos \alpha \end{bmatrix}$$

$$= \begin{bmatrix} \cos \alpha \left(\frac{u_x^2 u_z^2 + u_y^2 \overset{\text{red}}{u_x^2 (u_x^2 + u_y^2)}}{u_x^2 + u_y^2} \right) + u_x^2 (1 - \cos \alpha) & \cos \alpha \left(\frac{u_x u_y u_z^2 - u_x u_y + \overset{\text{red}}{u_x u_y (u_x^2 + u_y^2)}}{u_x^2 + u_y^2} \right) + u_x u_y (1 - \cos \alpha) - u_z \sin \alpha & u_x u_z (1 - \cos \alpha) + u_y \sin \alpha \\ \cos \alpha \left(\frac{u_x u_y u_z^2 - u_x u_y + \overset{\text{red}}{u_x u_y (u_x^2 + u_y^2)}}{u_x^2 + u_y^2} \right) + u_x u_y (1 - \cos \alpha) + u_z \sin \alpha & \cos \alpha \left(\frac{u_y^2 u_z^2 + u_x^2 \overset{\text{red}}{u_y^2 (u_x^2 + u_y^2)}}{u_x^2 + u_y^2} \right) + u_y^2 (1 - \cos \alpha) & u_y u_z (1 - \cos \alpha) - u_x \sin \alpha \\ u_x u_z (1 - \cos \alpha) - u_y \sin \alpha & u_y u_z (1 - \cos \alpha) + u_x \sin \alpha & \cos \alpha (u_x^2 + u_y^2 + \overset{\text{red}}{u_z^2}) + u_z^2 (1 - \cos \alpha) \end{bmatrix}$$

$$= \begin{bmatrix} \overbrace{\cos \alpha \left(\frac{u_x^2 (u_x^2 + u_y^2 + u_z^2) + u_y^2}{u_x^2 + u_y^2} \right)}^{=1} + u_x^2 (1 - \cos \alpha) & \overbrace{\cos \alpha \left(\frac{u_x u_y (u_x^2 + u_y^2 + u_z^2 - 1)}{u_x^2 + u_y^2} \right)}^{=0} + u_x u_y (1 - \cos \alpha) - u_z \sin \alpha & u_x u_z (1 - \cos \alpha) + u_y \sin \alpha \\ \overbrace{\cos \alpha \left(\frac{u_x u_y (u_x^2 + u_y^2 + u_z^2 - 1)}{u_x^2 + u_y^2} \right)}^{=0} + u_x u_y (1 - \cos \alpha) + u_z \sin \alpha & \overbrace{\cos \alpha \left(\frac{u_y^2 (u_x^2 + u_y^2 + u_z^2) + u_x^2}{u_x^2 + u_y^2} \right)}^{=1} + u_y^2 (1 - \cos \alpha) & u_y u_z (1 - \cos \alpha) - u_x \sin \alpha \\ u_x u_z (1 - \cos \alpha) - u_y \sin \alpha & u_y u_z (1 - \cos \alpha) + u_x \sin \alpha & \cos \alpha + u_z^2 (1 - \cos \alpha) \end{bmatrix}$$

$$= \begin{bmatrix} \cos \alpha + u_x^2 \cdot (1 - \cos \alpha) & u_x u_y \cdot (1 - \cos \alpha) - u_z \sin \alpha & u_x u_z \cdot (1 - \cos \alpha) + u_y \sin \alpha \\ u_x u_y \cdot (1 - \cos \alpha) + u_z \sin \alpha & \cos \alpha + u_y^2 \cdot (1 - \cos \alpha) & u_y u_z \cdot (1 - \cos \alpha) - u_x \sin \alpha \\ u_x u_z \cdot (1 - \cos \alpha) - u_y \sin \alpha & u_y u_z \cdot (1 - \cos \alpha) + u_x \sin \alpha & \cos \alpha + u_z^2 \cdot (1 - \cos \alpha) \end{bmatrix}$$

A.7 Figures - Appendix

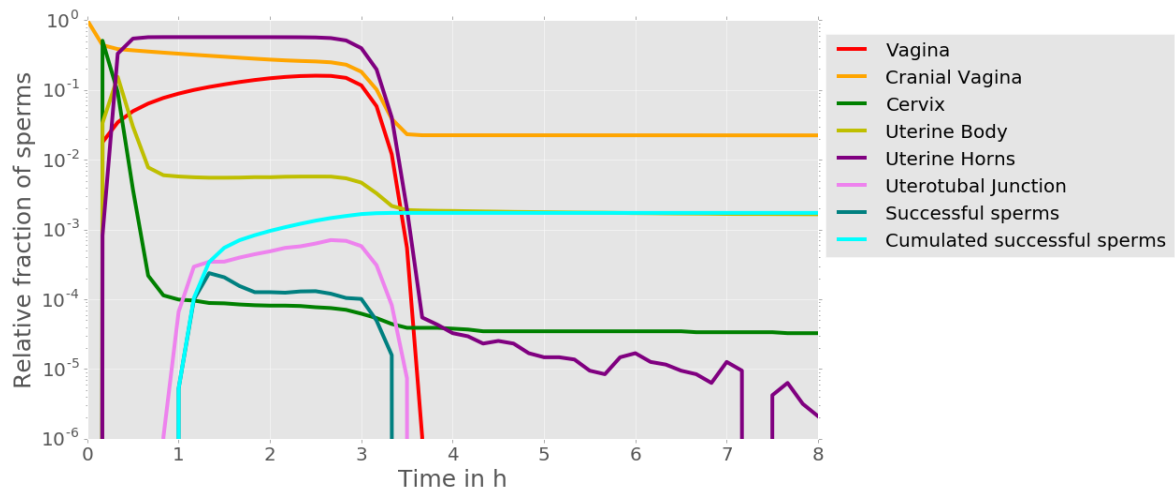


Figure A1: Relative number of sperm per compartment over time. Run *O_False*.

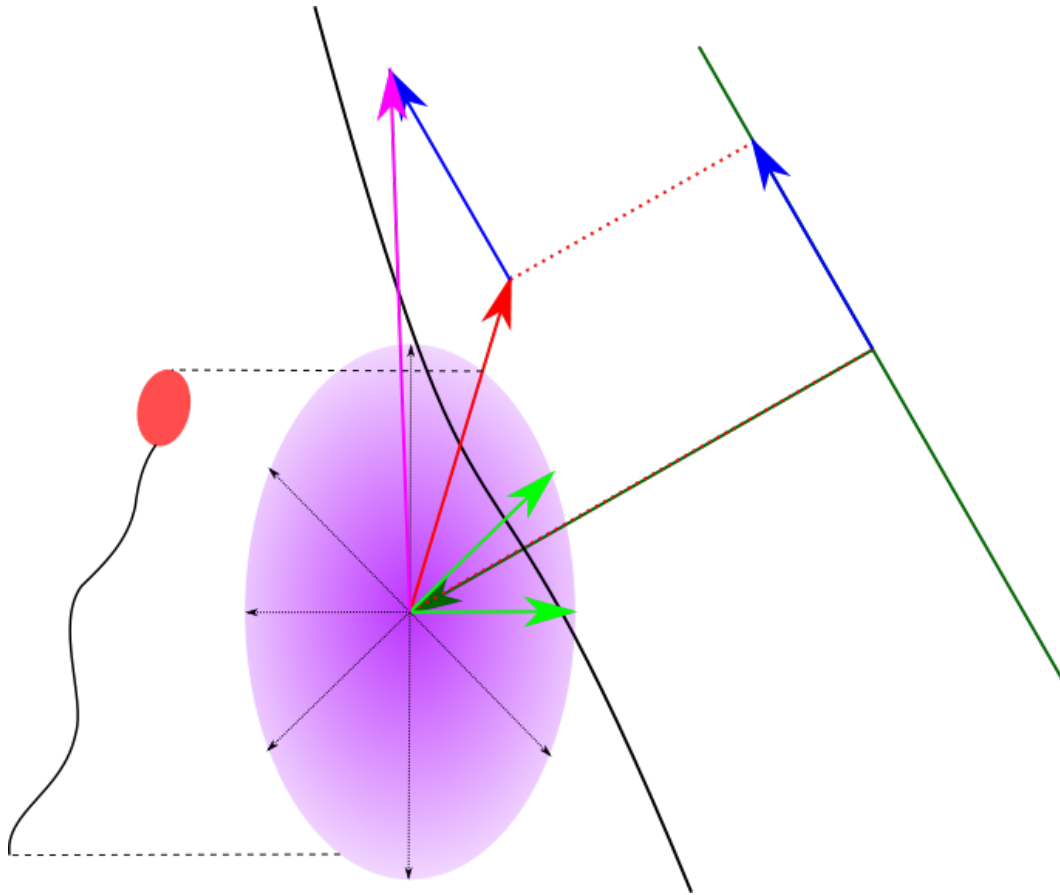


Figure A2: Red arrow indicates the orientation of the sperm shown in the left, originating from the sperm position. Small black arrows and thicker green arrows show the *checking directions*, while the latter are classified as *outliers*. By their average, these *outliers* define the normal vector for a plane (here line, because only two dimensional). The sperm orientation is projected on this plane resulting in the projection vector (blue arrow on plane). Adding the sperm orientation vector (red) and its projection on the plan (blue) one obtains the new sperm orientation (violet), which gives the new orientation vector has to be normalized afterwards.

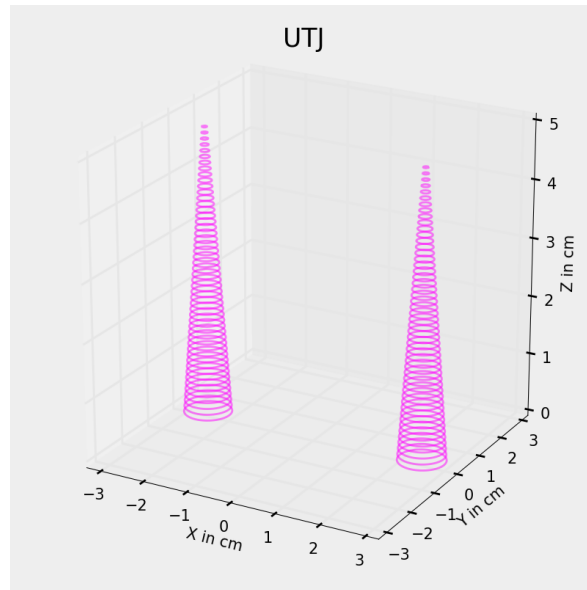


Figure A3: Mathematical representation of the uterotubal junctions. Lines indicate null surface.

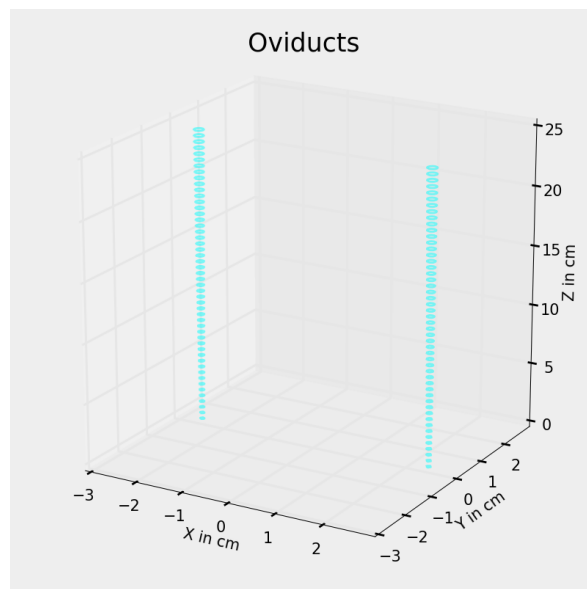


Figure A4: Mathematical representation of the oviducts.

Table A1: Simulation parameters. Here, global simulation parameters are shown.

Entity	Description	Value
N	Number of agents	-
t_s	Simulated time	28800
dt	Time step	0.25
Sim_{steps}	Simulation steps	115200
t_{out}	Time intervals between outputs	600
B_{pH}	pH change	False/True
B_{ir}	Immune response	False/True
Km_{IR}	Time of half maximal immune response	14400
n_{IR}	Hill coefficient of IR	4
B_{org}	Orgasm	False/True
P_{org_max}	Maximal probability of muscle contraction	0.1
t_{org}	Time of half-maximal muscle contraction intensity	60
n_{org}	Hill coefficient of muscle contraction probability	8
cw_{org}	Muscle contraction width	0.2
$\overline{cw_{org}}$	Mean of muscle contraction strength	2
cw_{org_sd}	Standard deviation of muscle contraction strength	3
B_w	Wall interaction	False/True
B_f	Fluid flow	False/True

Table A2: Sperm parameters. This table obtain global sperm population parameters. These parameters, except of λ_γ and $S_{speed.\sigma}$, are solely used to initiate a sperm population. Giving the sperms properties defined by probability distributions (Section 5.3).

Entity	Description
Value	
λ_γ	0.5
$\overline{S_{speed}}$	0.014
$\overline{S_{speed.sd}}$	0.0028
$\overline{S_{angle}}$	30.0
$\overline{S_{length}}$	0.0065
$\overline{S_{length.sd}}$	0.0005
$S_{speed.\sigma}$	10.0
$\overline{S_{lt}}$	86400.0
$\overline{S_{lt.sd}}$	21600.0
p_{mot}	0.8

Table A3: Compartment parameter. This table holds global parameters used to describe the reproductive tract.

Entity	Value	Entity	Value
r_{z_bif}	1.4 cm	r_{o2}	0.1 cm
r_v	2.5 cm	z_o	86.0 cm
pH_{semen}	7.5	A_{pf}	0.666667 cm
pH_{vagina}	4.5	k_A	0.8
C_{is}	144.0	A_{sf}	0.3
Km_{pH}	6.0	l_c	8.0 cm
l_{cv}	5.0 cm	l_{ub}	3.0 cm
z_{ub}	38.0 cm	λ_{pH}	900.0 s
ω_{sf}	32.0	r_c	1.0 cm
l_v	25.0 cm	z_{bif}	4.0 cm
l_o	25.0 cm	n_{pH}	25.0
z_{utj}	81.0 cm	r_{uh1}	1.5 cm
z_{uh}	41.0 cm	r_{uh2}	0.5 cm
l_{uh}	40.0 cm	z_v	0.0 cm
l_{utj}	5.0 cm	k_B	0.5
z_{cv}	25.0 cm	w_{pf}	8.0
z_c	30.0 cm	S_{fluid}	0.0018 $\mu m/s$
r_{o1}	0.05 cm		

E Eigenständigkeitserklärung

Hiermit versichere ich, dass ich die vorliegende Masterarbeit erstmalig einreiche, selbständig verfasst und keine anderen als die angegebenen Quellen und Hilfsmittel verwendet habe.

(Ort, Datum)

(Unterschrift)